D53687'85

120   *

D53687/85

TATE, T. J.

Coloured Diag'ms.

120

City of London Poly.

PIEZO-OPTICAL STUDY OF THE BEHAVIOUR OF SHORT CHAIN

LIQUID POLYMERS

by

Thomas John Tate, BSc MSc

Thesis submitted in partial fulfilment of the requirements of the
CNAA for the degree of

Doctor of Philosophy
City of London Polytechnic, November 1984

T J TATE

"Piezo-optical study of the behaviour of short chain liquid polymers"

ABSTRACT

The molecules of short chain liquid polymers exist in a dynamic mixture of conformations. Intermolecular interactions are important, rendering statistical mechanical models inappropriate: instead, free volume concepts are used.

Evidence of an ordered liquid state in the n-alkanes is disputed, and high-pressure Raman spectroscopy has shown the shorter homologues to become more globular with increasing pressure.

Brillouin laser light scattering is a powerful probe of molecular dynamics, and has been shown to be applicable to liquid polymers at high pressures. The present work has been concerned with relating molecular parameters, obtained by light scattering, to bulk properties of short chain homologous liquid series. To avoid thermal effects, pressure has been used to obtain pure volume-changes. Brillouin scattering, refractive index, density and viscosity data have been obtained at high pressure (up to 240 MPa) for members of four related homologous series, including some n-alkanes. Refractive index and density-cell piston movement were measured interferometrically; viscosity by falling ball and falling slug methods.

The refractive index, and density, data, both fit cubic polynomials in pressure, and the Lorentz-Lorenz equation applies with constant molar refractivity. Viscosity is exponentially, and hypersonic phonon velocity linearly, dependent on density, though Schaaff's equation is incorrect. A relaxation of 10^{-11} S was observed for the polyisobutenes.

In all cases, the important parameter is the density. A model of specific volume comprising contributions from chain segment- and chain end- volumes is proposed. This shows that packing is principally achieved by loss of free volume associated with chain ends for n-alkanes and polyisobutenes, and with chain segments for polyethylene glycols and polypropylene glycols, consistent with the freezing behaviour. The n-alkane data may be interpreted as showing some degree of molecular ordering above 150 MPa, analogous to the thermal observations of a mesomorphic liquid state.

INDEX

CHAPTER 1

INTRODUCTION

'With a name like yours, you might be any shape, almost.'

Lewis Carroll: "Alice's Adventures
Through the Looking Glass"

The liquid state of short chain polymers is characterised by the
flexible molecules existing in a dynamic mixture of conformations.
By contrast, the number of conformations is very limited in the solid
state: for example, the n-alkanes, which are an important group of
simple polymers with the repeat group - CH_2 -, exist only in the
all-trans conformation in the crystal [1]. A gas state often does not
exist, due to thermal degradation, but an important equivalent state
is that of infinite' dilution in a suitable solvent [2]. In this
case, the statistical mechanical concept of the 'random coil' may be
used to describe the molecular conformation. This bears some relation
to the bulk liquid, in that many distinct dynamic conformations are
available to the molecule: n-octane, for example, having a total of
34 distinct conformations, ranging from *all-trans* to those with five
gauche bonds. However, the statistical mechanical methods which may
be applied to the isolated molecule [2] are inappropriate to the bulk
liquid, in which intermolecular interactions play an important, if not
dominant, role.

Since statistical mechanical methods are currently unable to provide
a simple model of the polymeric liquid state, 'free-volume' theories
are often employed. There is a large number of definitions of 'free
volume' [3], depending to some extent on the chosen meaning of
'occupied volume', but it may conceptually be envisaged as the 'elbow
room' required by a molecule to be able constantly to assume new
conformations. In this case, the occupied volume comprises the total
Van der Waals' volumes of the constituent atoms.

Despite the extensive applications in modern materials of pressure-
extruded polymers, and of polymeric   components subject to high

stresses in lubricants, much of the literature is concerned with the properties of dilute solutions rather than those of the melt, from which the molecular conditions differ radically. This is no doubt due to the greater ease with which the dilute solution may be modelled. However, many molecular-weight dependent properties of polymers show asymptotic behaviour for long chain lengths, and so a consideration of the behaviour of a range of simple short chain homologues may provide useful insight into the behaviour of longer chains. In this way, linear polyethylene may be regarded as an n-alkane of very high molecular weight (> 1500 [2]). When crystalised from the melt, poly-ethylene chains extend to their full length - of the order of microns [4] - to form a lamellar structure, and evidence has been observed of a nematic-like ordered liquid phase as a step between the disordered liquid and the highly ordered solid states [5]. A similar local ordering of the melt has been suggested to account for observed discontinuities in thermal behaviour of sound velocity, magnetic susceptibility, and sound attenuation of n-alkane samples [6], occurring at a well-defined temperature, T_u, within the melt region. However, the observability and existence of this mesomorphic phase change are disputed [7]. In order to investigate this in the simple liquid state, Schoen et al [1,8] studied a range of liquid n-alkanes using high-pressure Raman spectroscopy. Their results indicated that, for the short-chain homologues, the number of *goucke* states increases with increasing chain length. This result is confirmed by the recent work of Ikawa and Whalley [9], in which the internal rotation angle of 1,2 dichloroethane ($ClCH_2CH_2Cl$) in solution, was measured as a function of pressure using both Raman and infra red spectroscopy. In this case, the ratio of *gauche* to *trans* was again found to increase with pressure. No work has been reported on longer chain homologues.

- 3 -

Dill et al [10] employed light scattering techniques at high pressure in order to obtain information on the pressure and temperature dependence of the viscoelastic properties of a polyphenyl ether lubricant, 5P4E. This showed light scattering to be a viable technique for the determination of viscoelastic (as distinct from static) data for use in the elastohydrodynamic model of the lubricant under working conditions. The methods described include polarised and depolarised 90° scattering up to pressures of 220 MPa, yielding high frequency experimental data which had been unavailable hitherto.

Apart from this pioneering study, however, there appears to be no literature concerning high pressure Brillouin light scattering from liquid polymers, although work has been reported for the liquids carbon tetrachloride [11], carbon disulphide, acetone and benzene [12] and benzene [13]. Nor were any of the earlier ultrasound investigations of Tait, Eden, and Richardson [14,15,16] specifically concerned with polymers.

Considering the potential of light scattering techniques for providing unique molecular data, the paucity of literature concerning its application as a function of pressure to polymer systems is surprising, especially following the work of Dill et al [10].

The aim of the present work has been to relate considerations based on molecular conformations to bulk properties of simple short chain liquid polymers. In order to avoid explicitly temperature-dependent changes in molecular parameters, the effects of pure volume changes have been investigated at constant temperature by varying the pressure. Molecular properties of various related homologous liquid series have been probed at high pressures, using polarised Brillouin laser light scattering. This technique analyses light scattered from thermal

- 4 -

motions of small sections of the polymeric chains [17], providing data on high-frequency molecular parameters related to the bulk properties of compressibility, viscosity and sound velocity. Analysis of the Brillouin data requires knowledge of the bulk parameters, ie refractive index, density, compressibility, and viscosity throughout the pressure range. Investigation of the literature reveals little such data for short chain polymers, and no instance of all these properties being evaluated by a single source, while variations in chemical purity, molecular weight distribution of samples, and pressure scale calibration, combine to render the compilation of data unreliable.

In view of these observations, the present work has been concerned with obtaining light scattering data for short chain liquid polymers in order to investigate the effect of pressure on molecular conformations. Interpretation of these data means that a large proportion of the work has involved the design and execution of experiments to determine refractive index, density and viscosity as functions of pressure for members of the four related homologous series investigated, thus standardising the purity and composition of the chemicals, together with a constant pressure scale calibration. The results of these investigations are presented in Chapter 4, and the dependence of the bulk and high-frequency effects on molecular conformation is discussed in Chapter 5.

CHAPTER 2

THEORETICAL CONSIDERATIONS

'Felix qui potuit rerum cognoscere causas'

Virgil: Georgics ii 490

Contents   Page Number

1 Introduction

(i) Free Volume

The model of the liquid state defined by Doolittle and Doolittle [18] describes it as being composed of material which occupies a limiting specific volume, v_o, the remaining free volume, v_f being empty so that

$$v = v_o + v_f \tag{2.1}$$

where v is the total volume occupied by the liquid. v_o corresponds to the limiting volume to which a real liquid would contract if it were to continue to behave as an nonassociated liquid without change of phase all the way to absolute zero. Matheson [20] modified this to allow v_o to be a function of temperature and pressure, ascribing solid-like behaviour to v_o and gas-like to v_f, so that the compressibility of v_o follows Bridgmann's [21] equation for solids

$$v_o(P) = a + bP + cP^2.$$

(ii) Optical Properties

(a) The Gladstone-Dale Equation

This equation has the advantage of simplicity, and is widely quoted in the earlier literature on high pressure. A slab of matter of refractive index n and thickness l comprises material (n' and l') and free space (refractive index = 1, thickness = l - l'). Thus the path length through the slab is

$$nl = n'l' + (l - l')$$

$$n - 1 = \frac{l'}{l} (n' - 1)$$

but $\frac{l'}{l} = \frac{v_o}{v}$ = relative volume of material

$$\rightarrow n - 1 = k\rho \qquad (2.2)$$

where ρ is the density. So long as n' remains constant the Gladstone-Dale [22] equation will hold.

(b)   The Lorentz-Lorenz Equation

A more rigorous derivation produces the Clausius-Mossotti equation [23] for spherical isotropic particles, relating the molecular polarisability, α, to the dielectric constant ε.

In the optical region, ε is replaced by n^2, producing the Lorentz-Lorenz [24,25] equation:

$$\frac{n^2 - 1}{n^2 + 2} = \frac{4\pi\alpha}{3} \frac{N_A \rho}{M} \qquad (2.3)$$

N_A is Avagadro's number; M the molecular weight, and ρ the density.

The molar refractivity, R, is defined from (2.3):

$$R = \frac{M}{\rho} \frac{(n^2 - 1)}{(n^2 + 2)}$$

and has been found to be an additive quantity for a wide number of

species [26,28]. Doolittle [19] reports finding a linear dependance of R on v_o in the n-alkanes, as predicted by Glasstone [26]. Bottcher [27] shows that the molar refraction of alkanes satisfies the rule of additivity, and it is reasonable to suppose that this will also hold for similar series: that this is so implies that the assumptions inherent in the Lorentz-Lorenz formula are met in these substances.

(iii)   Other Equations for Density and Refractive Index

Many more or less empirical equations exist linking pressure and density, including the Tait [29] equation

$$\frac{\Delta V}{V_o} = A \; \log \; \frac{(B + P)}{(B + P_o)}$$

where the initial volume V_o is defined at P_o and A, B are empirical constants. Vedam et al [30,33] report a linear relation between refractive index and the Eulerian strain, ϵ, ie

$$\epsilon = \tfrac{1}{2} \; (1 - (\frac{V}{V_o})^{-2/3}) \; \alpha \; \Delta n.$$

This was obtained using interpolated PV data from Bridgmann, and measured values of Δn, though there appears to be some uncertainty about the compressibility of the vitreous silica spacer used in their interferometer. Their finding is at variance with those of their earlier papers [31,32] and nullified by their own opening statement [30] 'Reliable experimental PV data on liquids over a wide pressure range are indeed sparse'.

(iv)   Viscosity

In order to explain the phenomenon of viscosity, Eyring [34] sees each
molecule as being surrounded by a cage of its neighbours [35]. For flow
to take place, the molecule must overcome the potential barrier of making
a hole in the cage and escaping through it irreversibly. The density
fluctuation in the cage is described as a rate reaction by the Arrhenius
equation:

$$\ln \eta = A + \frac{E}{RT} \qquad (2.4)$$

where R is the gas constant and E the activation energy for viscous flow.
For a chain molecule, which may escape in segments, E depends more on
the cross-sectional area and flexibility than on the molecular volume.
Cogswell and McGowan [36] give an estimate of these values by using the
parachor (an additive measure of the molecular volume), V*, deriving the
semiempirical   equation

$$\left(\frac{69RT}{p^*V^*}\right) \log \frac{\eta}{\eta^*} = (f(T))^{0.5} \left(9 \frac{p}{p^*} + (f(T))^{9/5}\right)^{5/9} \qquad (2.5)$$

where $f(T) = 32.5 \left(1 - \frac{T}{T^*}\right)$, T* being a characteristic temperature, and
p* is apparently constant for all liquids. By examination of literature
values, it appears that η^* is also constant for all liquids, and equal to
1.32×10^{-4} PaS. For measurement of η at constant temperature, this may
be rearranged to yield

$$(\log \eta + c)^{1.8} = a + bP \qquad (2.6)$$

where $c = \log \eta^* = -3.88$.

Doolittle [19] expressed (2.4) in terms of free volume, obtaining

$$\ln \eta = A' + B' \frac{v_o}{v_f} \tag{2.7}$$

This equation is generally found to apply to η:T data, but requires knowledge of v_f. Bridgmann's observation [21], that viscosity cannot be a function of volume only, since the η - V isotherms for a given liquid are observed to have different forms, is allowed for in (2.5) and (2.7) by the inclusion of $f(T)$ and by the fact that $\frac{v_o}{v_f}$ is a function of temperature.

(v)   Viscometry Relations

The viscometer used in this work consisted of a falling slug apparatus, where the slug was either a sphere or else a cylinder with rounded ends. In both cases, the slug diameter was comparable with the fall tube bore.

In the case of the sphere, of radius a, falling at terminal velocity V_T in an infinite sea of Newtonian fluid, Stoke's relation is:

$$\eta = \frac{2a^2 g}{9 V_T} (\rho_s - \rho_1) \tag{2.8}$$

where ρ_s is the density of the sphere, ρ_1 that of the liquid, and g is the acceleration due to gravity. Since the sphere is falling in a tube, correction must be made for the effect of the walls: the correction due to Faxen [37] is given by Flude and Daborn [38]:

$$V_T(\text{corrected}) = V_T (1 - 2.104 \, (\frac{d}{D}) + 2.09 \, (\frac{d}{D})^3 - 0.95 \, (\frac{d}{D})^5)^{-1} \tag{2.9}$$

with d and D the sphere and fall tube diameters.

- 11 -

The slug's motion is also constrained by the tube ends, and a correction for this is given by Lorentz [39]. However, this has been found to be negligible [40,41] except when the slug is within one fall-tube diameter of the tube end, and so it has not been applied in this work. The Reynold's number gives the critical values for laminar flow; if it is not exceeded then the flow will be laminar. For a solid sphere, this Reynold's number is given by

$$a \, \rho_1 \, V_T < \eta \qquad\qquad (2.10)$$

combining (2.8) and (2.10)

$$\frac{2a^3 g \, \rho_1}{9} (\rho_s - \rho_1) < \eta^2$$

and putting in values of $\rho_1 = 1$ g/cc, $\rho_s = 8$ g/cc for a steel sphere of 1 mm diameter (the smallest size generally available, and approaching the threshold of detection of the apparatus used), gives a minimum viscosity which may be measured in this way as

$$\eta_{min} = 0.04 \text{ Pa S.}$$

The viscosity of octane at 20 °C is 5.6×10^{-4} Pa S, whereas that of the lowest molecular weight polyisobutene investigated is around 0.18 Pa S. This shows that the simple falling sphere method is not applicable to the lower viscosity samples, and instead, the cylindrical fall slug was used. In this case, the flow is through the narrow annular gap between the slug and fall tube, similar to a capillary flow between the quasi-stationary slug and the wall, due to the pressure difference between the bottom and top of the slug. The equation for a right cylindrical body

- 12 -

falling axially down a closed vertical tube is given by Isdale and Spence [42] to be

$$V_T = \frac{- M_s \, g(1 - \frac{\rho_L}{\rho_s})}{2\pi \, l_s \, \eta} \left[\ln \left(\frac{D}{d} \right) - \frac{(D^2 - d^2)}{(D^2 + d^2)} \right]$$

substituting $M_s = \rho_s \, \pi r_s^2 \, l_s$, and rearranging, gives

$$\eta = \frac{r_s^2 \, g(\rho_s - \rho_L)}{4 \, V_T} \left[\ln \left(\frac{r_t}{r_s} \right) - \frac{(r_t^2 - r_s^2)}{(r_t^2 + r_s^2)} \right] \tag{2.11}$$

where r_t is the tube radius, and r_s that of the slug.

The Reynold's number [42] is given by

$$R_e = \frac{2r_s^2 \, \rho_L V_T}{(r_t - r_s)\eta}$$

This is for a cyliner with flat ends: for a cylinder with rounded ends we should expect to obtain laminar flow with Reynolds' numbers in excess of 1, as may be seen from the data of Isdale and Spence [42], who obtained laminar flow with Reynolds' numbers up to 1000, using a similar fall slug. In this work, the maximum experimental Reynolds' number is of the order of 10, for octane at one atmosphere pressure. Chen and Swift [43] found that laminar flow obtained for a Reynolds' number of $\sim$ 100 for flat ended fall slugs. The effects of non-vertical alignment of the fall-tube, and of the slug falling non-axially have been assumed negligible, since the fall tube was held vertical to a very high degree, and observation of the slug falling in a separate fall tube showed it to

- 13 -

be self-centring even for non-vertical alignment of up to about 3°. By use of the equations (2.8), (2.9) and (2.11), it would be possible to measure absolute viscosities. However, since (2.11) applies strictly only to a right circular cylinder, and since the viscometer constants will all be functions of pressure as the components compress in the hydrostatic field, only relative viscosities were measured, equations (2.8), (2.9) and (2.11) being used to compute corrections due to the changes of viscometer dimensions with pressure.

(vi) Rayleigh-Brillouin Scattering

Polarised Brillouin scattering arises from thermal fluctuations in the local dielectric tensor, producing longitudinal phonons with velocity V_s given by [44]

$$V_s = \frac{\nu_B \lambda}{2n \, \sin(\frac{\theta}{2})} \tag{2.12}$$

with an attenuation coefficient α:

$$\alpha = \frac{\pi \, \Gamma_B}{V_s} \tag{2.13}$$

where ν_B is the Brillouin shift, or separation of the Brillouin peaks from the central Rayleigh line, Γ_B is the Brillouin half-width at half height, λ the wavelength of light and θ the scattering angle (90° in this work). Schaaffs [50] proposed the equation

$$V_s = W(B\frac{\rho}{M} - \frac{1}{1 + B\beta})$$

relating the sound velocity to the molecular structure, where B is the

- 14 -

molar molecular volume:

$$B = \sum_i (z\ A)_i$$

with $A = \begin{cases} 1.06 \text{ cm}^3 \text{ for H atoms} \\ 3.06 \text{ cm}^3 \text{ for C atoms} \end{cases}$

and z is the number of atoms of each species in the molecule. The space-filling coefficient β is given by

$$\beta = \sum_i (z\ a)_i$$

where $a = 0.10$ cm^3 for each C – CH$_3$. This relationship was found to be incorrect for thermal data by both Michels [51] and Champion and Jackson [44]. Medina and O'Shea [13] found a linear dependence of V_s on density for Brillouin scattering from benzene at high pressures, but (2.14) still does not appear to apply.

The phonon attenuation is governed by the viscous loss and may be shown [44] to be

$$\alpha = \frac{2\pi^2 \nu_B}{\rho V_s^3} \left(\frac{4}{3} \eta_s(\omega) + \eta_V(\omega)\right) \tag{2.14}$$

where $\eta_s(\omega)$ is the shear and $\eta_V(\omega)$ the volume viscosity, measured at frequency $\omega = 2\pi\nu_B$. The frequency-dependent viscosities may then be expressed as:

$$\eta_V(\omega) = \frac{\eta_V(0)}{1 + \omega^2\tau_V^2} \qquad : \qquad \eta_s(\omega) = \frac{\eta_s(0)}{1 + \omega^2\tau_s^2}$$

where $\tau_{s,V}$ are the shear and volume relaxation times. If there is no relaxation, then $\eta(\omega) = \eta(0)$. By considering an average relaxation time, $\bar{\tau}$, (2.14) may be written as

$$\frac{\alpha}{\nu_B^2} = \frac{z}{V_s^3(1 + \omega^2\bar{\tau}^2)} \tag{2.15}$$

where z is a constant.

The elastic modulus of a system will be a combination of the compressional modulus K and the shear modulus G [47]:

$$M = K + \frac{4}{3}G = M' + iM''$$

where $M' = \rho V_s^2$ \hfill (2.16)

is the real part of the elastic modulus.

Relaxation will cause a dispersion in M' with frequency, from a low frequency limit

$$V_o^2 = \frac{\dot{K}_o}{\rho}$$

to a high frequency limit, where

$$V_\infty^2 = \frac{1}{\rho}(K_0 + K_r + \frac{4}{3}G_\infty)$$

where K_o is the bulk modulus and K_r t'e relaxational modulus. Clearly, for a liquid, the shear modulus is zero at zero frequency.

The Landau-Placzeck ratio is the integrated intensity ratio of the central peak to that of the Brillouin peaks, $I_C/2I_B$. If the spectra are

assumed to be composed of Lorentzian line shapes [48,49], then the Landau-Placzeck ratio is given by

$$LP_r = \frac{H_R \Gamma_R}{2H_B \Gamma_B} \qquad (2.17)$$

where $H_{R(B)}$ is the height of the Rayleigh (Brillouin) line, and $\Gamma_{R(B)}$ the half-width at half-height. For a non-relaxing liquid, $LP_r = \gamma - 1$, whereas for a relaxing liquid [49] $LP_r = (\gamma M'/M_o) - 1$. ($\gamma$ is the ratio of specific heats.) In general, the LP_r is difficult to measure, since any stray light or light scattered off dust particles will vastly increase I_c. For this reason, the LP_r is often useful as an indicator of the sample cleanliness rather than a measure of γ. For polymer samples, a reasonable value of γ at high temperature or low pressure is 1.25: if a sample approaches this then it may be assumed to be reasonably clean, so long as there is no relaxation causing $M' > M_o$.

CHAPTER 3

EXPERIMENTAL PROCEDURES

'You boil it in sawdust, you salt it in glue
You condense it with locusts and tape ,
Still keeping one principle object in view,
To preserve its symmetrical shape'

Lewis Carroll: "The Hunting of the Snark"

CHAPTER 3

Contents	Page Number

CHAPTER 3 EXPERIMENTAL PROCEDURES

1 (i)   Brief Review of High Pressure Techniques

The sensitivity of interference effects meant that the small changes
produced by small pressures could easily be measured by early investigators
However, the findings reviewed by Bridgman [52] show great disparity. Gibson
and Kincaid [53] used an immersion method in which the pressure of the
sample was adjusted until immersed fragments of glass of known refractive
index (at atmospheric pressure) were observed to disappear. Langer and
Montalvo[54] used an interferometer with a pure iron (assumed isotropic)
spacer, and observed fringe movement as sample pressure was changed in a
controlled manner. Waxler and Weir [55] used a similar method, claiming
greater dimensional stability. The Newton's rings interferometer of
Vedam et al [56], employing a semi-silvered plano convex lens appears
suspect because of the dependence on lens curvature and compressibility
of a silica spacer.

Three basic methods have been used to measure compressibility.
Canton [57], and Tait [58] used an arrangement similar to a glass
thermometer, with the sample in the bulb and the pressure applied
via the mercury column. In Aime's [59] "lobster pot" method, mercury
replaced any volume lost due to sample compression, the trapped mercury
being weighed on depressurisation. This method was modified by
Bridgmann [52]. The third method measures the movement of a piston,
either by means of a sliding collar [60], or by electrical resistance [52]
or, as in the present work, by interferometry. In Bridgmann's work, a
sylphon or bellows was used to contain the sample.

- 20 -

Measurement of viscosity is complicated by the enormous range that this parameter can take (in the present work, a dynamic range of 10^8 was encountered). This, together with the need to compile data at differing shear rates, leads to the wide range of methods which have been devised, many of which have been applied to high pressures. Thus, high pressure methods include: swinging vane [61], falling weight [52], capillary flow [52,62], light scattering from poly-styrene spheres within the sample [63], and Covette-Hatschek (concentric cylinders) [64,65]. The vast majority, however, have been of the falling ball or falling cylinder type, with electrical [66,42,67,68] or optical [69,70] detection of the sinker movement. Dandridge and Jackson [71] used intensity variation spectroscopy to measure the doppler shift of light reflected off the back of the fall slug, to obtain data on two of the polyisobutene samples investigated in this work.

The only high pressure Brillouin scattering reported from liquids employed pressure bombs similar to that described in this work [2,11,72,13]; the technique of optical mixing in which the scattered light is reintroduced

into the laser cavity for amplification, being used in ref [72], the others using Fabry-Perot interferometers. The Diamond anvil cell, because of its straight-through optical configuration, is not suitable for 90°-scattering, though it has been employed for Raman studies.

(ii)   Materials Investigated

The liquids investigated are members of four homologous series of short-chain polymers, as detailed below.

(a)   Alkanes

Samples of n-alkanes, referred to by the number of carbon atoms in the chain, as C_8, C_{10}, C_{11}, C_{12}, C_{13}, C_{15}, and an isomer of C_8, 2-2-4 trimethylpentane, were obtained as puriss grade, from Koch-Light Chemicals Ltd. These were chosen because the freezing pressures at room temperature, of the higher molecular weight samples, were attainable with the available equipment. In addition, data for the refractive index and density variation with pressure, for C_8 and C_{10} are available [30], [73], giving a comparison. Isooctane was studied because the molecule is globular compared with that of n-octane. It was envisaged that other globular isomers, notably that of C_{10}, 2-2-4-6-6 pentamethylheptane, would also be studied, but were not commercially available.

Having chosen the range of alkanes (summarised in table 3.1), the other series were chosen to cover a similar range of molecular weights.

(b)   Polyisobutenes

Polyisobutene (PIB) samples were obtained from BP Chemicals Ltd under the trade name 'HYVIS', with molecular weights ranging from 340 to 2400. These highly branched chain alkanes (with a C = C double bond near one end), were included because of their large range of viscosity, from around 65 c St to 195,000 c St at one atmosphere pressure, and room temperature. The samples are designated by BP as HO4, HO7, H5, H30 and H200, and are summarised in table (3.2).   [This kinematic viscosity range is equivalent to 0.07 - 200 PaS]

(c)   Polyethylene Glycol and Polypropylene Glycol

Polyethylene glycol (PEG) and polypropylene glycol (PPG) samples, both

series starting from the monomer, were obtained from BDH Chemicals, and are summarised in tables (3.3) and (3.4).

(iii)   Sample Preparation

Measurements of refractive index, density, and, for all except the alkane samples, viscosity, were performed on samples direct from the bottle. Dust in the alkane samples was found to introduce large discrepancies in the viscosity measurements and so filtering was necessary. In addition, rigorously dust-free samples were imperative for the light-scattering experiments, and so the samples were filtered using standard 'Millipore' PTFE (0.2 μm) filters. These were first flushed through with several millilitres of sample and the resulting samples found to be adequately dust-free when scattered laser light was examined using a hand lens. A larger pore size (1.0 μm), and heating to 40 °C were found to be necessary for filtering the polyisobutene liquids.

2 Design and Description of Apparatus

All the pressure vessels and associated tubing were made from stainless steel and used within a safety margin of at least X4.[75]

(i)   The Pressurising System

The pressurising system is shown in fig 3.1. The standard gauge had a range up to 1600 bar. The other gauge read up to 70,000 PSI (4.83 k bar), though a pressure of 40,000 Psi was never exceeded. For convenience, all measurements were made in Psi, and afterwards converted. Calibration by comparison of the gauges in increments of 100 bar was performed every six months and showed no appreciable changes over the period of use. Beyond 1600 bar, the calibration was extrapolated.

A detail of the tubing connections is given in fig 3.2. The seal is formed by excess pressure at the metal-to-metal contact.

(ii) The Separator

The separator is shown in detail in fig 3.3. The plug, or piston, was made of brass and, together with the single 'O' ring, sealed the hydraulic oil from the sample while transmitting pressure with a pressure difference of less than 1 bar. Positive location of the end cones was provided by the conical section and sealing effected by the 'O' ring being forced by internal pressure into the very small clearance (< 25 μm) between the shoulder and separator bore.

The four separate experimental bombs will now be described.

(iii) (a) The Refractive Index Bomb

The bomb for refractive index measurement was externally similar to the separator (fig 3.4), but with a thermal probe cavity at one end and a glass window at the other. The probe cavity was formed from a piece of high pressure tubing brazed to the end cone and sealed with a steel ball, allowing a thermocouple to be placed in close proximity to the sample. The window was cut from float glass 6 mm thick and glued directly onto the ground face of the end cone using cyanoacrylate adhesive. This method of sealing was found to be very satisfactory, the adhesive formed the seal at low pressure, and the force on the glass at high pressure. A thin film of cyanoacrylate adhesive was found to be superior to a beading of epoxy, which tended to crack the glass.

(b) The Optical System

The method selected to measure change in refractive index is based on the alteration in path length due to varying refractive index causing

movement of interference fringes. Two mirrors were set up parallel in the beam from a helium-neon laser so that the first obscured half the beam (fig 3.5). The path difference was thus 2 tn where t is the mirror spacing, and n the refractive index of the material between the mirrors. The separation was defined by means of a stainless steel spacer holding the mirrors apart. Both mirrors were front silvered using a vacuum evaporation apparatus. As may be seen from the figure, the reflecting surface of the front mirror is always in the same plane as the end of the spacer, irrespective of compression of the glass or spacer. This is not so, however, for the rear mirror, and compression of the components will cause a change in path length. A discussion of this path length change and of the choice of optimum dimensions of components is given in paragraph (4.1).

The mirror spacing was measured, using a travelling microscope, to be $t = 3.79 \times 10^{-3}$ m. The complete interferometer system screwed on to the end of the thermal probe cavity, and the bomb was set in a mount on an optical bench as shown in fig (3.6).

Setting up was performed with the window removed. The lens was adjusted so that the beam was bisected by the first mirror, and the mirror then adjusted until the reflected beams overlapped. The window was then inserted, the bomb filled with the sample, and the separator and associated tubing connected up.

(c) The Detection System

Interference fringe movement was detected by a photodiode, the amplified output being fed to a bistable (fig 3.7) which supplied the input to the counter. The bistable was arranged so that the positive- and negative-going trigger voltages differed by about half a volt, giving

- 25 -

meaningful counting even from quite a noisy signal (fig 3.8). The amplified output was displayed on an oscilloscope so that the signal could be easily monitored and, if necessary, the iris in front of the detector opened or closed to adjust the intensity.

(d)   Experimental Procedure

Having been set up and filled as outlined, the system was pressurised slightly in excess of the maximum datum point (just below the freezing pressure if that was lower than 250 MPa).   It was then left for about half an hour to attain thermal equilibrium, during which time the pressure would fall slightly. The pressure was then increased back to the original, the metering valve opened slightly, to give a counting rate of a few fringes per second, and the electronics adjusted. As the pressure passed through the highest datum the counter was switched on, and the cumulative number of fringes recorded for constant pressure changes down to atmospheric pressure. The temperature was monitored throughout each run, and if it was observed to fluctuate by more than 0.5 °C, then the run was aborted. The average temperature was used in calculating the mirror spacing.

In general, five sets of data were obtained for each liquid, showing agreement to within 1%, over a total count of around 500 fringes.

(e)   End-Point Refractive Index Measurement

An Abbe-type refractometer was used to measure refractive index at one atmosphere, illuminated using a helium-neon laser at the same wavelength (632.8 nm) as for the high pressure measurements. Since no tables exist for the instrument at this wavelength, calibration was performed using a fused silica test piece. Data on the dispersion of silica were obtained from ref [70]. The refractometer was calibrated at

- 26 -

546.07 nm (Hg line), using the silica test piece, and readings of the prism angle taken for spectral lines from Hg, Na, He and Kr sources, the He-Ne laser, and at 488.6 nm and 541.8 nm using the argon-ion laser.

Comparison of these data with the silica refractive index from ref [74] provided a Cauchy fit for the Abbe prism, of the form:

$$N(\lambda) = a + \frac{b}{\lambda^2} + \frac{c}{\lambda^4} + \frac{d}{\lambda^6} + \cdots$$

using

$$n = \sin A (N^2 - \sin^2 B)^{\frac{1}{2}} + \cos A \sin B$$

where a, b, c ... are least-squares fitted parameters

- N = Abbe prism refractive index
- n = sample (silica) index
- A = prism angle, 68.00° for this instrument
- B = (scale reading - intercept value), where the intercept value = 38.00°.

The resulting calibration is accurate to four decimal places over a wavelength range of 450 - 650 nm.

(iv) Density and Compressibility Measurements

The measurement of density change with pressure also depended on an interferometric fringe-counting technique. The bomb was similar to that used for refractive index measurement, and held a glass piezometer in a stainless steel mount (figs 3.9, 3.10).

(a) The Piezometer

The piezometer was fabricated from a 1 ml Chance all-glass syringe. Both

- 27 -

ends were ground off the (hollow) plunger, a 'quickfit' connection fused one end, and the sample volume sealed with a 'quickfit' stopper. A supporting ring, glued to the plunger near the stoppered end, fitted into a recess in the holder, allowing free movement to the body of the syringe.

The holder provided a mount for the front mirror, and incorporated an end stop to define the initial sample volume and mirror separation. The front mirror was mounted as for the refractive index measurement.

(b) Experimental Procedure

Initially, the empty syringe was weighed. It was then placed in the holder, with the body pushed down into contact with the end stop, and filled through the 'quickfit' opening using a long-needled syringe. After removal of any bubbles, the stopper was inserted and held in place using a light spring while the holder was screwed together, thus defining the sample volume and allowing any excess to leak out by slightly compressing the spring. The syringe was then removed from the holder, and the whole re-weighed. Knowledge of the sample density thus allowed the sample volume to be computed, and it was found to be 0.774 ± 0.001 cc for all samples. The system was then reassembled with a stronger spring to hold the end seal in place, and the whole mounted in the bomb. Setting-up was the same as for the refractive index system except that the bomb was filled with the polyisobutene sample, H07. This was used throughout as a pressure transmitting medium since its rela- tively low compressibility guarded against the separator reaching the end of its travel due to too large a volume change,and the viscosity was high enough to discourage leakage along the ground glass faces causing sample contamination. Correction was made for the changing refractive index of the H07.

The system was then pressurised and allowed to reach equilibrium.

Partial opening of the metering valve then allowed the pressure to leak

down and a count to be made over given pressure intervals. Five sets
of data were obtained for each liquid and generally found to agree
within 1% over a total count of order 20 000, obtained over an average
run time of about two hours. If the bomb temperature varied by more
than 0.5 °C over this time then the run was abandoned, thus these
data give isothermal measurements of density change.

Because of the movement of the rear mirror with changing volume, the
alignment of the optics tended to shift slightly throughout the
experiment, affecting the position of the fringe pattern. To compen-
sate for this, the iris in front of the detector was adjusted, or the
detector moved (along a fringe) to maintain clear counting. This was
a small effect, the mirrors remaining parallel to a surprising extent:
however, it was large enough to preclude measurement of fast volume
change and hence adiabatic compressibility, quite apart from the neces-
sity which would ensue for instantaneous pressure measurement.

(c) End-Point Density Measurement

The sample densities at one atmosphere pressure were obtained using an
Anton-Paar digital densitometer, accurate to 0.01%. This was not used,
however, for the polyisobutene samples, since their high viscosity made
it difficult to introduce them into the fine bore of the instrument.
Instead, density bottles were used, giving an accuracy of 2%.

The average molecular weights of the polyisobutene samples were deter-
mined using quantitative microanalysis.

(v) Viscosity Determination

(a) The Viscometer Bomb

The viscometer body (fig 3.11) was a vertically-mounted cylinder with
three pairs of windows looking across the axis, and provision for
electromagnets to be attached to the end cones. To ensure that the

- 29 -

internal diameter of the fall tube was parallel and smooth, a length of precision bore glass tubing, of internal diameter 12.00 mm, was supported within the bomb by spacers which held it vertical and away from the bomb walls. One of these spacers was glued to the fall tube and sealed to the bomb wall with an 'O' ring to prevent liquid flowing around the outside of the tube. Measurement, using a travelling microscope, of rings cut from the tubing were within the makers' quoted tolerances of ± 0.001" (25 μm) in diameter and circularity.

The end cones were designed to have concave conical interior faces so that the fall slug would centre itself on reaching the bottom one: it would then be in close proximity to the soft iron core of the cone, and so could be held in place by an external electromagnet while the viscometer was turned upside-down in readiness for the next run (fig 3.12). To overcome the problem of residual magnetism in the bobbin holding a light ball after the current had been switched off, an AC supply was used at a frequency of about 1 kHz: decreasing the voltage smoothly to zero removed any residual field. This system was found to be capable of holding balls of up to 40 g weight.

In order to hold the bomb vertical, while allowing its easy removal, inversion and replacement, a 'Dural' socket was made and bolted to the bench. This was designed as a deep cup allowing the bomb very little (< 0.1°) play, and was set up using a plumb line.

(b)   The Fall Slug

Measurement of the viscosity of the polyisobutene samples was possible using spherical steel balls as the fall slugs without exceeding the Reynold's numbers. However, in the case of the other, less viscous, samples, the ball would have to be extremely small (and so invisible

- 30 -

to the timing system), or else of a density comparable with that of the sample - leading to very large errors. Instead, for these samples, a cylindrical fall slug was used with only a small annular clearance between it and the fall tube. As shown in paragraph (2.v), the viscosity in this geometry is still simply related to the fall velocity.

In order that the slug should fall smoothly without any wobble, it is necessary that it should be self-centring in the fall tube, and that the centre of mass should be as far below the centre of action of the viscous drag as possible (ref [42]). Since the viscometer was to be used either way up, the leading and trailing ends of the slug had to be symmetrical, and there had also to be a magnetic component to hold the slug before the commencement of a run. For these reasons a composite 'jumping-bean' was made with a loose steel ball inside it (fig 3.13 (a)). At first, both ends were left open to maintain symmetry, with the ball sealing the lower hole: however, trials showed that the ball tended to vibrate, allowing liquid past, and so one end was sealed with shaped brass shim (fig 3.13 (b)). This was observed to fall smoothly and centrally even for the lowest viscosity samples. Two such slugs were made, with outside diameters of 11.5 mm and 11.9 mm. Each was polished and finished to an accuracy of ± 12 μm. Because of the thin walled construction (∿ 1 mm), concentricity of the internal and external surfaces was hard to attain: however, any variations in wall thickness were within tolerances of ± 15 μm, and a slug with the ball removed rolled freely down a smooth inclined surface. The mass distribution at the two ends of the slug is clearly not the same, and different viscometer constants were found to apply, depending on the slug orientation (open end up or down).

(c)   The Optical System

The passage of the fall slug was sensed by its interrupting light beams at the three pairs of windows. The light source was a 100 W Quartz halogen lamp, focused on to a bunch of three optic fibre cables which transferred the light to the inlet windows. Light was detected by built-in photodiodes at the exit windows, which triggered the electronics (see fig 3.11).

A detail of the window assembly is given in fig (3.14). The 3.81 mm OD float glass window was sealed using an 'O' ring since the usual window arrangement (3.2.iii (a)) presented machining difficulties when scaled down. The optic fibres were bonded to the inlet windows with cyano-acrylate adhesive to reduce reflection losses.

(d)   The Timing System

The photodiode output was amplified (with adjustable gain), and fed to a discriminator. Interruption of the beam causes a change of state of the discriminator, switching over a latching relay (fig 3.15 (a)). The slug, moving on, re-establishes the beam without affecting the (latched) relay. This happens at each pair of windows, causing the input to the relays to be switched to the first timer, then the second, and then open circuit. Provision is made for adjusting the amplifier gain and offset, resetting the system, setting the triggering to leading or trailing edge, and reversing the photodiode sequence to allow for inverting the viscometer. The input signal switched by the relays was a TTL clock pulse, switchable in half-decades between 1 Hz and 1 MHz: since each counter had a maximum of 8 decades this allowed measurement of a very wide range of fall times by adjustment of the input pulse rate. The automatic system could be left to record for days on end if necessary.

In addition to timing the rate of fall between windows, three four-decade counters (fig 3.15 (b)) were used to assess the 'dark' time for which each window was obscured. If these times were similar, it was assumed that terminal velocity had been attained by the time the slug reached the first window.

(e) Experimental Procedure

The setting-up procedure for the bomb was as follows. The fall-tube support ring, tensioning spring, end cone and 'O' ring were assembled. One pressure port was blanked off, and the other had a length of pressure tubing and a valve screwed into it. The window assemblies, complete with optic fibres and photodiodes, were bolted in place and the bomb was placed, open end uppermost, in its socket, and filled with sample using a long-needled syringe to expel trapped air. The more viscous samples were then allowed to settle before the glass fall tube was lowered into place and pushed into its seat. The ball or (filled) fall slug was introduced, allowing a dynamic test of the detection system. Care was taken always to introduce the fall-slug open end uppermost to obtain reproducible fall times.

The remainder of the bomb was assembled, and the trigger levels set by lowering the lamp voltage from 10.5 V to 8 V, and adjusting the amplifier gain and offset controls until the trigger threshold was just attained. This method of adjustment ensured that each part of the circuit triggered at the same fraction of its usual light level, eliminating individual differences in response, window transmission, etc. Although the absolute position of the slug to produce a change of state of the discriminator output will perforce change from run to run, the separations between these points will be constant.

- 33 -

A few runs were performed with the viscometer at atmospheric pressure, to find the optimum pulse frequency and to check that the slug moved freely in the fall tube - any dust or dirt causing irregular fall times - and then the bomb was pumped to the maximum pressure, and left for a few hours to reach equilibrium, and any gross drop in pressure investigated. The valve was then closed, and the pressurising system depressurised and disconnected, leaving the bomb pressurised but free to be inverted. Four or six experimental runs were performed at each pressure datum, with a thermocouple in contact with the topmost cone. A temperature variation of ± 2 °C was allowed since some runs took several days and the room temperature fluctuated. It was assumed, however, that viscosity changes due to these fluctuations would be far exceeded by those due to the pressure, and that the fluctuations would, to some extent, cancel to the mean temperature.

Once data had been collected, the bomb was reconnected and the system pumped to the original pressure. If the gauge reading changed appreciably on opening the valve, the data were rejected and the source of the leak investigated, the pressure difference due to the movement of the valve from 'shut' to 'open' being below the sensitivity of the gauges.

(vi)   Rayleigh-Brillouin Light Scattering

(a)   The Light-Scattering Apparatus

The apparatus used to obtain 90° - scattered Rayleigh - Brillouin (VV) spectra has been described elsewhere [76], and is shown diagrammatically in fig (3.16). The argon-ion laser was tuned to a wavelength of 488.6 nm and used at a power of around 300 mW (single mode), with the light polarised vertically relative to the scattering plane. The Fabry-Perot etalon was scanned piezo-electrically, and three further piezo-

- 34 -

electric stacks, together with three micrometer screws, used for adjust-
ment of the plates. Control of the scanning system is shown in
fig (3.17).

(b) The Scattering Bomb

The bomb is shown in fig (3.18). The cones sealing the ports were of
the same design as for the refractive index bomb, though the windows used
were of 'spectrosil B' fused silica. Since it was found impractical to
attempt to fill the bomb, separator, and tubing with the filtered sample
without some dust getting in, a cell containing the filtered sample was
used inside the bomb, containing the volume 'seen' by the detection
system as the scattering volume. So long as the sample in the cell is
rigorously dust-free, it is unnecessary to ensure absolute cleanliness
of the rest of the fluid in the system.

(c) The Sample Cell

The use of a sample cell within the bomb poses the problems that it
must be held rigidly within the sample volume without being strained,
and must have some mechanism to equalise the pressure within and without
the cell, while not allowing contamination of the sample.   This must
be able to cope with the 13% change in volume observed for C_8 at 240 M Pa.
The method used is shown in fig (3.19): a truncated glass syringe was
glued to a 1 cm cubical quartz sample cell. Ideally, the two parts
would be fused together: this was not feasible since the cell was of
silica and the syringe of borosilicate pyrex. Cyanoacrylate glue was
again found to be satisfactory, though generally coming apart when the
cell was cleaned after use. The cell allowed for a 40% volume change
without any extra stress.

The cleaned cell assembly was filled with filtered sample and the cut-
off end of the syringe plunger pushed in to seal the cell. By pushing

- 35 -

and rotating it was possible to expel any air bubbles and force the plunger in flush, though removal after use presented some difficulty.

The effect of parasitic scattering and stray light within the sample volume is greatly to increase the unshifted central peak height. In order to obtain spectra it is therefore imperative to minimise reflections within the bomb, and the cell holder (fig 3.20) was designed with this in view, while holding the cell rigidly in position without strain. The scattering volume was visible through the slot to within a short distance from the cell walls, thus eliminating flare from the walls. The cell was held in place in the holder by a light spring wrapped around the barrel, bearing on the top of the cell, and the cell holder screwed on to the end of the top cone so that the centre of the cell was level with the centre of the bomb windows.

The bomb was mounted on a platform which was clamped to the optical bench: the height and orientation were adjustable by means of screws.

(d)   Experimental Procedure

(i)   Alignment

The bomb was filled with the low molecular weight polyisobutene, HO7, as a pressure medium, and a sample cell containing a colloidal suspension placed in the cell holder. By looking through the incident window towards a light source the other side of the bomb, it was possible to check the orientation of the cell as the retaining bolt was tightened down. The bomb was then placed on the platform and slid into position on the optical bench. It was roughly adjusted to bring the incident beam normal to the centre of the input window, and the 90° exit window central and square to the detection system.

Because the amount of unshifted light scattered by the colloidal sample is large, it was now possible to adjust the alignment by observing the scattering volume using a telescope placed behind the etalon. To focus the image of the scattering volume at the etalon it was found necessary slightly to move the lenses L_1 and L_2 (fig 3.16): however, pressurising the bomb (and so changing the apparent depth of the scattering volume within the bomb) did not affect the focus significantly. It was however found necessary to adjust Lens L_3 as the pressure changed, to focus the light on to the photomultiplier tube aperture. This is because the incident window tended to 'settle' slightly, deviating the beam by a small amount, and so moving the scattering volume up or down a little.

Having positioned the bomb, the finesse of the etalon was tuned to a maximum by setting the clock on a fast rate and adjusting the tilt of the non-driven mirror by use of the three piezo-electric stacks. The voltage to these stacks was varied to give sharp, narrow peaks for the instrumental function. The lens L_3 was then adjusted in the vertical plane to maximise these peaks.

After this, while obtaining spectra, it was necessary to tune the finesse slightly before each experimental run. Rather than removing the bomb to do this, a sample cell containing colloidal sample and illuminated by the laser using a bunch of optical fibres, was placed just before L_1. The plates could then be made parallel by observation of the instrumental function in the usual way, without disturbing the sample or bomb. The finesse, measured from this method of illumination was rather lower than the true finesse, since the scattering cell was not quite in focus,

- 37 -

and there was no pinhole immediately after it. However, the
finesse obtained in this way would be when the plates were
parallel.

The free spectral range was computed from measurement of the
plate spacing (of the order of 1 cm) using a travelling micro-
scope, and the finesse measured using a colloidal sample in place
of the bomb each time that the FSR was changed.

(ii) Procedure for Obtaining Spectra

A clean sample cell containing filtered sample was placed in the
cell holder which was placed in the bomb. The bomb was put in
position and the pressure increased to the maximum to which the
sample was to be subjected.

After the system had been left to reach equilibrium, the plates
were adjusted using the colloid and optic fibre, as outlined
above, and then with high photon counting system gain, and fast
clock speed, the lens L_3 was adjusted to maximise the peak
heights observed. The gain and clock speed were then decreased
to give a collecting time of 15 - 20 minutes, and spectra were
obtained. Each spectrum, containing 1024 data points covering
three orders, was output from the transient recorder on to
paper tape. The pressure was decreased and the process repeated.
Three or four spectra were obtained at each pressure.

The temperature was monitored throughout, and the plate spacing
measured after each spectrum had been obtained.

(iii) Liquids Investigated

Initially, it was hoped to investigate all the liquids looked at
in the other experiments. However, various problems were
encountered.

and there was no pinhole immediately after it. However, the finesse obtained in this way would be when the plates were parallel.

The free spectral range was computed from measurement of the plate spacing (of the order of 1 cm) using a travelling microscope, and the finesse measured using a colloidal sample in place of the bomb each time that the FSR was changed.

(ii) Procedure for Obtaining Spectra

A clean sample cell containing filtered sample was placed in the cell holder which was placed in the bomb. The bomb was put in position and the pressure increased to the maximum to which the sample was to be subjected.

After the system had been left to reach equilibrium, the plates were adjusted using the colloid and optic fibre, as outlined above, and then with high photon counting system gain, and fast clock speed, the lens L_3 was adjusted to maximise the peak heights observed. The gain and clock speed were then decreased to give a collecting time of 15 - 20 minutes, and spectra were obtained. Each spectrum, containing 1024 data points covering three orders, was output from the transient recorder on to paper tape. The pressure was decreased and the process repeated. Three or four spectra were obtained at each pressure.

The temperature was monitored throughout, and the plate spacing measured after each spectrum had been obtained.

(iii) Liquids Investigated

Initially, it was hoped to investigate all the liquids looked at in the other experiments. However, various problems were encountered.

- 38 -

(1)   The PEG and PPG samples were found to attack rapidly the cyanoacrylate bond between the quartz sample cell and the pyrex glass syringe body. Although epoxy resins were tried, it was found that their large shrinkage on curing caused stress in the sample cell leading to breakage under pressure.

(2)   Problems of filtering arose for the higher viscosity (PIB) samples. Even in a dust-free sample, however, the central Rayleigh peak was found to swamp the Brillouin peaks. This follows from an increase in the Landau-Placzeck ratio for a relaxing liquid.

In view of this, and because of a failure in the photon counting system, spectra were recorded only for the n-Alkane samples, for iso-octane, and for the PIB samples Hyvis 04, 07, and 5.

TABLE 3.1

ALKANES   Data for atmospheric pressure at 20 $^{\circ}$C

General formula $H-(CH_2)_n-H$

Sample	n	R.I. 632.8 nm	M_n	Density,Kgm^{-3}
Iso octane	8	1.39061	114.23	689.6
n - Octane	8	1.39594	114.23	694.9
n - Decane	10	1.41228	142.29	723.9
n - Undecane	11	1.41659	156.31	734.9
n - Dodecane	12	1.41957	170.34	745.3
n - Tridecane	13	1.42526	184.37	761.5
n - Pentadecane	15	1.43050	212.42	765.6

TABLE 3.2

POLYISOBUTENES   Data for atmospheric pressure at 20 $^{\circ}$C

General formula $Me-(CH_2CMe_2)_n-C\,{}^{=CH_2}_{-Me_2}$

Sample	n	R.I. 632.8 nm	M_n	Density,Kgm^{-3}
H 04	~6	1.46608	342	777.8
H 07	~8	1.47615	460	793.5
H 5	~14	1.48995	758	830.5
H 30	~22	1.49676	1318	852.2
H 200	~43	1.50209	2469	862

TABLE 3.3

POLYETHYLENE GLYCOLS data for atmospheric pressure at 20 $^{\circ}$C

General formula HO-$(CH_2CH_2O)_n$-H

Sample	n	R.I. 632.8 nm	M_n	Density,Kg m^{-3}
Monomer	1	1.43048	62.07	1109.0
Trimer	3	1.45062	150.17	1118.9
PEG 300	-6	1.46452	300	1121.7
PEG 400	-8	1.46496	400	1123.4

TABLE 3.4

POLYPROPYLENE GLYCOLS data for atmospheric pressure at 20 $^{\circ}$C

General formula HO-$(CH_2CHMeO)_n$-H

Sample	n	R.I. 632.8 nm	M_n	Density,Kg m^{-3}
Monomer	1	1.42721	76.10	1032.2
Dimer	2	1.43870	134.18	1022.4
PPG 425	-7	1.44649	440	1007.4
PPG 1025	-17	1.44862	1055	1002.3
PPG 2025	-37	1.44936	2156	999.6

Metering valve

Separator.

Pump handle.

Reservoir.

To bomb.

Pump.

Standard gauge. (0—1600 bar)

Gauge. (0-70,000 Psi)

Isolating valve.

Fig. 3.1   The pressurising system.

60° inclusive angle.

59° inclusive angle.

Nut.

$\frac{1}{4}'' \times \frac{1}{16}''$ tubing.

L.H. Threaded collar.
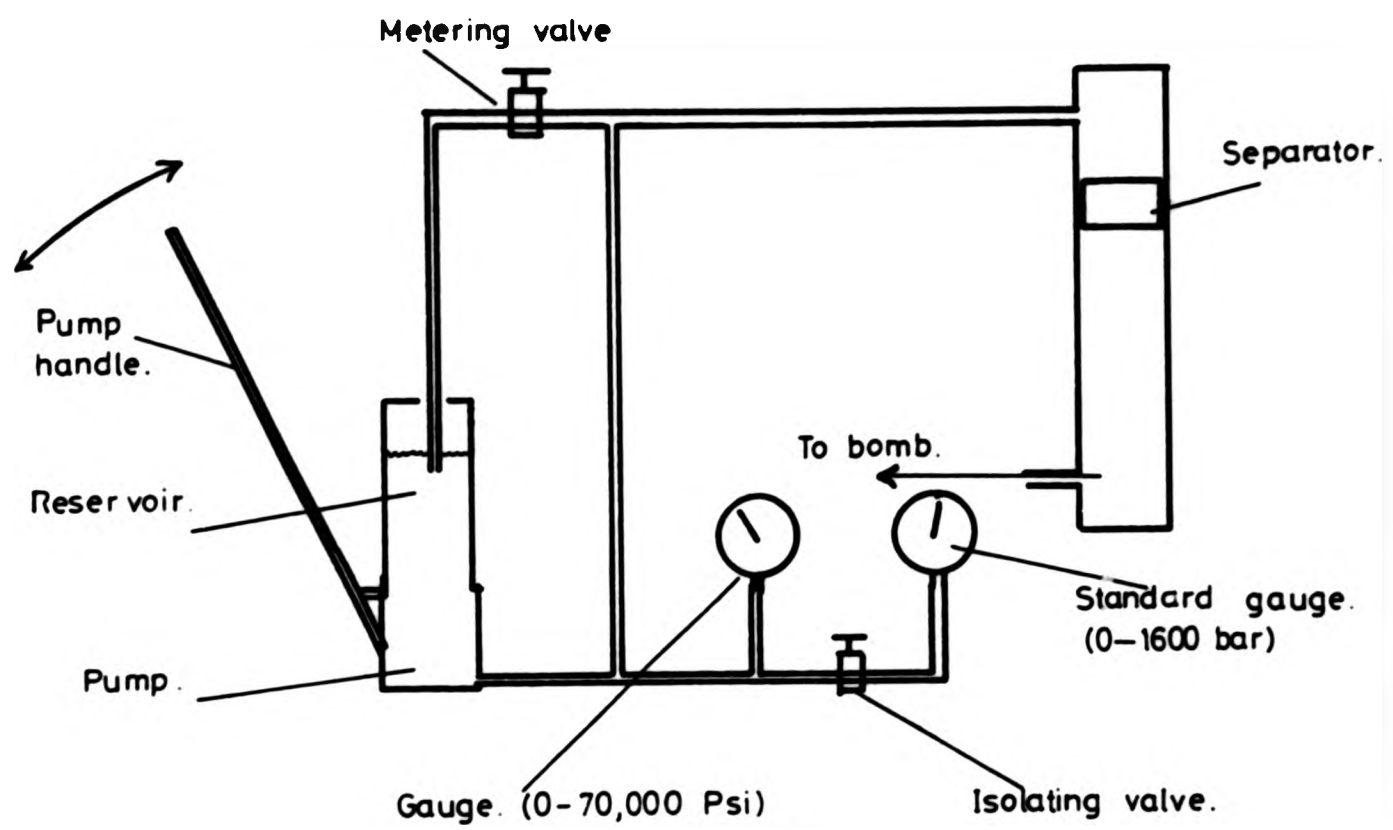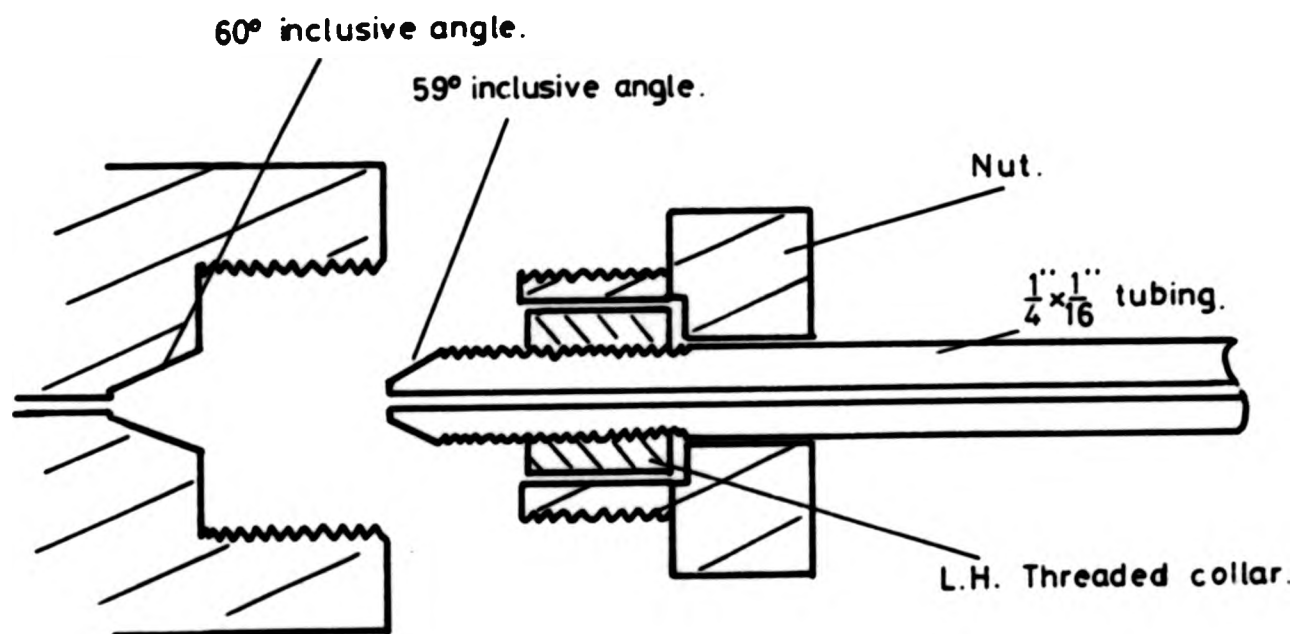
Fig. 3.2   Detail of pressure connection.
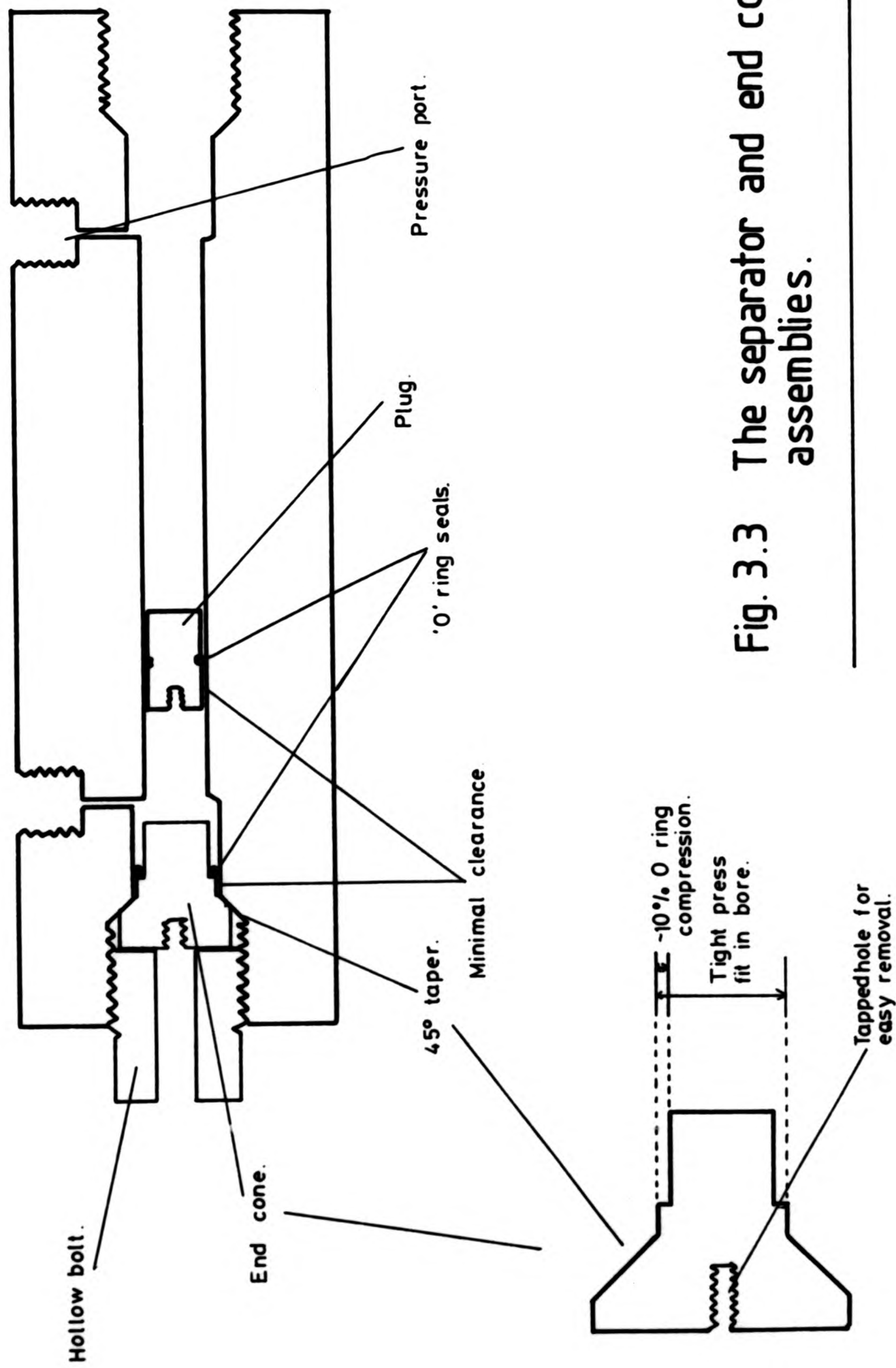
Fig. 3.3   The separator and end cone assemblies.

Labels on figure:
- Pressure port.
- Plug.
- 'O' ring seals.
- Minimal clearance
- 45° taper.
- Hollow bolt.
- End cone.
- ~10% O ring compression.
- Tight press fit in bore.
- Tapped hole for easy removal.

- 43 -

To meter.

Thermocouple.

pressure tubing brazed to end cone.

Steel ball
to seal

Float glass window.   Interferometer (fig. 3.5)

Cyanoacrylate
glue film.

Fig. 3.4   The refractive index bomb

- 44 -

Spring.

Support ring.

Mirrors.

12 B.A.
Adjusting screws

Steel spacer.
(other two screws
have springs.)

Mirror.

Fig 3.5   The interferometer.

Rigid 'V'- block
mounting.

Bomb.

Lens.

Iris & photodiode.

To amplifier.

He-Ne laser.

Optical bench.
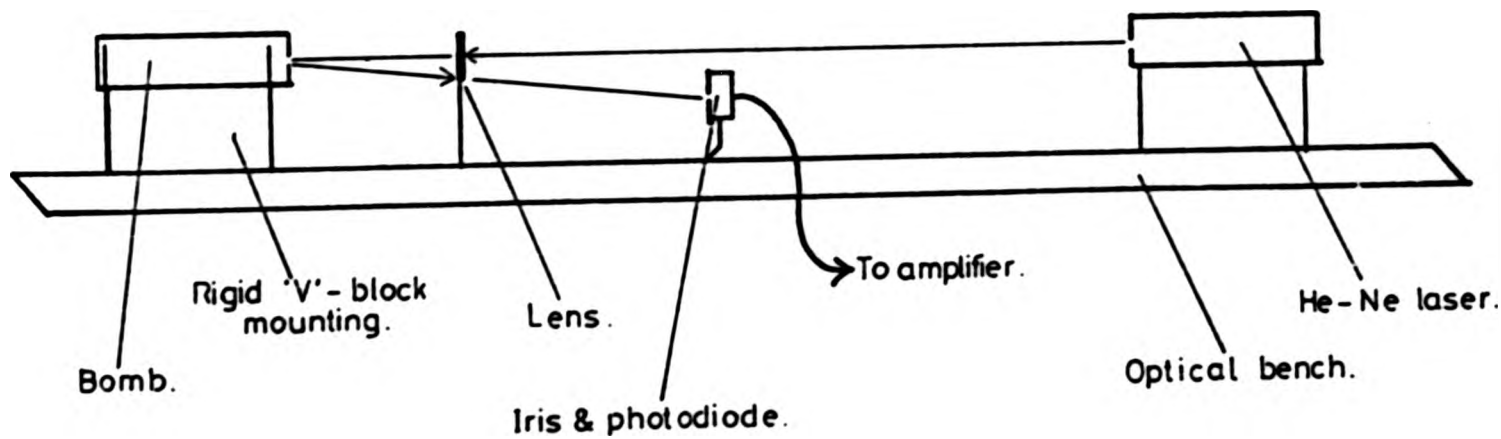
Fig. 3.6   The experimental system

(refractive index & compressibility).
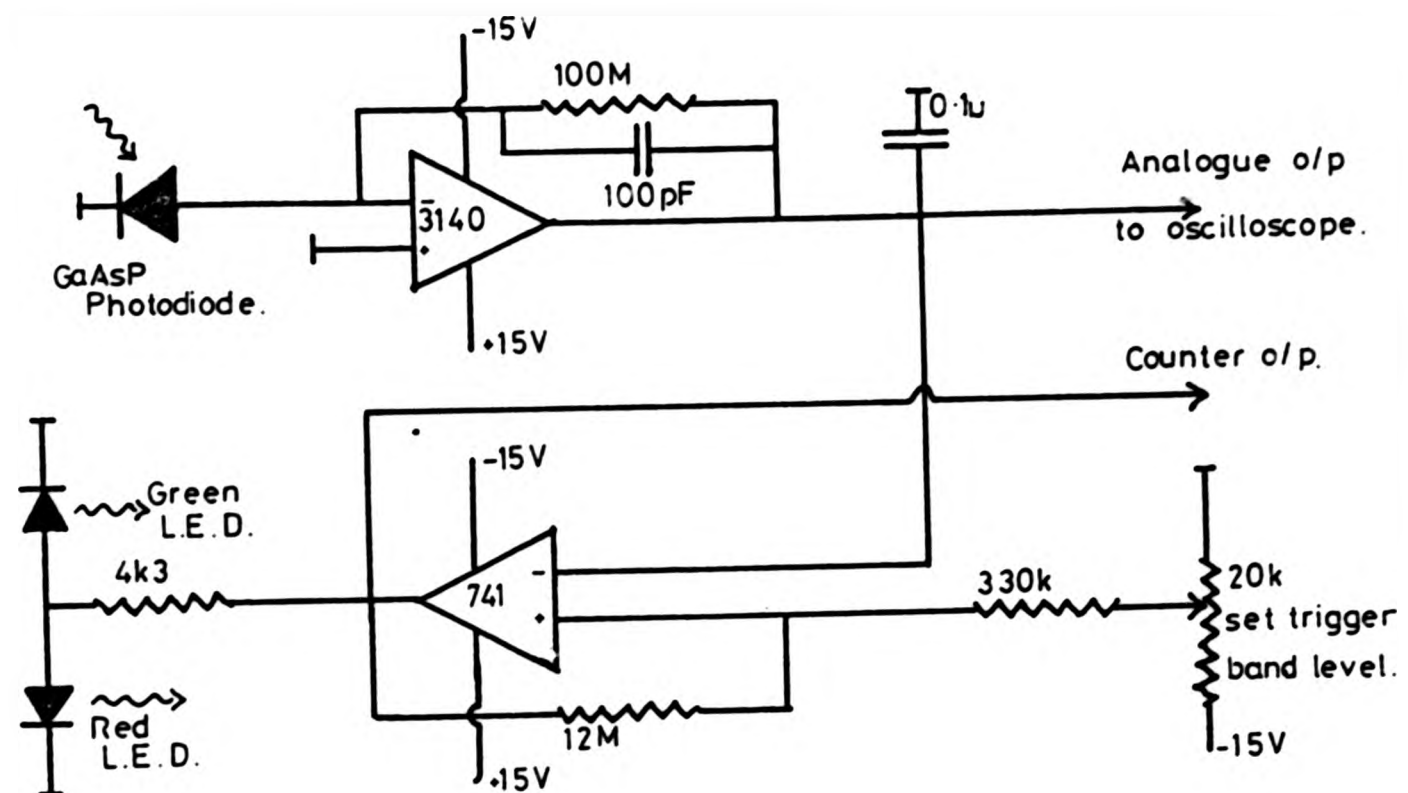
Fig 3.7　Photodiode & bistable amplifiers.
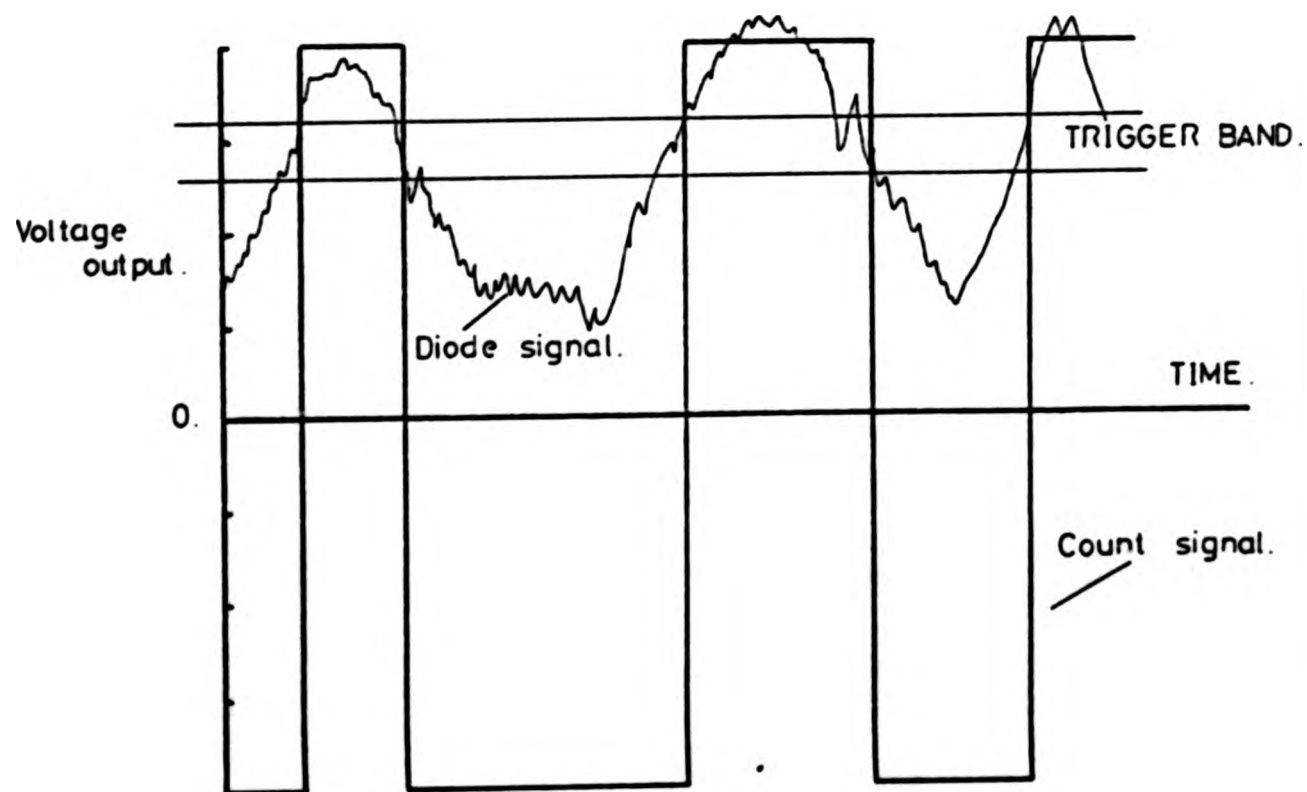
Fig. 3.8　Amplifier outputs.
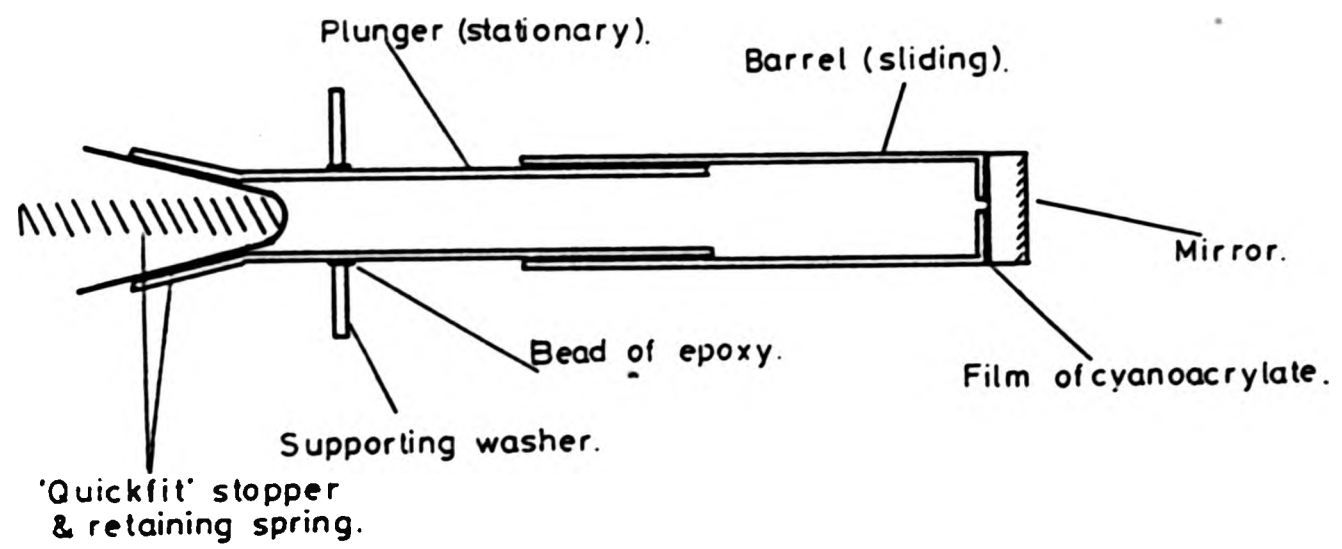
Fig 3.9   The glass piezometer.
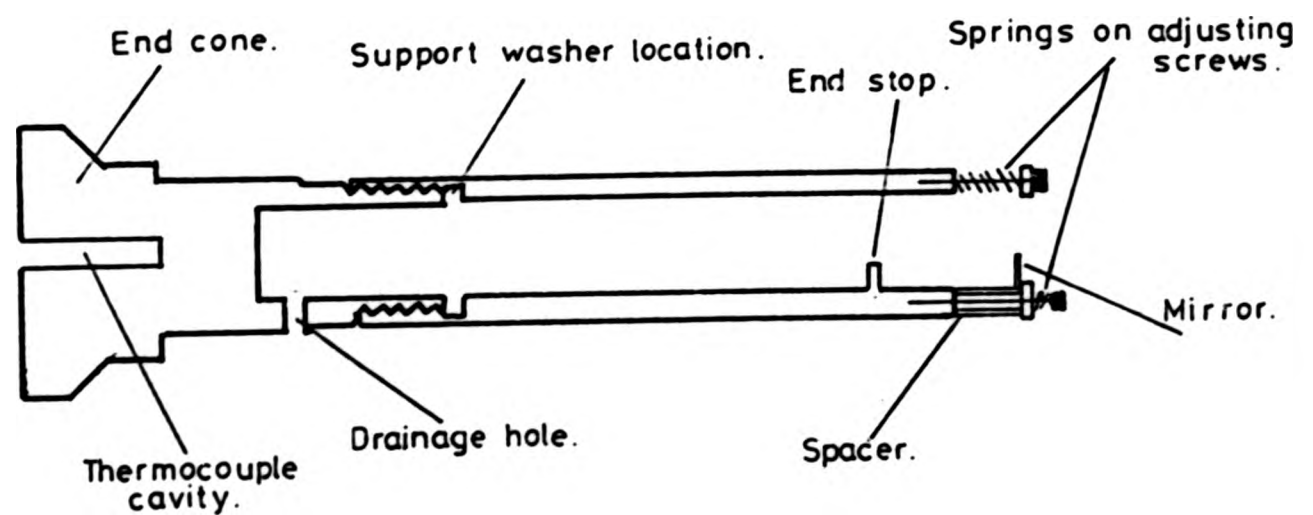
Fig 3.10   Piezometer and front mirror support.

Support ring glued to fall tube.

'O' ring.

Window ports.

12mm. i.d. precision bore tube.

Support ring.

Spring.

End cone. (fig. 3.12)

Electromagnet. (fig. 3.12)
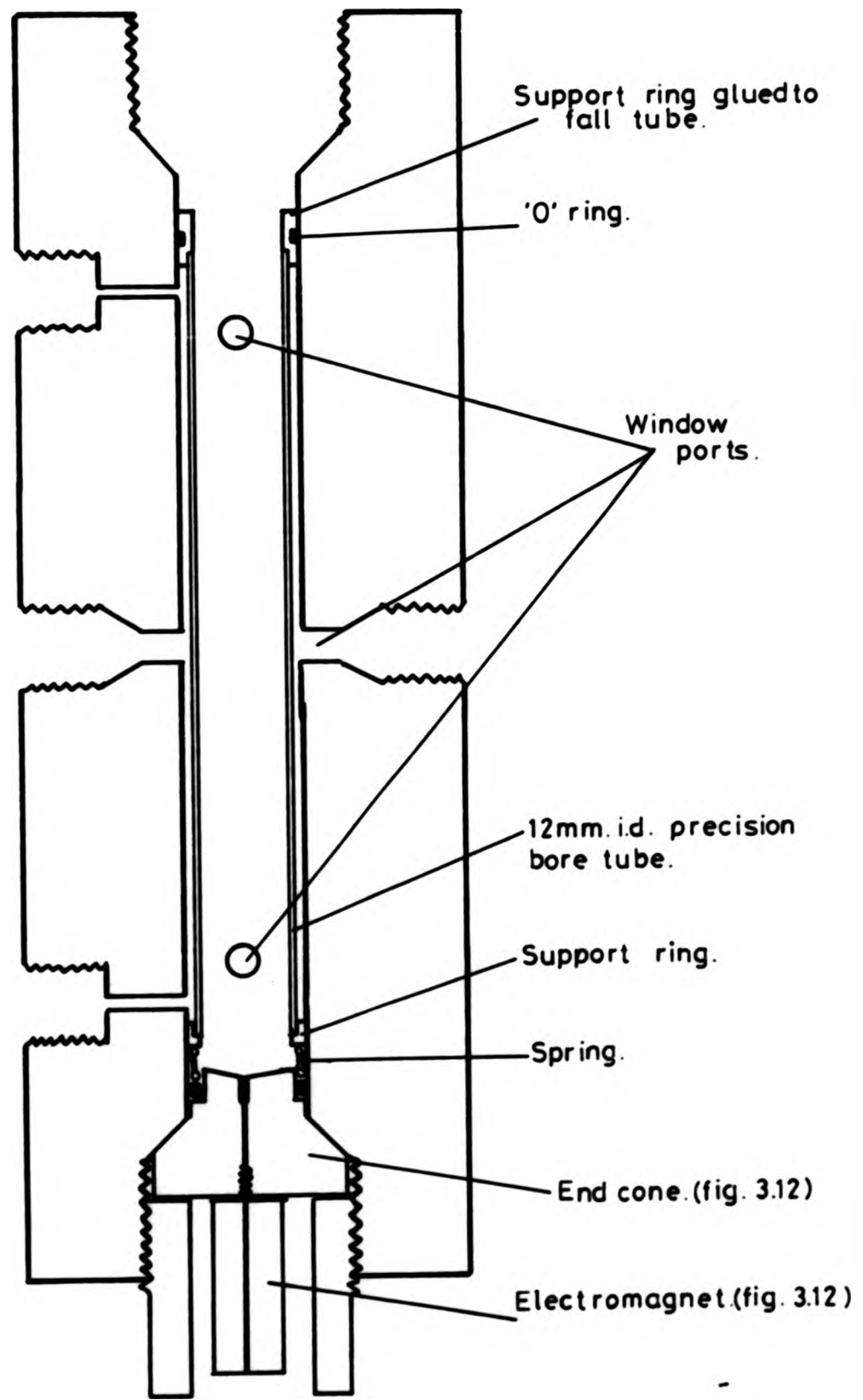
Fig 3.11   The viscometer bomb.

Electromagnet

Soft iron core brazed into cone.

Locating thread.

Stainless steel end cone.
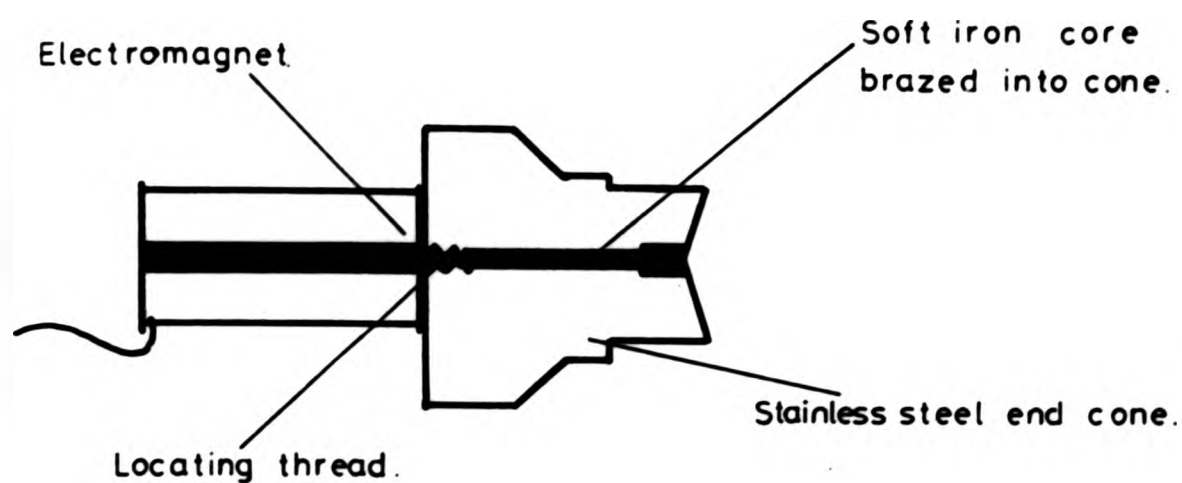
Fig. 3.12 End cone with magnetic bobbin.

Brass shell.

Overlap joint, soldered & buffed.

Captive steel ball.

Shaped end cap, soldered & buffed.
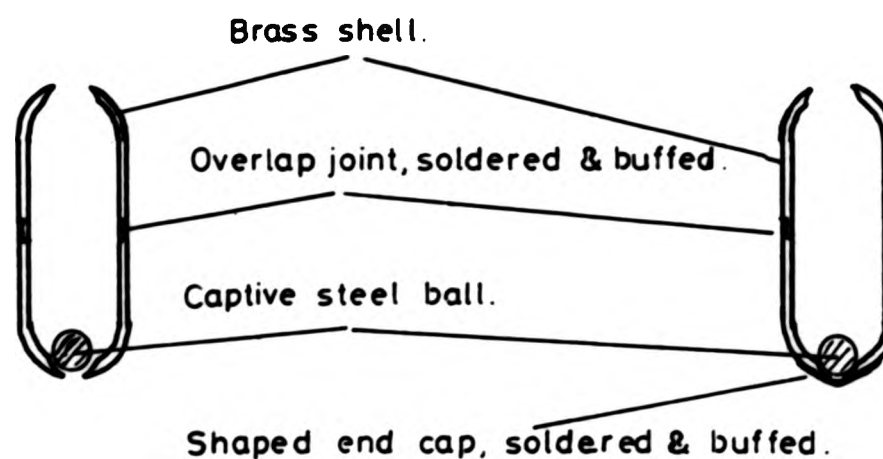
Fig. 3.13 (a) & (b) The 'jumping bean' fall slug.

Bomb body.

Fall tube.

Window.

1mm. hole.

Photodiode or optic fibre.

'O' rings.

Nut.
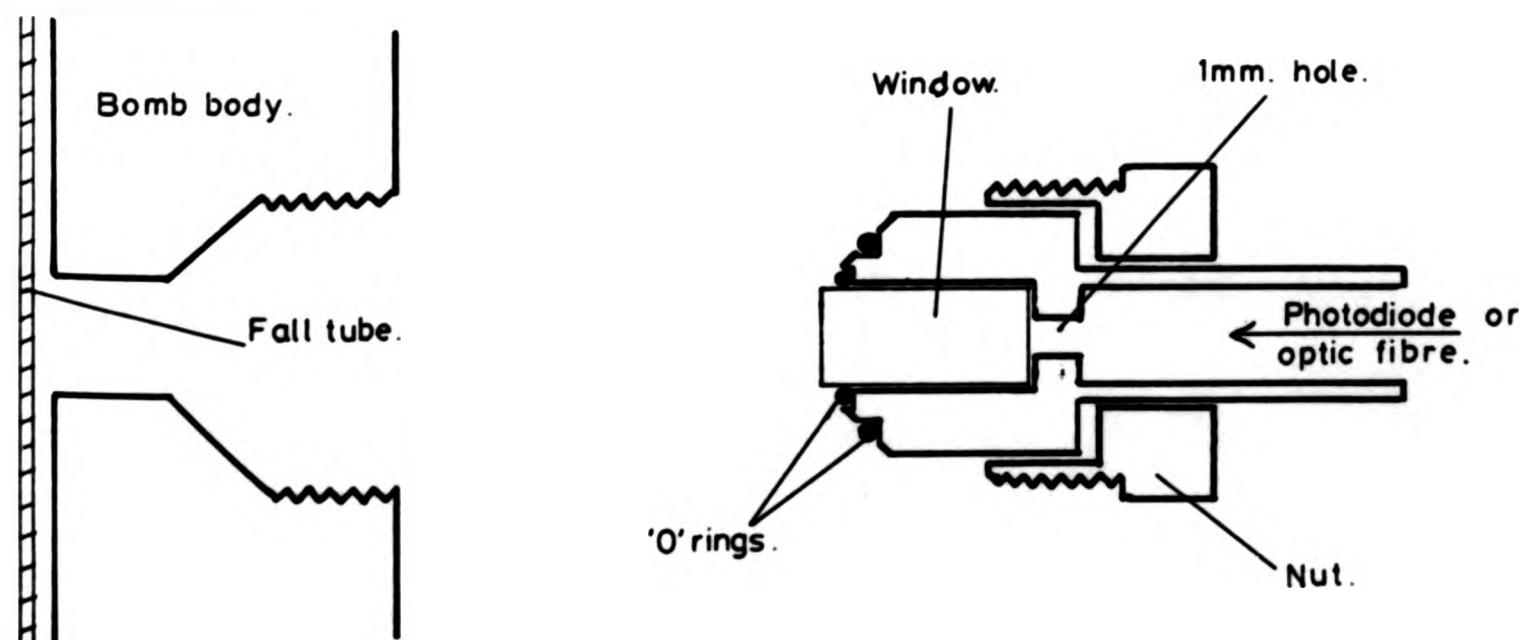
Fig. 3.14 Viscometer window assembly.
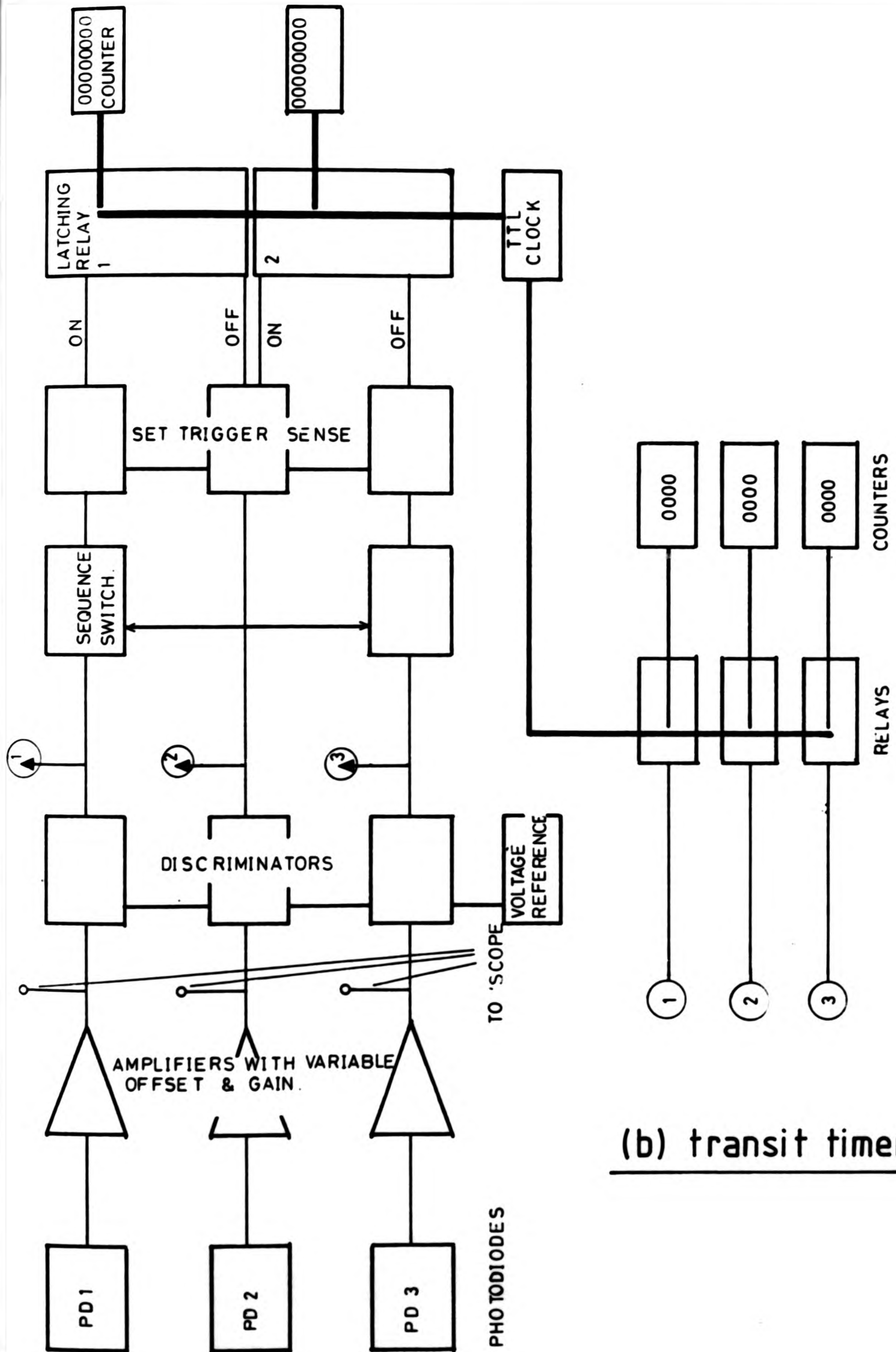
Fig. 3.15 a & b.   Viscometer timers.

Argon - ion laser
488·6 nm , ~ 300 mW single mode.

Light - proof enclosure.

GT - Polariser. (V.)

I - Iris.

L - Lens.

GT L₀ I₀ Bomb. Attenuator

GT Bulkhead.
L₁   I₁
I₂
L₂
I₃
I₄

Fabry - Perot
etalon.

L₃

Pinhole.
P.M.T.
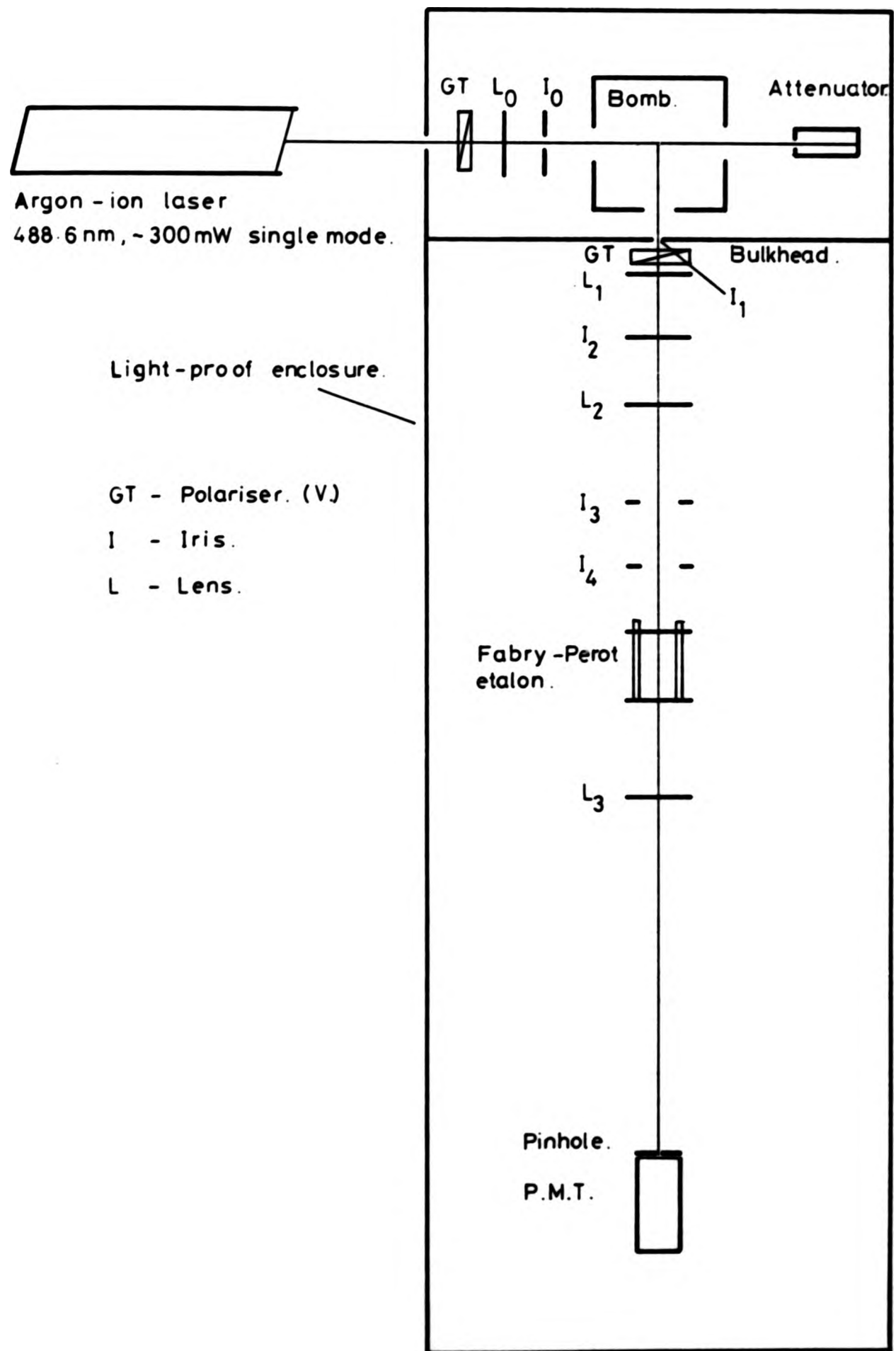
Fig. 3.16   The light-scattering apparatus.
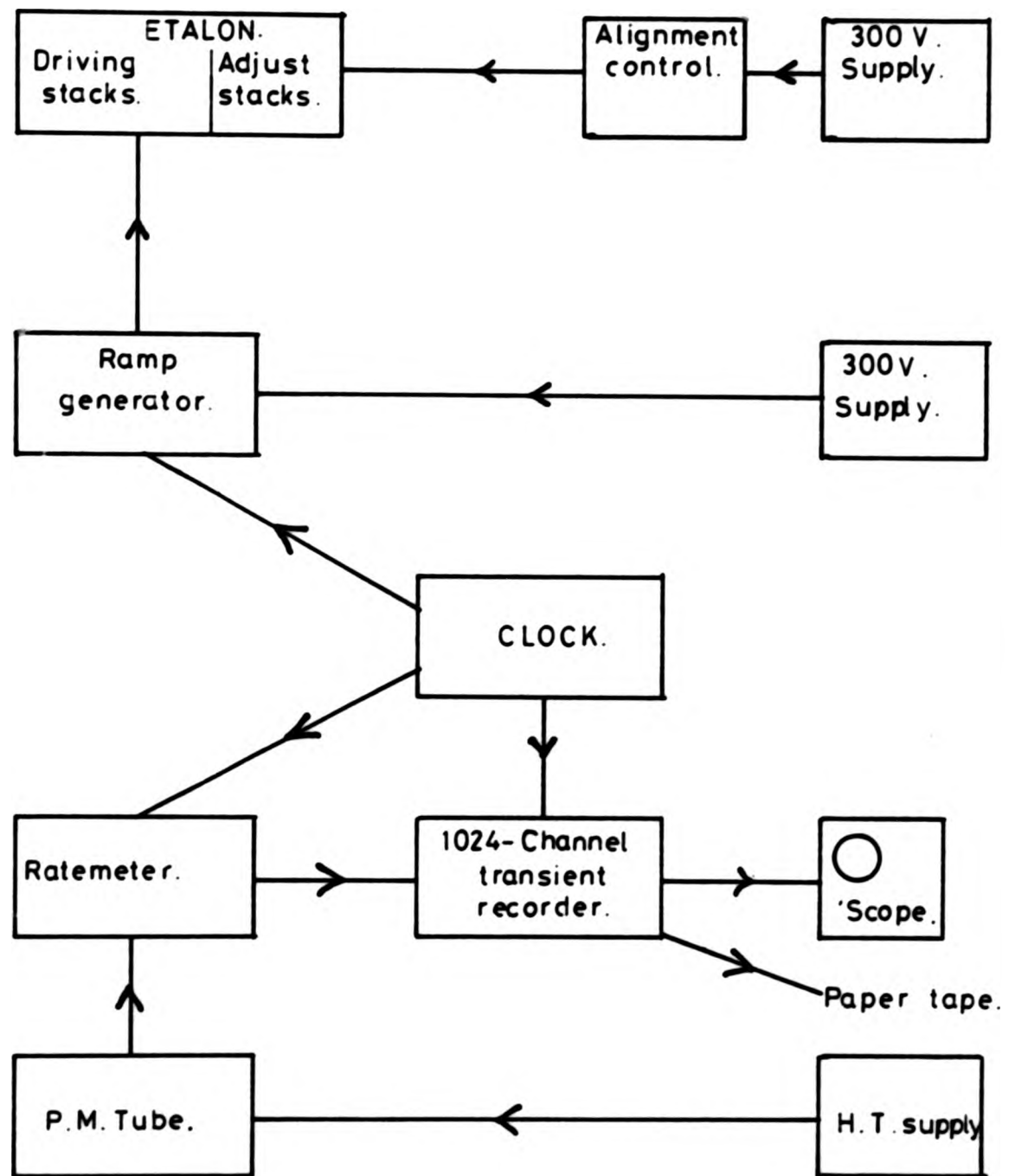
Fig. 3.17   Schematic of data collection.

Unscattered light.

Pressure port.

90° Scattered light.

Cell holder.

O' rings.

Sample cell.

Spectrosil B Windows.

Incident laser light.
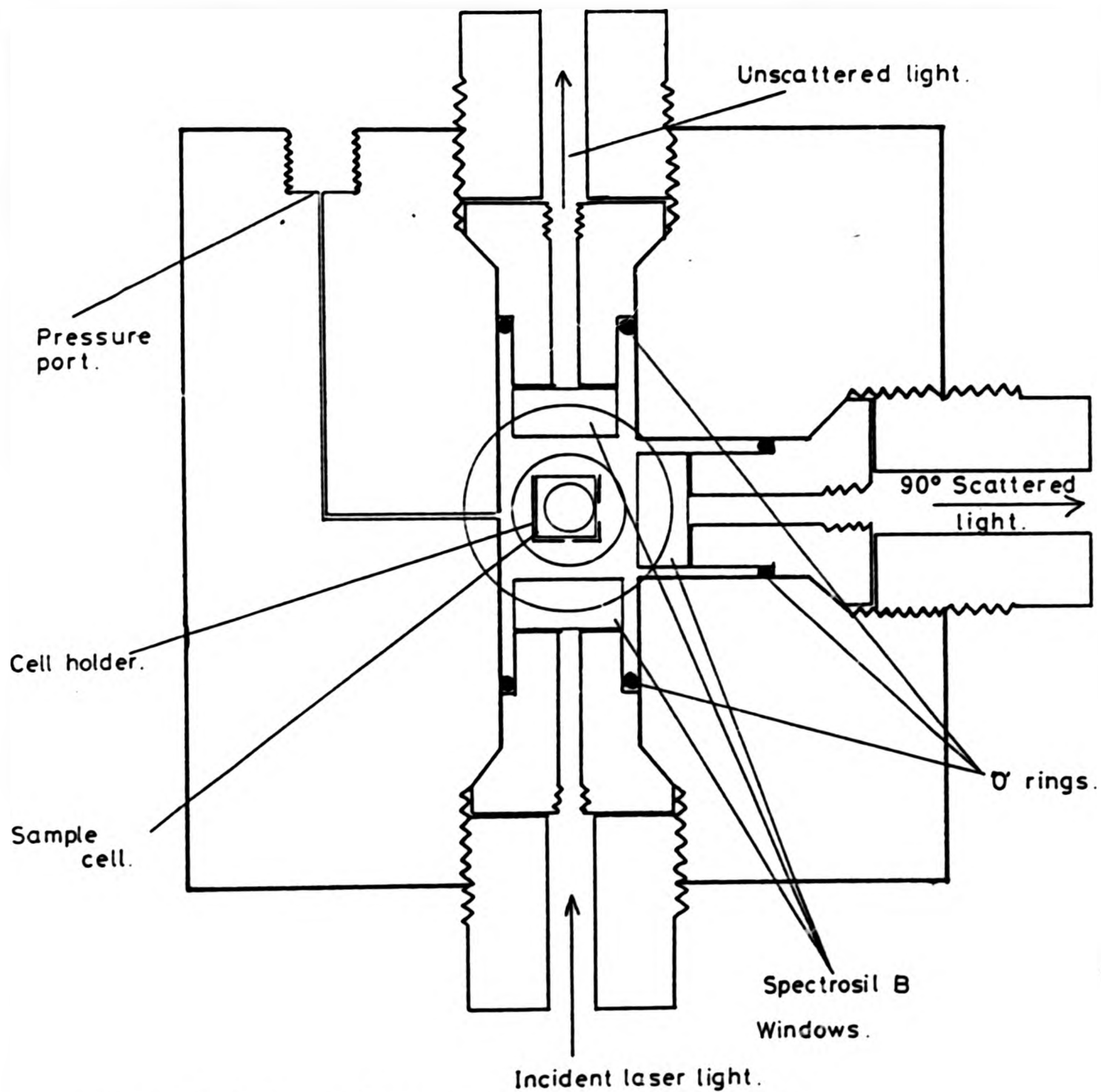
Fig. 3.18   The scattering bomb.

Syringe plunger.

5mm. hole.

Syringe barrel glued to cell.

1cc. silica cell.
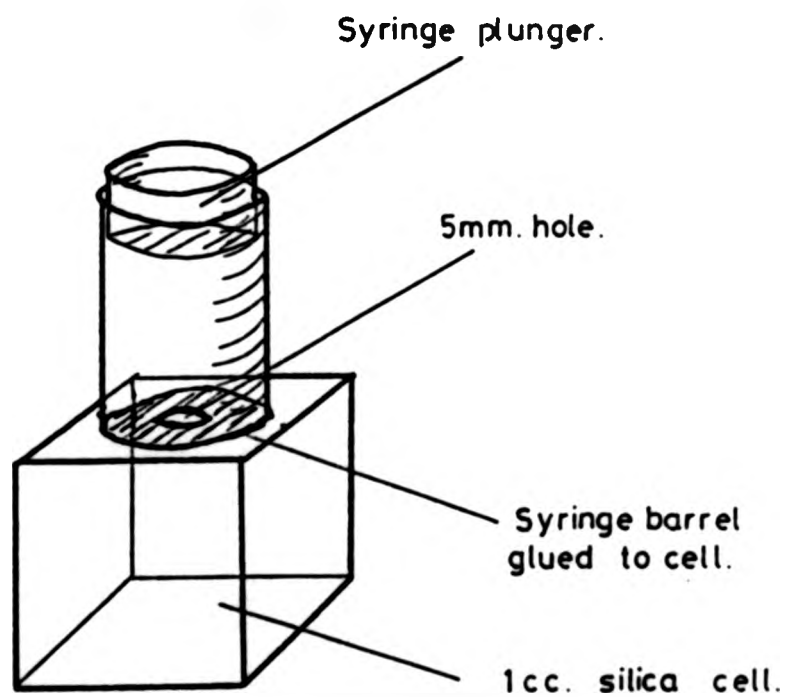
Fig. 3.19   Variable volume sample cell.

Top provides location
for cell – retaining
spring.

Rear baffle.

To laser.

Incident window.

Exit window.

To detecting
optics.

Retaining lip.

Supporting
end cone.
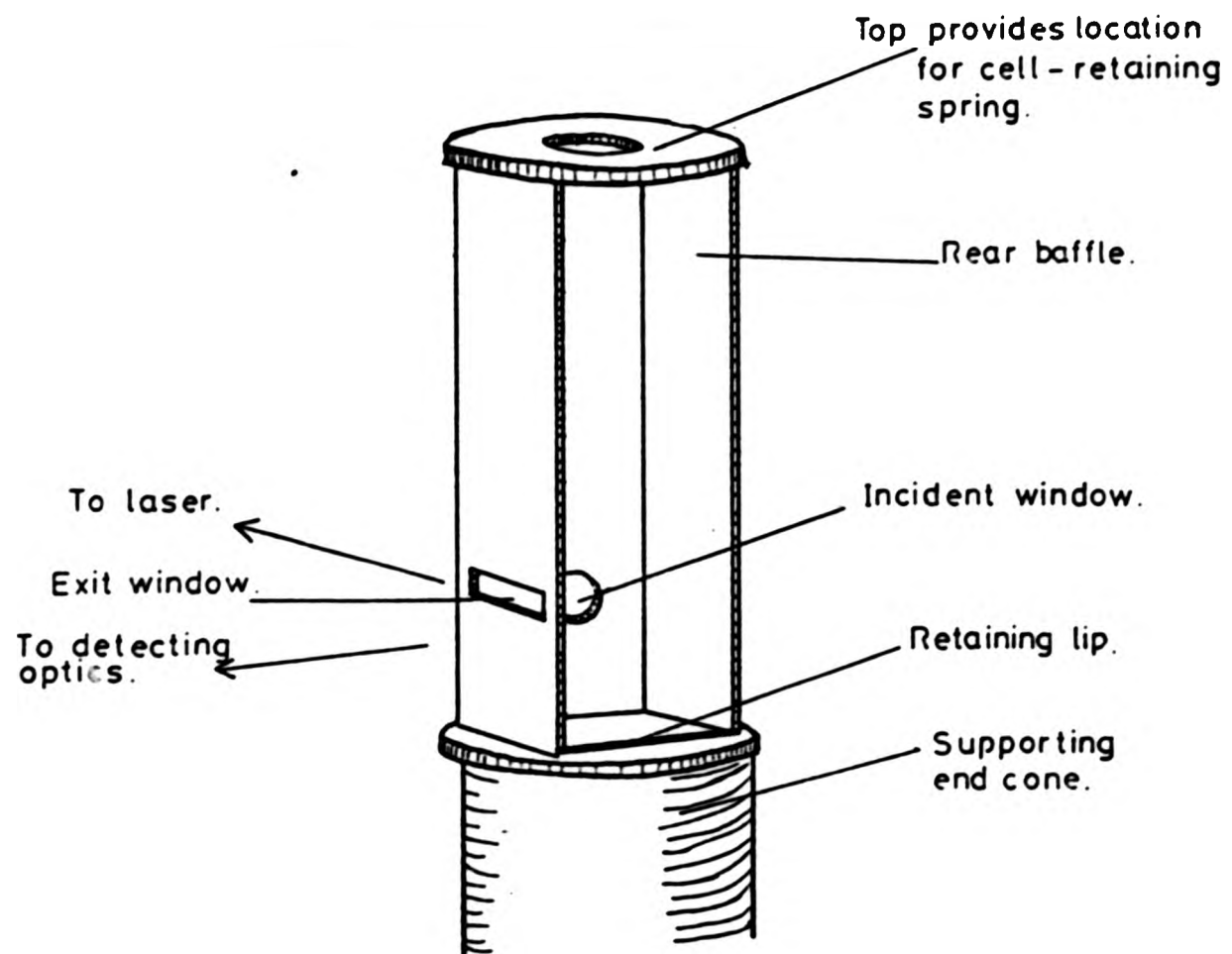
Fig. 3.20   The cell holder.

CHAPTER 4

ANALYSIS AND PRESENTATION OF DATA

*'I am at a loss to give a distinct idea of the nature of
this liquid, and cannot do so without many words'*

E A Poe: "Narrative of A G Pym of
Nantucket"

CHAPTER 4 ANALYSIS AND PRESENTATION OF DATA

1 Compression of Components in a Hydrostatic Field

(i)   General

Three of the experimental systems described in Chapter 3 depend on
knowledge of the dimensions of components which are compressed in a
hydrostatic pressure field. While it is reasonable to state that, for
example, the compression of the glass in the piezometer will be much
less than that of the fluid under test, it is nonetheless necessary to
quantify this statement. We shall assume that the materials are iso-
tropic, that no visco-elastic changes occur, and that the change in
volume is given to a sufficient degree of accuracy by the bulk modulus,
K (Vedam et al [31] report linearity of $\Delta V/V_o$ vs P for vitreous silica
up to 4.5 k bar).

Consider a cube of isotropic material subject to a hydrostatic pressure,
P. The bulk modulus is defined in terms of the change in volume:

$$\frac{\Delta V}{V} = \frac{P}{K} \tag{4.1}$$

If the linear dimensions of the cube are given by X, Y, Z, which
decrease to $X - \Delta X$, $Y - \Delta Y$ and $Z - \Delta Z$ (fig 4.1), at pressure P, then
the change in volume is given by

$$\Delta V = XYZ - (X - \Delta X)(Y - \Delta Y)(Z - \Delta Z)$$

since the material is isotropic,

$$\frac{\Delta X}{X} = \frac{\Delta Y}{Y} = \frac{\Delta Z}{Z} = C$$

$$\frac{\Delta V}{V} = 3C - 3C^2 + C^3 = \frac{P}{K} \qquad (4.2)$$

$\frac{P}{K}$ is of the order of 10^{-3} or less, and so we may neglect 2nd and higher orders in C, giving

$$C \approx \frac{P}{3K} \qquad (4.3)$$

where C is the fractional compression of an arbitrary linear dimension.

Values of bulk moduli of the critical component materials used in the various bombs are given in table 4.1.

(ii)   Applications of Compression Calculation to Bomb Components

(a)   Refractive Index

The dimensions of the steel spacer and the glass mirror are shown in fig 4.2a. To find Δt, the change in path length due to compression of the components, we require $\Delta l_g - \Delta l_s$ as a function of pressure. Writing

$\begin{cases} K_s = \text{bulk modulus of steel} \\ K_g = \text{bulk modulus of glass} \end{cases}$

$$\Delta t = \frac{Pl_g}{3K_g} - \frac{Pl_s}{3K_s} = \frac{P}{3} \left(\frac{l_g}{K_g} - \frac{l_s}{K_s} \right) \qquad (4.4)$$

Thus for the values given in fig 4.2a and table 4.1, the maximum value of Δt, at 250 M Pa, is 7.7×10^{-7}m, or of the order of one fringe shift.

TABLE 4.1 (after ref [79])

Material	K (GN/m^2)	Function in Bomb	C Max(%)
Stainless Steel	166.0	Bomb body. Mirror mounts and spacers.	0.050
Glass (Pyrex)	36.9	Piezometer body. Viscometer fall tube. Refractometer mirrors.	0.226
Brass	111.8	Viscometer slug body.	0.075
Steel	165.2	Viscometer balls.	0.050

(b) Density Measurement

The change in mirror spacing due to compressional effects in the apparatus will be given by: (fig 4.2b).

$$\Delta t = \Delta t_1 + \Delta t_2 - \Delta t_3 + \Delta t_4$$

where Δt_4 is produced by the increase in sample length Δl necessary to maintain constant volume V as a radial compression of the syringe decreases the sample cross-section. The dimensions of the system used are:

plunger

l_2 = 31.00 mm

d_1 = internal diameter = 3.00 mm

barrel

l_4 = 31.00 mm

d_2 = 6.48 mm

total length of barrel and plunger = l_5 $\sim$ 50 mm.

- 58 -

$$V = \frac{\pi}{4} \left(l_2 d_1{}^2 + (l_5 - l_2) d_2{}^2 \right)$$

if $d \rightarrow d - \Delta d$, and noting that Δl_1 is already covered in Δt_2:

$$\rightarrow \Delta l_5 = l_2 - l_5 + \frac{\left(l_2 (d_1{}^2 - d_2{}^2 - (d_1 - \Delta d_1)^2 + l_5 d_2{}^2 \right)}{(d_2 - \Delta d_2)^2} \qquad (4.5)$$

This gives a maximum value of Δl_5 (at P = 250 M Pa) of 3.4×10^{-5} m.

Thus $\Delta t_{tot}(\text{max}) = 1.8 \times 10^{-5}$ m, which is of the order of 30 wavelengths of the red laser light used.

(c) Compression Effects in the Viscometer

Whether a steel ball or a composite fall slug is used in the viscometer, the radius will decrease with pressure as predicted by equation 4.3. Similarly, the glass fall tube will contract, and in general, the gap will lessen. Writing subscript g for glass, and m for metal (steel or brass, for the ball or slug), then the radius of each component will become:

$$\begin{cases} R_g(P) = R_g(O) \left(1 - \dfrac{P}{3K_g} \right) \\[3mm] R_m(P) = R_m(O) \left(1 - \dfrac{P}{3K_m} \right) \end{cases} \qquad (4.6)$$

These effects were included in the programs used to compute the quantities being measured.

2 Analysis of Experimental Data

(i) Refractive Index Data

In the measurement of refractive index, the movement of interferance fringes was observed as the pressure, and hence the refractive index

of the medium between the mirrors, decreased. For a refractive index
change Δn measured at wavelength λ, due to a pressure change Δp, Δf
fringes will move across the detector, where

$$\Delta f = \frac{2 \Delta n \bar{t}}{\lambda}$$

where $\bar{t}$ is the average mirror spacing, which may be computed from (4.4).
In addition, $\bar{t}$ will be affected by temperature, but since all the
experiments were performed at 20 ± 2 °C, this variation was negligible.
A computer program was written to give average values of Δn for each
pressure datum and the results were fitted, using a least-squares
routine, to a range of polynomials in pressure. On the basis of the
variance of fit, a cubic polynomial was found to describe the data
adequately. The data are plotted as Δn against pressure in figs (4.3 -
4.7), and the fitted coefficients giving absolute refractive index at
λ = 632.8 nm for pressure in M Pa, in table (4.2).

(ii)   Density Data

In the case of the measurements of volume change with pressure, there
will be two main contributions to the number of fringes observed to
pass the detector for a given pressure interval: those due to move-
ment of the mirror (ie due to sample volume change and compressional
effects in the piezometer and support) and those due to variation in
refractive index of the medium between the mirrors. The number of
fringes counted will be an integrated value comprising these two
mechanisms.

Consider the system starting at one atmosphere. The mirror separation
is defined by the spacer and the rear mirror stop, to be t_o = 5.203 mm.
As the pressure increases by a small amount, then t_o will increase by

Δt, and the refractive index by Δn. Assuming that Δt and Δn are both linear for a small pressure increment, then the order of the fringe at one atmosphere is given by:

$$f_o = \frac{2n_o t_o}{\lambda}$$

and at pressure p:

$$f_p = \frac{2(n_o + \Delta n)(t_o + \Delta t)}{\lambda}$$

while the difference gives the number of fringes shifted across the detector:

$$\Delta f = \frac{2}{\lambda} (\Delta t(n_o + \Delta n) + t_o \Delta n)$$

Thus Δt is given by:

$$\Delta t = \frac{\Delta f \ \lambda}{2(n_o + \Delta n)} - \frac{t_o \Delta n}{(n_o + \Delta n)} \qquad (4.7)$$

Since t_o is known, and n has been found as a function of pressure for the fluid between the mirrors, measurement of Δf will give values of Δt. Applying the pressure correction given in equations (4.5 - 4.7), the mirror movement is obtained. Since this is the movement of the syringe body, the change in sample volume, ΔV, may be calculated. This was done by computing $\frac{\Delta V}{V_o}$, ie the ratio of the change in volume to the initial volume. Again, cubic least-squares polynomial fits to the data were performed, and are presented as curves of $\Delta V/V_o$ against pressure in figs (4.8 - 4.12), and as coefficients giving density

61 -

(in g/cc) for pressure (M Pa), in table 4.3.

(iii)   The Lorentz-Lorenz Equation

Whereas the present measurements have been made at a wavelength of
632.8 nm, most of the literature values are not, and in particular,
the Brillouin data have been obtained at a wavelength of 488.6 nm.
It is therefore necessary both for comparison and interpretation of
data, to find how the dispersion affects the refractive index.

The variation of $\dfrac{n^2 - 1}{n^2 + 2}$ with ρ/M is shown in figs 4.13 and 4.14 for
the alkane samples.   Curves for the other samples also show constant
gradient.   The gradient of the curves is equal to the molecular
refractivity, R, which may be seen to be constant.   In view of this
linearity, the Lorentz-Lorenz equation has been used to calculate
values of the refractive index for the blue laser light used in the
light scattering experiments.   The variations in Eulerian and Lagrangian
strains, when plotted against refractive index, are very much larger
than any scatter on the Lorentz-Lorenz data.

(iv)   Analysis of Viscosity Data

The viscosity data comprise five time intervals for each pressure datum:
the two fall times, between windows, and the times for which each light
beam was interrupted.   The latter three times were used simply as a
check that terminal velocity had been attained;   so long as they
showed no systematic decrease (which would imply an acceleration), and
were within 5% of each other, they were ignored: the value of 5% was
chosen because the (non-latching) relays controlling the counters
switched on the change of state of the discriminator and so were able
to switch off and on several times at each edge if the signal was slowly
varying and with superimposed mains hum.   In fact, only systematic

- 62 -

variations occurred when there was dust or obstructions in the bomb:
at other times, terminal velocity had been attained by the time the
slug reached the first window, after a minimum fall of two slug lengths.

It was observed that the window separations were not quite equal, and
that the fall times were in the ratio 1.15:1.00, equal to the measured
difference in separations.

In order to compute the viscosity, the fall velocity is required. Since
the data were used only to find the change in viscosity, the reciprocal
total fall time was used to give the velocity in arbitrary units.

In the experiments using the fall slug rather than spheres, the slug
orientation affected the fall time. However, since the same number of
runs were performed in each orientation at each pressure datum, it is
permissable to take the simple average of the fall times for both
orientations: the standard deviation of the resulting quantity will be
compounded of the deviations of the quantities for each orientation.
Thus for each liquid, we have a set of fall velocities for the various
pressures. These were found to have a standard deviation amounting to
± 1.5%, in part due to thermal fluctuations, but also attributable to
changes in the lamp output and photodiode sensitivity with time. (It
was observed that the lifetime of the (RS 305462) photodiodes was short
and showed large variation. Over the five months of experiments, nine
photodiodes failed, due perhaps to being subjected to high light levels
for long periods. Corroborating this is the observation that it was
usually necessary to readjust the threshold levels before starting a
new run.) Two different steel balls were used, with diameters of
8.727 mm and 3.175 mm. It was assumed that their measured density of
7.772 g/CC was not appreciably affected by pressure. The density of

the composite fall slug was also assumed to be independent of pressure, and was computed by weighing the separate components.

The density of the fluid was computed at each pressure datum using coefficients from table 4.3, and the radii of slug (or ball) and fall tube computed using equations (4.6).

In the case of the simple ball, we may write, (equations 2.8, 2.9):

$$\eta = \frac{2}{9} \frac{a^2(\rho_s - \rho_1)g(1 - 2.104\,(\frac{a}{b}) + 2.09\,(\frac{a}{b})^3 - 0.95\,(\frac{a}{b})^5)}{V}$$

where a is the ball radius, b the fall-tube radius, and V the ball velocity.

The ratio $\eta' = \frac{\eta(\rho)}{\eta(0)}$ was computed, while allowing a, b and ρ to vary as described. Similarly, in the case of the fall slug, the program evaluated η' while calculating a, b and ρ in the equation (2.11):

$$\eta = \frac{g}{4V}\,a^2(\rho_s - \rho_1)(\ln\,(\frac{b}{a}) - \frac{b^2 - a^2}{b^2 + a^2})$$

The viscosity was measured at one atmosphere pressure and 25 °C using capillary viscometers in a constant temperature water bath. The equation (2.6) of Cogswell and McGowan [36] was applied:

$$(\log \eta + C)^{1.8} = a + bP$$

This equation does not fit the present data, though a program which allowed C to vary gave curves approximating to those found for the alkanes, with C ranging monotonically from -3.22 (ISO C8) to -2.58 (C 15).

More data are necessary if the free volume equation of Doolittle [19] is to be applied. Since the present work shows R (the molar refractivity) to be constant, this would imply (see 2.ii.b) that v_o is constant, (and, incidentally, the solid-like compressibility of v_o predicted by Matheson [20], does not occur in this pressure regime) and so:

$$\frac{\Delta v_f}{v_o} \propto \frac{\Delta v_p}{v_{p=0}}$$

The Doolittle equation for viscosity may thus be expressed as:

$$\ln \left(\frac{\eta}{\eta_o}\right) = B \; \frac{\Delta v_o}{v_f}$$

where η_o is the viscosity at one atmosphere pressure and B a constant.

Thus we should expect straight-line fits for $\ln \eta$ against density. These fits were used to find the curve of best fit in figs (4.15 - 18).

(v)   Analysis of Light Scattering Data

(a)   The Computer Fitting Program

(1)   Linearisation

The spectral data were output from the transient recorder on to punched tape as a sequence of 1024 data points, ranging in magnitude from zero to 256 and proportional to the PM tube count ra_e. The maximum observed count rate was of the order of 2000 counts, in a time interval dictated by the clock rate. Thus, for a total scan time of 20 minutes the counting interval for each data point was 1200/1024 = 1.17 sec. At the end of this interval, the

- 65 -

voltage ramp to the Fabry-Perot scanning stack was
incremented. Thus, if the magnitude of each data point
is taken as the y-axis, then the time axis will be a linear
measure of stack voltage. In general, the plate separation
will not, however, be a linear function of stack voltage,
and so the x-axis is related in a non-linear manner to
the plate separation. This mechanism causes the information
in the data sequence to become more compressed as the scan
progresses, (see fig 4.19). In addition to this is the
effect of order number in the etalon. As the plate spacing
varies, the FSR changes, introducing a nonlinearity of plate
spacing with respect to frequency. However, this is a
negligibly small effect, being of the order of

$$\Delta FSR = \frac{-\lambda}{2c} \quad \text{per order.}$$

Before attempting to reduce the data, it is necessary to
linearise the x-axis so that it may be calibrated in terms
of frequency. The voltage/frequency dependence was
determined by adjusting the voltage ramp so that the scan
covered five orders. Spectra were collected, using a
colloidal sample which produced narrow, sharp peaks at the
exciting wavelength, and the separation of these peaks were
determined as the number of points between them. Since the
scattered peaks were all of the same wavelength, the
frequency separation was 1 FSR in each case, and so five
data points were available, giving frequency vs points
(ie voltage). These data were fitted to a polynomial least
squares fit and it was found that a quadratic fit was

adequate to describe the data. It was therefore possible
to linearise any experimental spectrum by taking the
separations of the central peaks as 1 FSR, and performing
a least-squares quadratic fit to the 1024 x-points.

(2)   Initial Estimates

The data were fitted to a spectral shape comprising a sum
of three Lorentzian lines for each order allowing for two
orders either side of the collected data, to allow for the
overlapping orders increasing the heights of the observed
data using the FORTRAN NAG minimisation routine, E04GAF.
This routine requires initial estimates for each of the
fitted parameters, eight of which were used to describe
the spectra:

        Base height

        Rayleigh (central Lorentzian) height

        Brillouin height

        Rayleigh width at half-height

        Brillouin width at half-height

        Brillouin shift

        Starting position

        FSR.

The last two parameters allow the routine slightly to
expand or contract the scale and move the origin if
necessary.

In addition, the positions of the central peaks need
to be known in order that the data may be linearised before
fitting.

- 67 -

To find the initial estimates it was necessary to overcome
the problem of random noise in the data, and this was done
by making the program smooth the data points in a copy of
the input data: these smoothed data were only used to find
initial estimates, the unsmoothed data being used in the
fitting routine. Once smoothed, a numerical differentiation
was performed, and the number of turning points found. This
process was repeated until 19 or fewer turning points had
been found: these were sorted to find the Rayleigh and
Brillouin peak positions, and the data were then linearised,
initial estimates found, and E04GAF called. The vast
majority of the program was written by Tatam and Crilly, and
details reported elsewhere [80].

(3)   Observations on the Fitting Routine

The output from the minimisation routine consists of the
eight fitted parameters and a value of chi-square for the
fit. In addition, two statistical tests were performed on
the data: the correlation coefficient and the one sample
runs test. These tests are both extremely sensitive, and
the correlation coefficient, like the chi-square test,
depends on correct weighting of the data to give meaning-
ful results. A full statistical investigation of the data
is beyond the scope of this work: suffice it to say that
finding the correct weighting is complicated by the fact
that the scaling of the y-values performed by the transient
recorder (from 0 - 2000 to 0 - 256) causes the distribution
to deviate from Poisson statistics, and the correct weights
to account for this have not been found. In the meantime,

- 68 -

fig 4.20 shows a typical set of (linearised) experimental data together with the fitted function, which will be seen to follow the points very well. The sample spectra shown in fig 4.19 are for Octane at pressures of one atmosphere, 122, 208 M Pa, in which it will be seen that as the pressure increases, the Brillouin shift, the central peak height, and the Brillouin half-height width, all increase.

The main advantage of the fitting routine over graphical methods, is that the shifting of the Brillouin peak positions due to overlap with the central peak is deconvoluted. In addition, the program allows for the effects of two orders to each side of the data, so that overlap effects are minimised.

Because the instrumental function has a finite width, any linewidths measured on spectra will be a convolution of the true linewidth and the instrumental linewidth, and no feature smaller than the instrumental width will be resolved. In order to calculate the attenuation coefficient, α, the true Brillouin halfwidth is needed. So long as the observed width is greater than twice the instrumental width, and assuming both to be Lorentzian in shape, it is reasonable [82] simply to subtract the instrumental width from the observed width. The instrumental width was known from the measured finesse.

(b) Physical Interpretation of the Light Scattering Data

The hypersonic phonon velocity, V_s, attenuation coefficient α, modulus M and Landau-Plackzeck ratio LP_r were computed from the fitted data

using equations (2.12,13,16,17), together with measured values of density, compressibility, and shear viscosity at zero shear rate. Since the Lorentz-Lorenz equation has been shown adequately to describe the refractive-index data, it was used to caculate $n(\lambda,P)$ for λ = 488.6 nm.

(1) **Hypersonic Phonon Velocity**

Figures (4.22a, b) show the hypersonic phonon velocity plotted against density, from which it may clearly be seen that V_s may be described by the empirical equation:

$$V_s = A + B\rho$$

where B appears to be constant for a given series, and A is a constant for each liquid (see table 4.4) and increases with molecular weight. Although this has the same form as the equation (2.14) of Schaaffs [50], it may be seen that there are large discrepancies between the fitted and predicted values of the constants.

Molecular Sound Velocity

The molecular sound velocity, R, calculated from Rao's equation [81]

$$R = V_s^{1/3} \frac{M}{\rho}$$

gives the same variations of R as those of Rajagopalan [78] using the data of Boelhouwer [45] for octane and dodecane at pressures up to 1400 bar ($\sim$ 140 M Pa). These data were obtained at a frequency of 2 MHz, but do not show the 1% dispersion reported by Champion and Jackson [44] when compared to the present data.

Free Volume

Champion and Jackson [44] found a linear dependence of the free volume as defined by Doolittle [19] on the cube of the sound velocity, independent of molecular weight and over a large temperature range. If the mechanism of the change in free volume is the same, then it should be possible to use this data to predict the free volume directly from V_s. However, since Champion and Jackson's data may be fitted to

$$V_s = A' + B' \left| \frac{V_f}{V_o} \right|^{-1/3}$$

and a linear dependence of ρ on $\frac{V_o}{V_f}$ has been shown from the viscosity data (4.2.iv), while a linear dependence of V_s on ρ holds for these data, it would appear that V_s cannot be used to predict the free volume in pressure experiments.

(2)   Attenuation Coefficient and Relaxation Time

From equation (2.15):

$$\frac{\alpha}{\nu_B^2} = \frac{K}{V_s^3 (1 + \omega^2 \bar{\tau}^2)}$$

it may be seen that a value of an average relaxation time $\bar{\tau}$ for viscous relaxations, may be obtained by fitting:

$$\frac{1}{(2\pi\nu_B)^2} = \frac{K}{\alpha \, V_s^3 (2\pi)^2} - \bar{\tau}^2$$

when applied to the alkane data, this gives a value of zero for the relaxation time. However, the polyisobutene

- 71 -

data yield the following values for $\bar{\tau}$:

HO4 1.14×10^{-11}

HO7 1.27×10^{-11}

H5 4.24×10^{-12}

in view of the uncertainty ($\pm$ 10%) on these figures, this would appear to be a relaxation of $\tau = 9.4 \times 10^{-12}$ s common to all three samples.

(3)   Modulus and Landau-Placzeck Ratio

The modulus $M(\omega)$ is given [47] by

$$M(\omega) = K(\omega) + \frac{4}{3} G(\omega) = \frac{v_s^2}{\rho}$$

where $K(\omega)$ is the compressional modulus and $G(\omega)$ the shear modulus. Since a liquid is incapable of sustaining zero frequency shear, the limit must be

$$M(O) = K(O) = \frac{1}{\beta}$$

where β is the isothermal compressibility. The variation of $M(\omega)$ as a function of $M(O)$ is shown in fig 4.21(a) and is seen to be linear with a gradient of unity and a common intercept at the origin for all the n-alkanes studied. The implication, that $K(\omega) = K(O)$ and $G(\omega) = O$ substantiates the observation that there is no relaxation process occuring within this pressure and temperature range in the alkane samples. In the case of a non-relaxing liquid, the ratio

- 72 -

of specific heats may be obtained from the Landau-
Placzeck ratio:

$$\gamma = (LP_r + 1),$$

however, the apparent increase in LP_r is more likely to
be due to the presence of fine particulate matter than an
increase in γ, since increasing sample viscosity will slow
down the particle velocity, increasing the spurious elastic
scattering.

The curves of fig 4.21(b) show that, in the case of the
polyisobutene samples, $M > \frac{1}{\beta}$, supporting the observation
that a relaxation is taking place.

TABLE 4.2

Pressure coefficients of Refractive index : $n_{632.8} = A + BP + CP^2 + DP^3$

SAMPLE	A	B	C	D
Iso octane	0.13908E+01	0.53321E-03	-0.19347E-05	0.36916E-08
Octane	0.13961E+01	0.45475E-03	-0.12416E-05	0.18622E-08
Decane	0.14170E+01	0.42882E-03	-0.12541E-05	0.19292E-08
Undecane	0.14167E+01	0.39426E-03	-0.10018E-05	0.15055E-08
Dodecane	0.14197E+01	0.41529E-03	-0.15107E-05	0.41508E-08
Tridecane	0.14253E+01	0.39716E-03	-0.13435E-05	0.36770E-08
Pentadecane	0.14304E+01	0.40672E-03	-0.16120E-06	-0.22082E-07
PEG 3	0.14506E+01	0.14985E-03	-0.13617E-06	0.33506E-10
PEG 300	0.14645E+01	0.17360E-03	-0.20655E-06	0.13074E-09
PEG 400	0.14650E+01	0.11274E-03	-0.17767E-06	0.37944E-09
PEG 1	0.14305E+01	0.14959E-03	-0.18708E-06	0.18288E-09
PPG 1	0.14271E+01	0.39489E-03	-0.67352E-06	0.67460E-09
PPG 2	0.14388E+01	0.45539E-03	-0.83233E-06	0.80132E-09
PPG 425	0.14466E+01	0.52602E-03	-0.11322E-05	0.13041E-08
PPG 1025	0.14487E+01	0.54896E-03	-0.12223E-05	0.14679E-08
PPG 2025	0.14494E+01	0.55317E-03	-0.12656E-05	0.16060E-08
Hyvis 04	0.14663E+01	0.35758E-03	-0.92794E-06	0.14347E-08
Hyvis 07	0.14762E+01	0.31717E-03	-0.61921E-06	0.83284E-09
Hyvis 5	0.14900E+01	0.28809E-03	-0.49065E-06	0.50965E-09
Hyvis 200	0.15020E+01	0.26863E-03	-0.48192E-06	0.62539E-09
Hyvis 30	0.14968E+01	0.27691E-03	-0.49208E-06	0.55504E-09

TABLE 4.3

Pressure (MPa) coefficients of Density (g/cc) $Rho = A + BP + CP^2 + DP^3$

Sample	A	B	C	D
Iso octane	0.68946E+00	0.12563E-02	-0.49749E-05	0.97183E-08
Octane	0.69486E+00	0.11109E-02	-0.37605E-05	0.59870E-08
Decane	0.72380E+00	0.90032E-03	-0.27097E-05	0.42279E-08
Undecane	0.73477E+00	0.92052E-03	-0.28939E-05	0.46212E-08
Dodecane	0.74522E+00	0.80321E-03	-0.28260E-05	0.62676E-08
Tridecane	0.76136E+00	0.77295E-03	-0.26076E-05	0.61709E-08
Pentadecane	0.76549E+00	0.82258E-03	-0.36939E-06	-0.44897E-07
PEG 1	0.11090E+01	0.28959E-03	-0.47054E-06	0.43628E-09
PEG 3	0.11189E+01	0.32049E-03	-0.36486E-06	0.96206E-10
PEG 300	0.11217E+01	0.36287E-03	-0.51833E-06	0.31053E-09
PEG 400	0.11234E+01	0.34231E-03	-0.48240E-06	0.10101E-08
PPG 1	0.10322E+01	0.18042E-03	-0.25494E-06	0.23406E-09
PPG 2	0.10224E+01	0.21646E-03	-0.38910E-06	0.47371E-09
PPG 425	0.10074E+01	0.25130E-03	-0.47126E-06	0.58100E-09
PPG 1025	0.10023E+01	0.25566E-03	-0.46471E-06	0.51999E-09
PPG 2025	0.99957E+00	0.27212E-03	-0.53794E-06	0.73381E-09
Hyvis 04	0.77763E+00	0.61202E-03	-0.15482E-05	0.20654E-08
Hyvis 07	0.79344E+00	0.58753E-03	-0.14843E-05	0.19915E-08
Hyvis 5	0.83044E+00	0.51598E-03	-0.12174E-05	0.16335E-08
Hyvis 30	0.85215E+00	0.47594E-03	-0.10180E-05	0.11593E-08
Hyvis 200	0.86295E+00	0.42586E-03	-0.75364E-06	0.70327E-09

The isothermal compressibility is given by the first derivative:

$$\beta = B + 2CP + 3DP^2$$

TABLE 4.4

Comparison of fitted hypersonic phonon velocities with Schaaffs´ equation

Sample	$-A$ ms^{-1}	B $m^4 Kg^{-1}s^{-1}$	$W\beta/(\beta+B)$ ms^{-1}	WB/M $m^4 Kg^{-1}s^{-1}$
	(Slope)	(Intercept)	(Slope)	(Intercept)
Iso Octane	4840	8.52	39.5	1.08
Octane	4570	8.23	23.8	1.45
Decane	5150	8.81	18.6	1.45
Undecane	5150	8.69	16.8	1.50
Dodecane	5230	8.73	15.3	1.52
Tridecane	5960	9.53	14.1	1.53
Pentadecane	4980	8.26	12.1	1.54
H 04	9560	14.3	41.87	16.34
H 07	9200	13.8	42.04	16.26
H 5	9610	14.2	42.18	16.25

This work : $V_s = A + B\rho$

Schaaffs´ equation : $V_s = W\left((\beta/\beta+B) + B\rho/M\right)$

TABLE 4.5

Table of density coefficients of viscosity : $\eta = e^{(-A + B\rho)}$

Viscosity in Pas , Density in Kgm^{-3}

SAMPLE	A	B
Iso octane	16.77	0.0137
Octane	17.25	0.0141
Decane	17.45	0.0146
Undecane	17.06	0.0143
Dodecane	19.82	0.0179
Tridecane	19.81	0.0177
Pentadecane	19.73	0.0181
Hyvis 04	60.84	0.0747
Hyvis 07	80.56	0.1000
Hyvis 5	81.76	0.1020
Hyvis 30	78.61	0.0972
PPG Monomer	65.03	0.0578
PPG Dimer	89.71	0.0791
PPG 425	93.15	0.0879
PPG 1025	114.42	0.1103
PPG 2025	96.23	0.0932
PEG Monomer	30.11	0.0209
PEG Trimer	36.76	0.0275
PEG 300	37.55	0.0285
PEG 400	56.37	0.0454
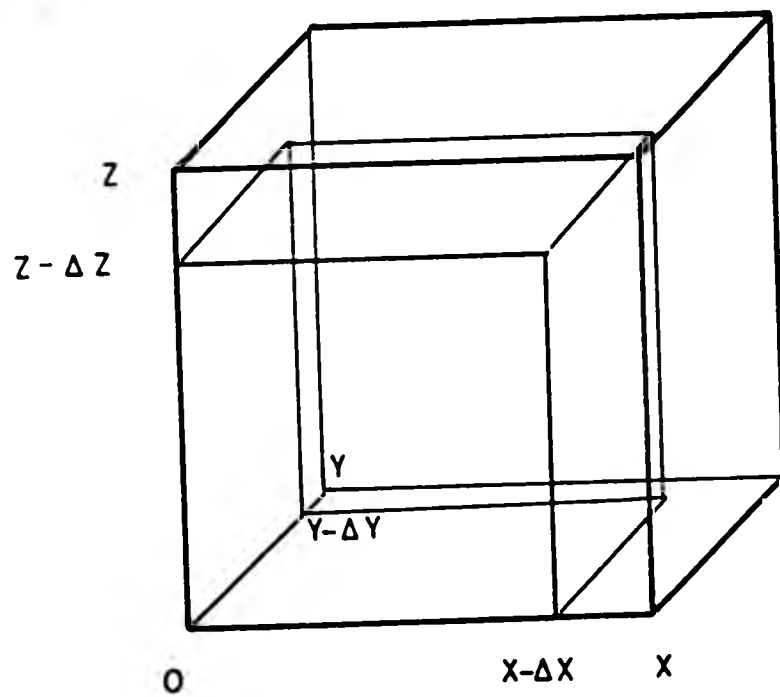
Fig. 4.1 Coordinate system for calculation of component compression.
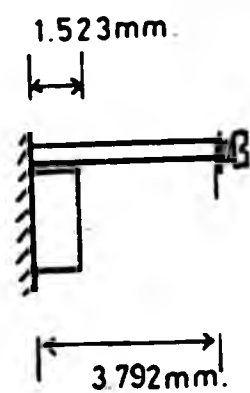
(a) Refractive index
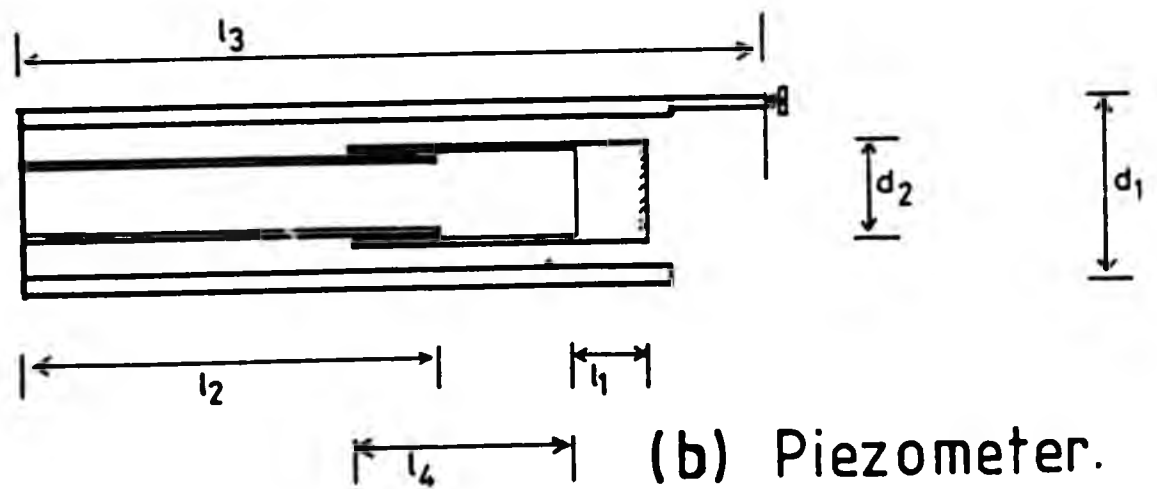
(b) Piezometer.

Fig. 4.2 Component dimensions.
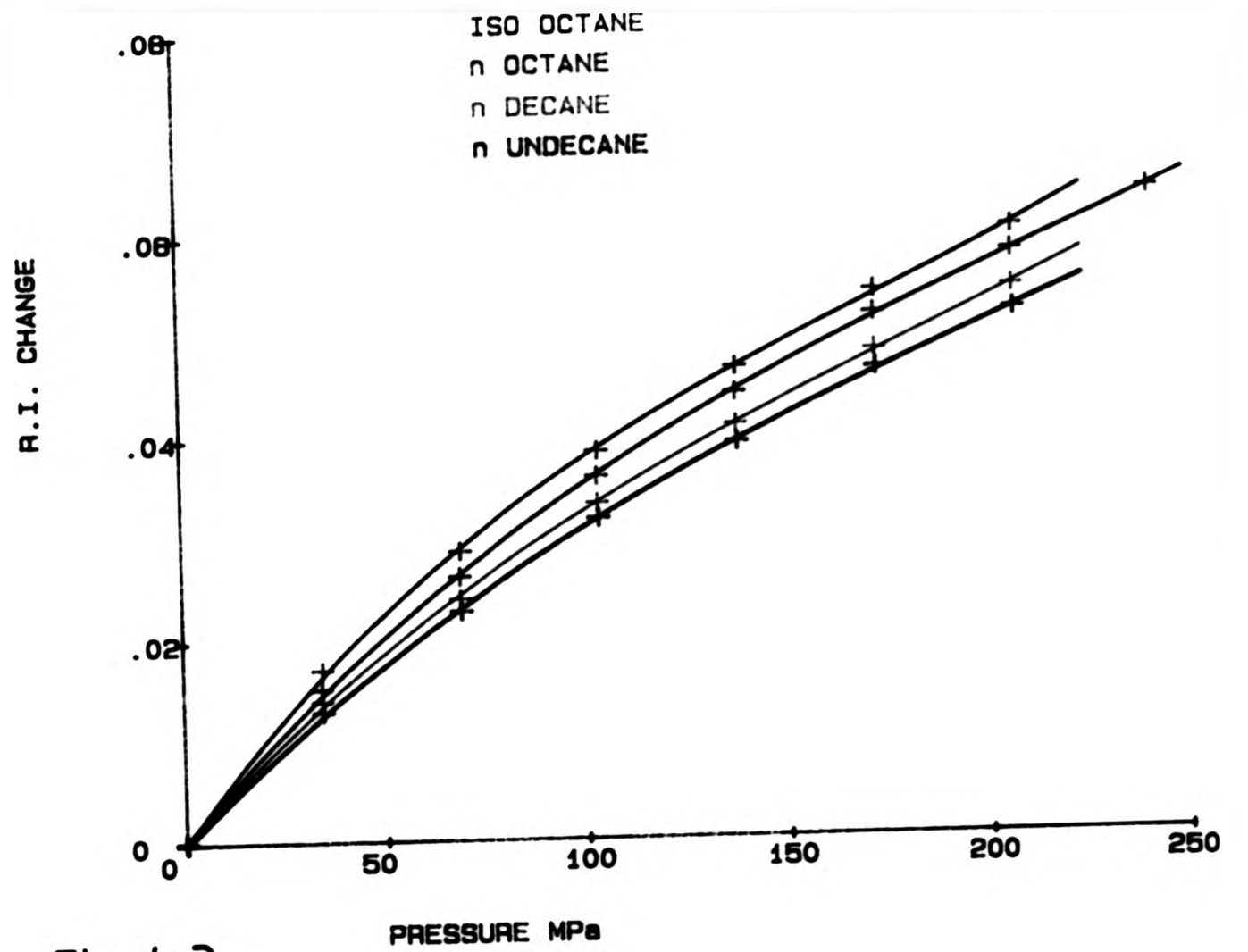
Fig. 4.3

ALKANES C8-C11 R.I. vs PRESSURE
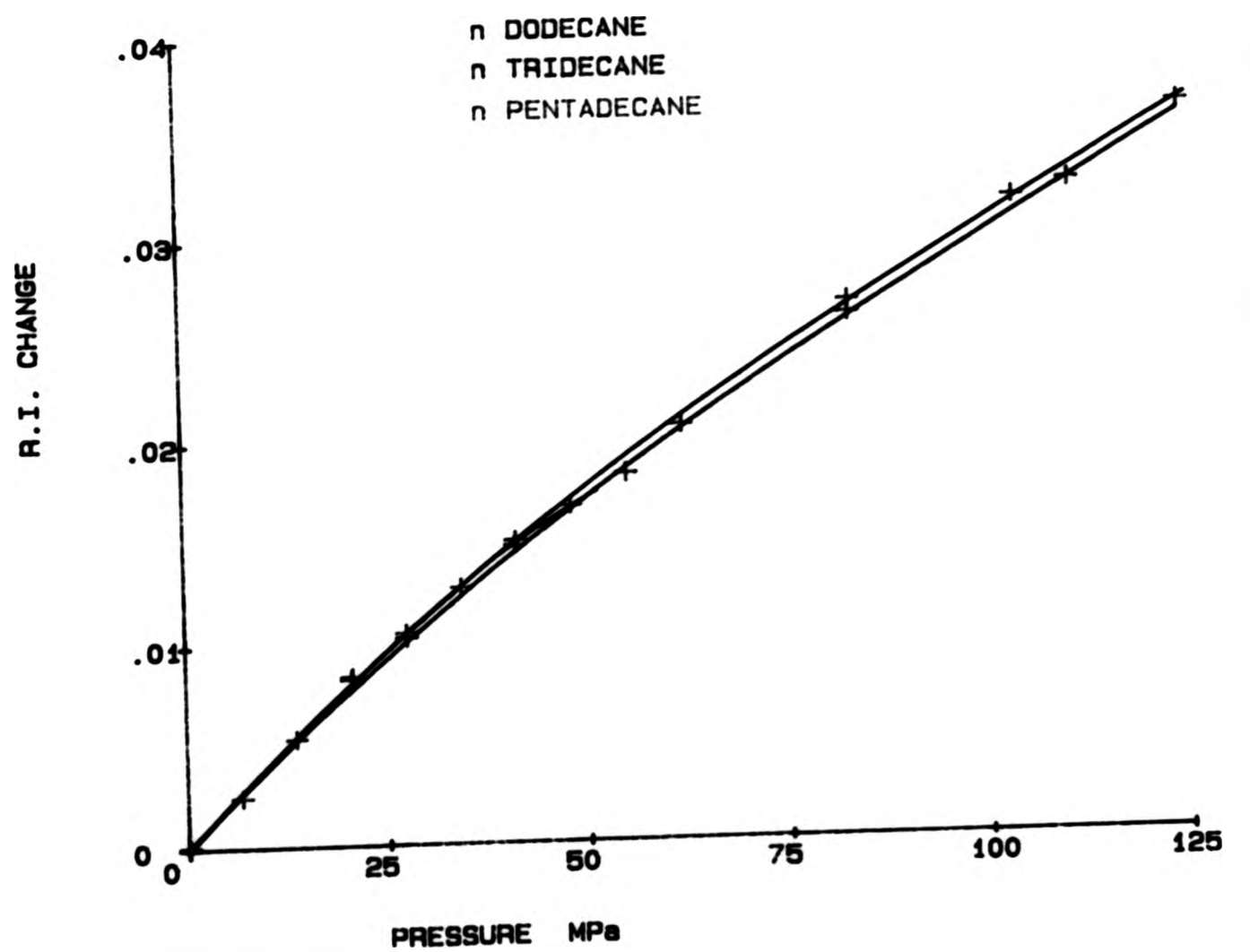
Fig. 4.4

ALKANES C12-C15 R.I. vs PRESSURE

Fig. 4.3

ALKANES C8-C11 R.I. vs PRESSURE

Fig. 4.4

ALKANES C12-C15 R.I. vs PRESSURE

- 79 -
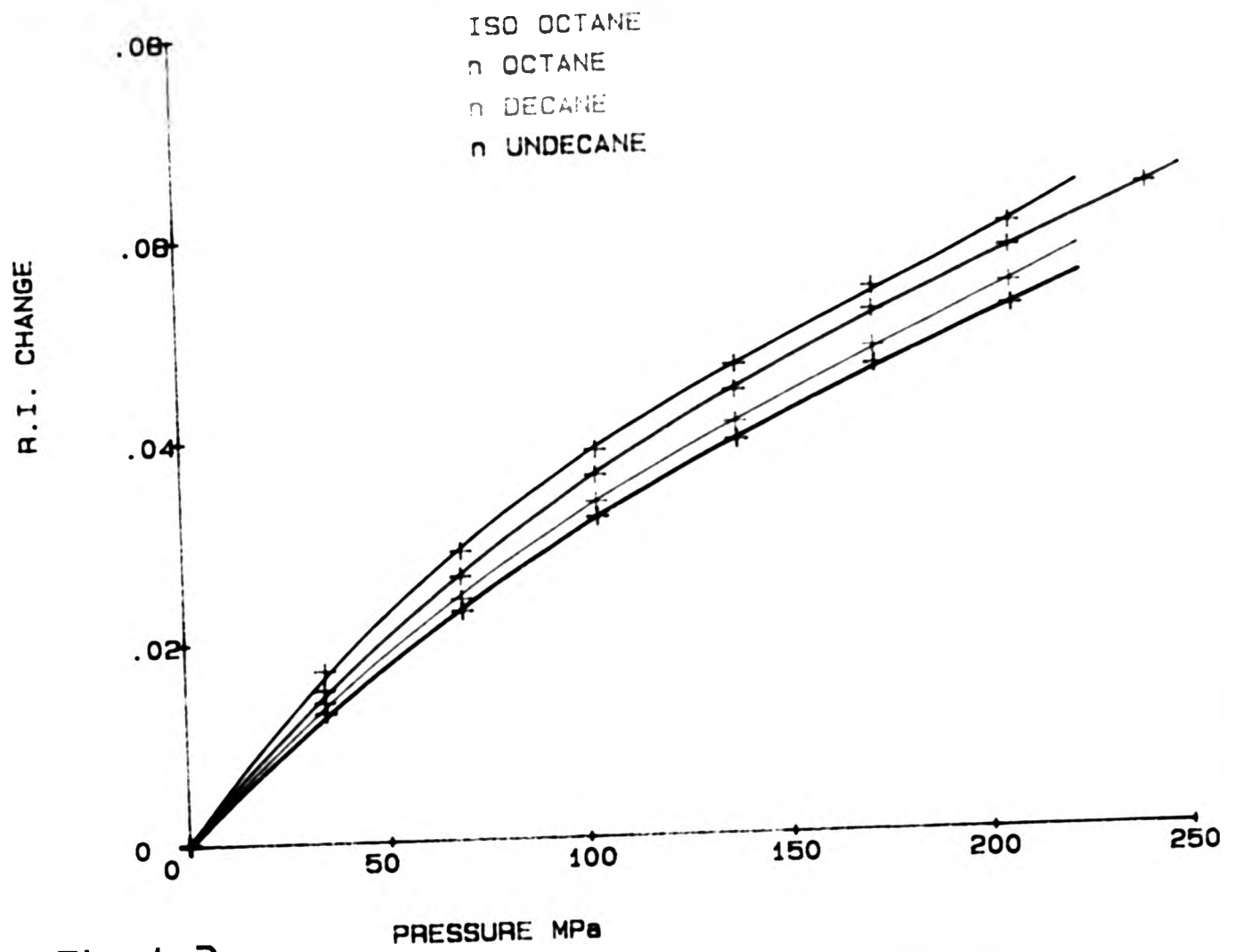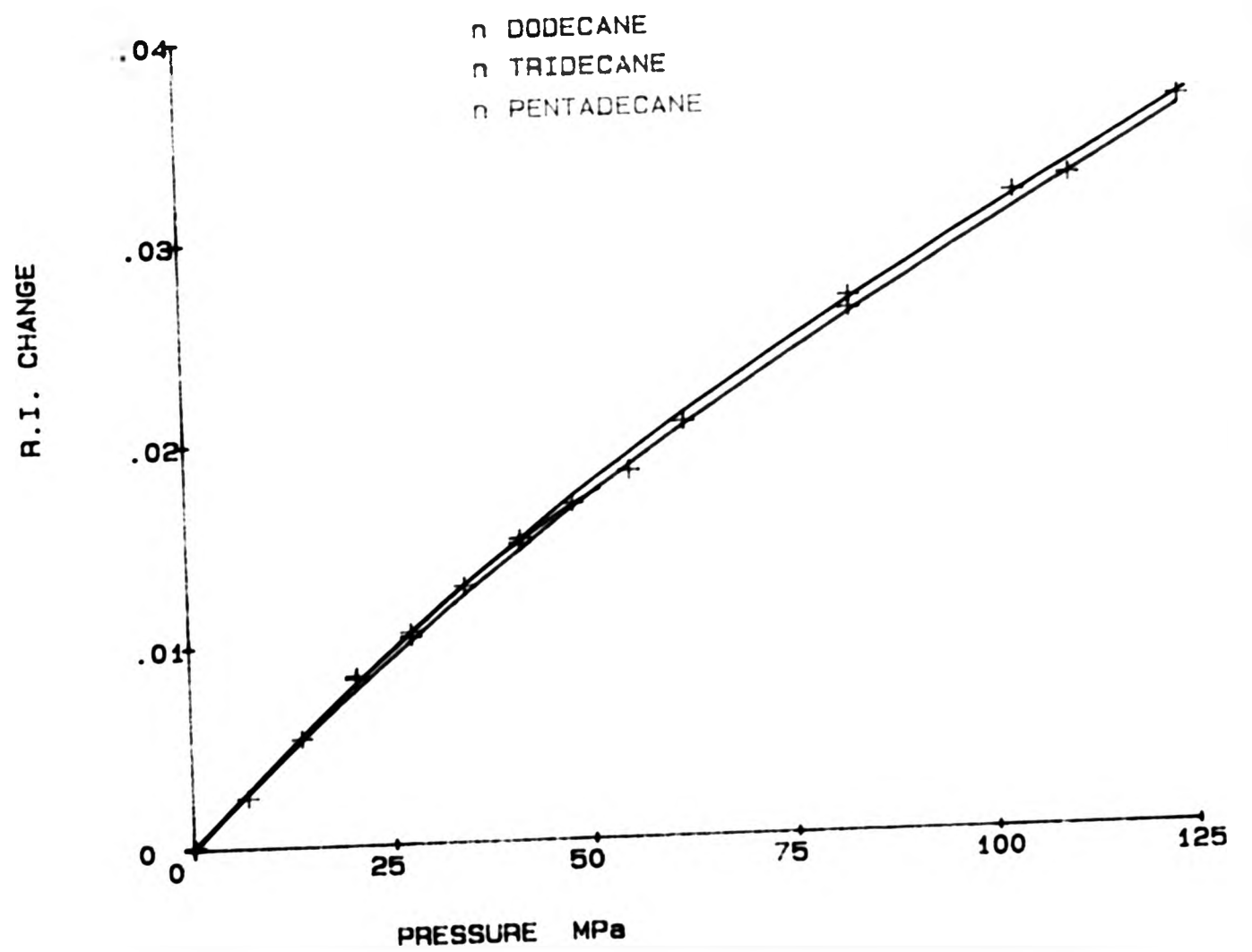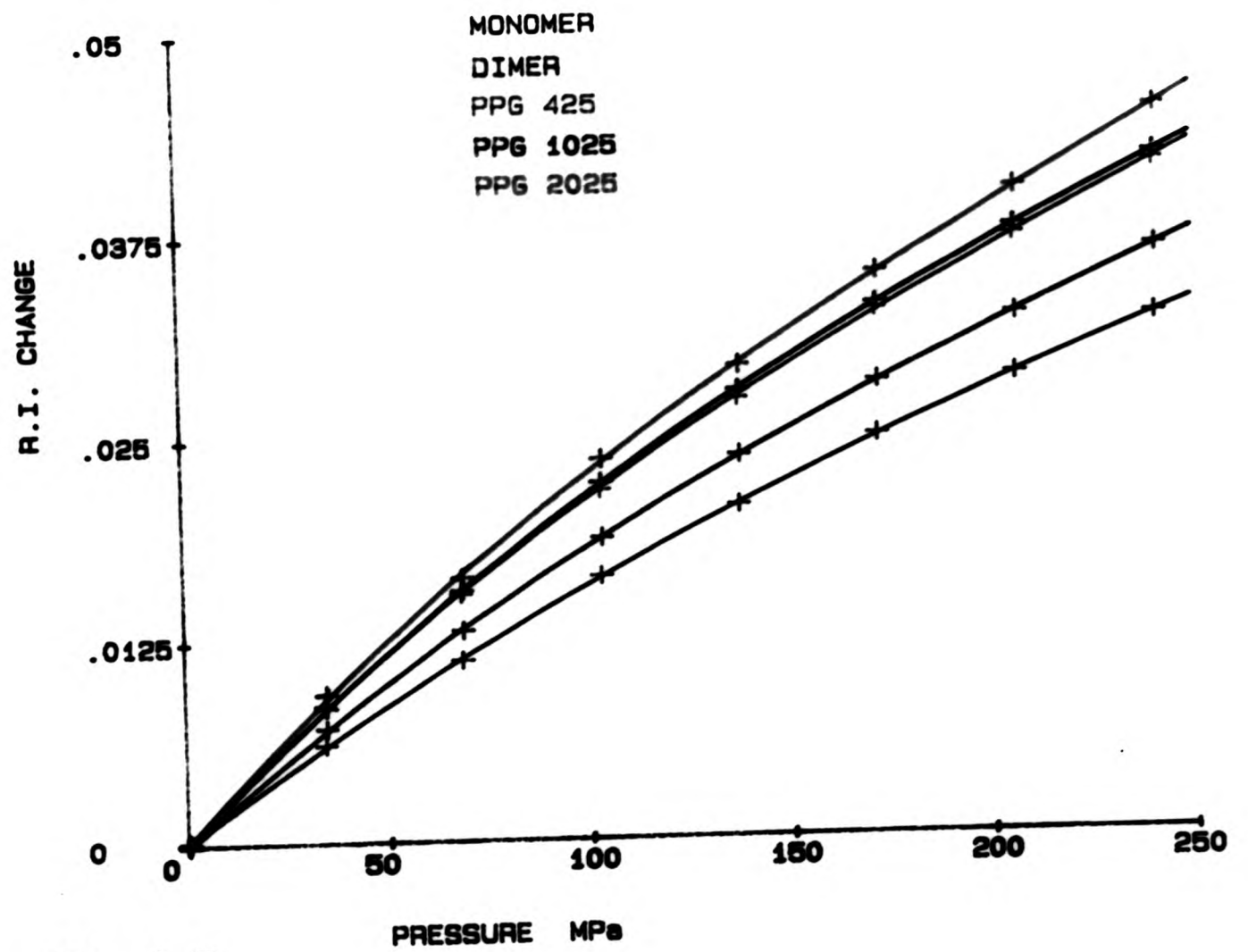
Fig. 4.5

PPG R.I. vs PRESSURE
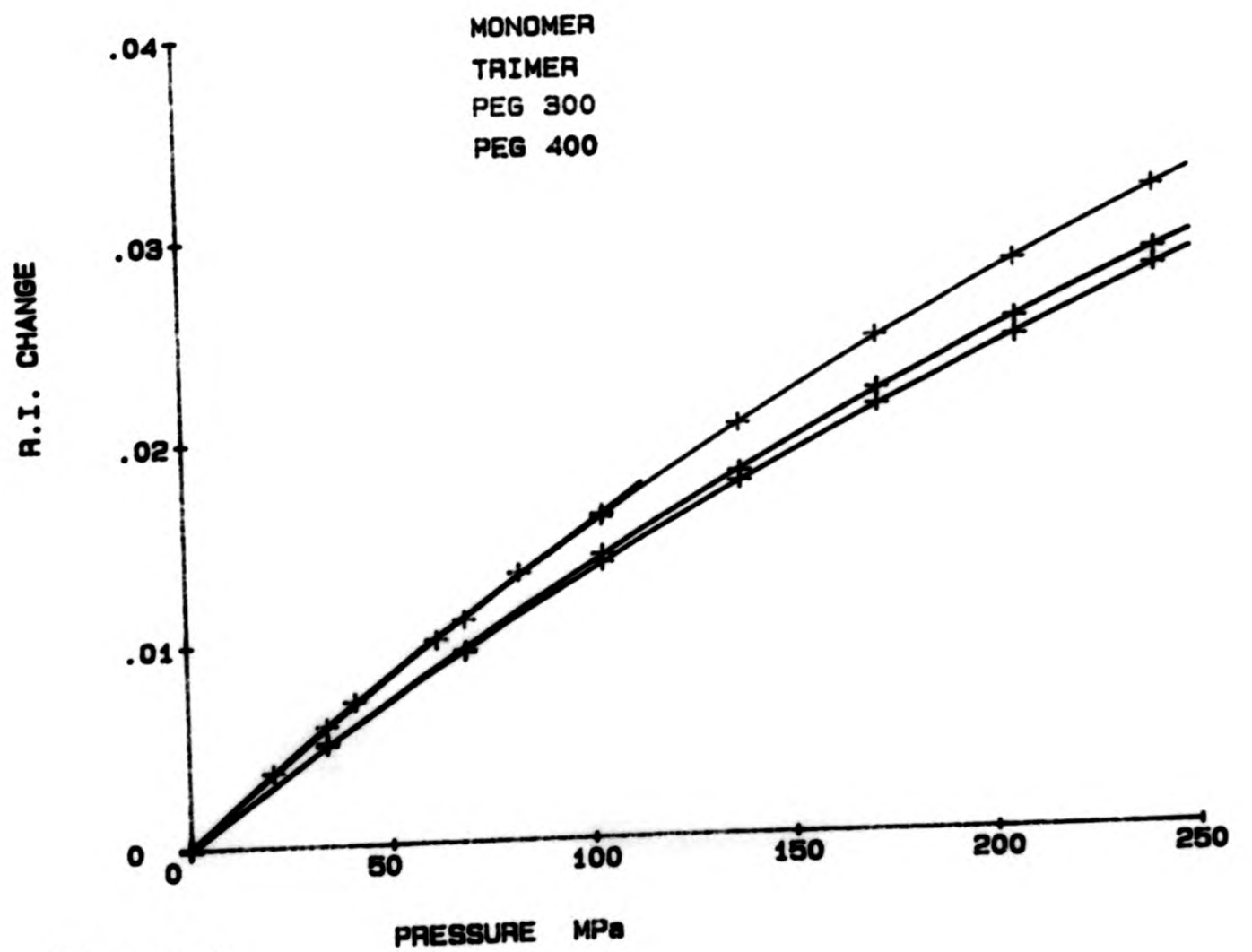
Fig. 4.6

PEG R.I. vs PRESSURE
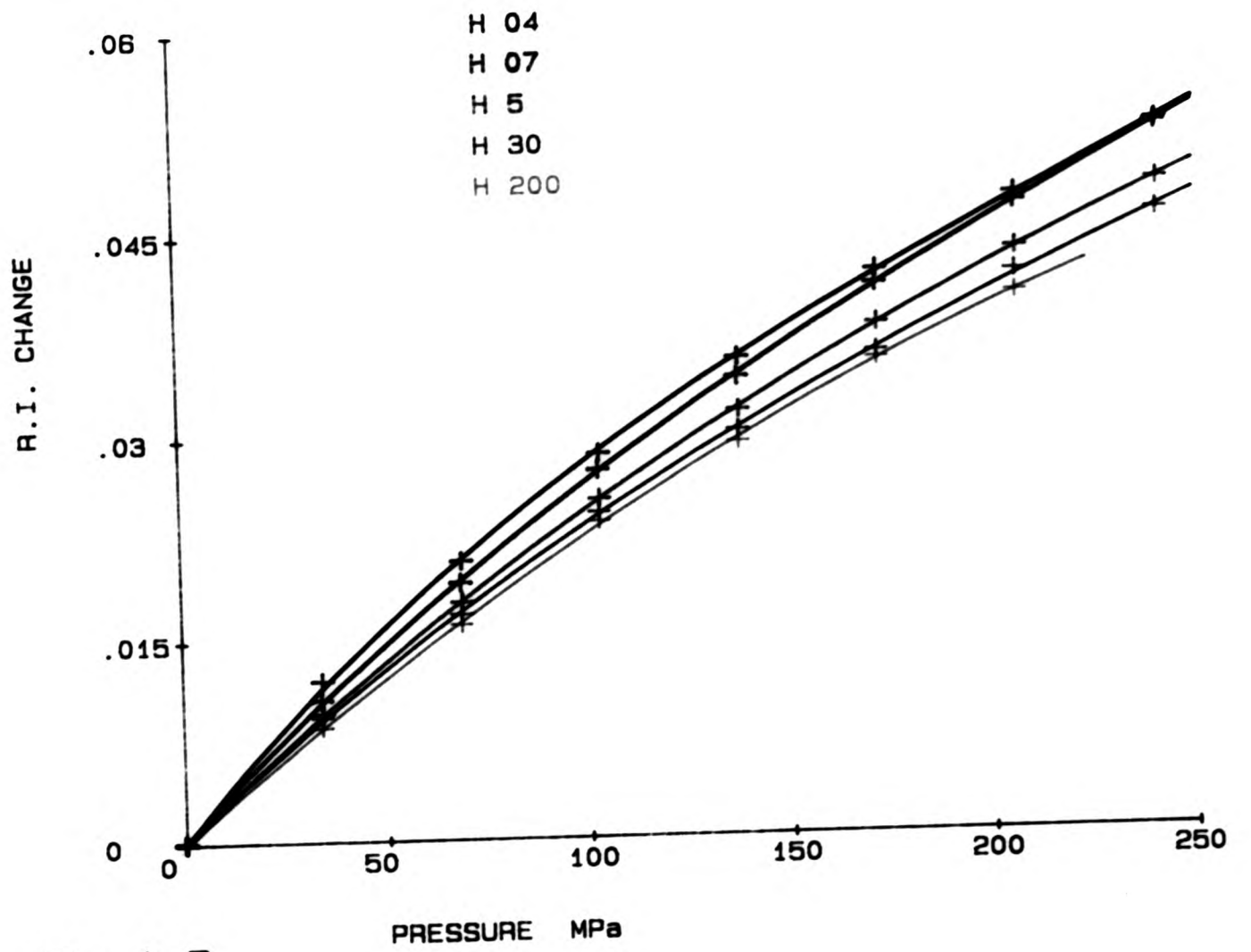
Fig. 4.7

POLYISOBUTENES R.I. vs PRESSURE
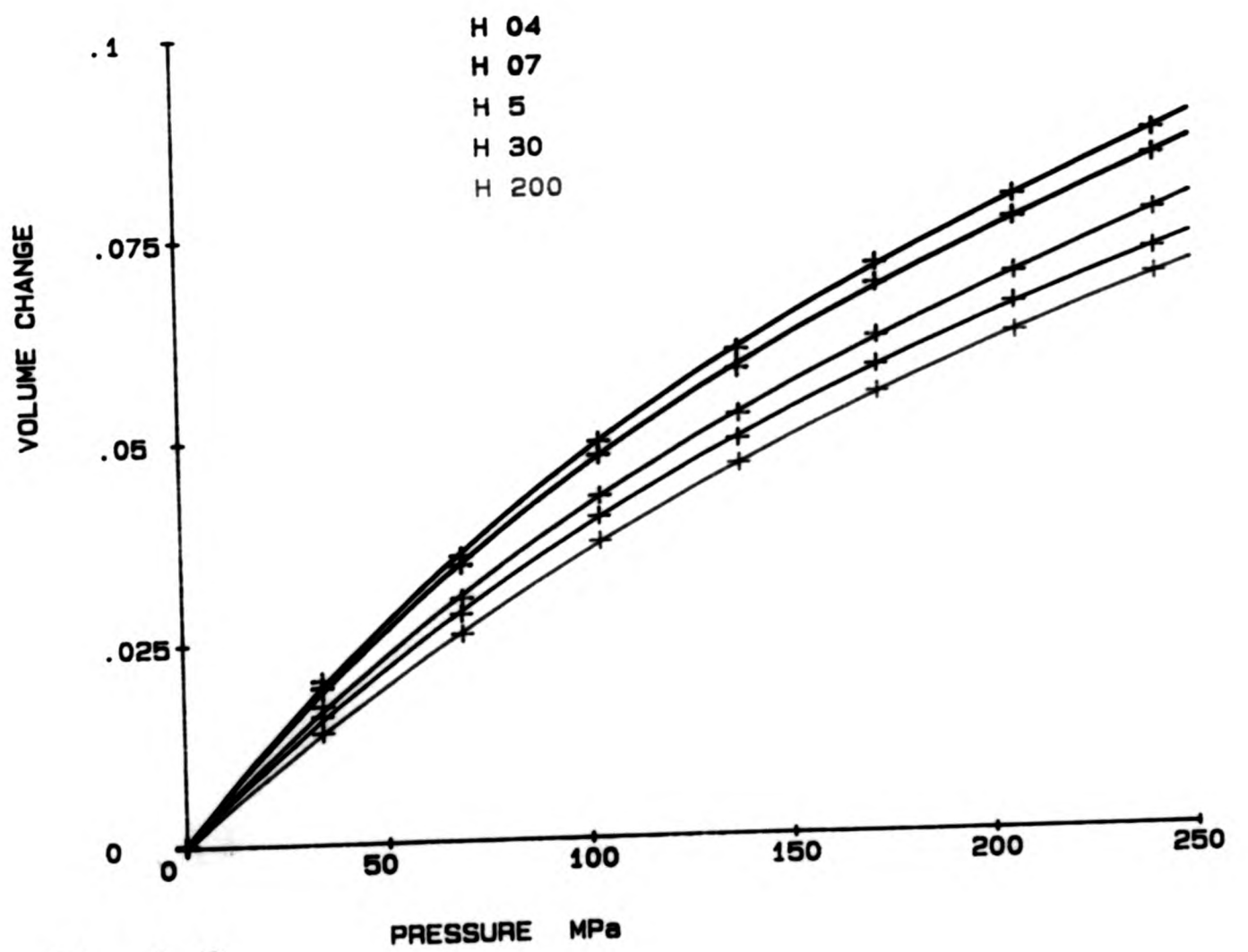
Fig. 4.8

POLYISOBUTENES VOLUME CHANGE AS A FUNCTION OF PRESSURE
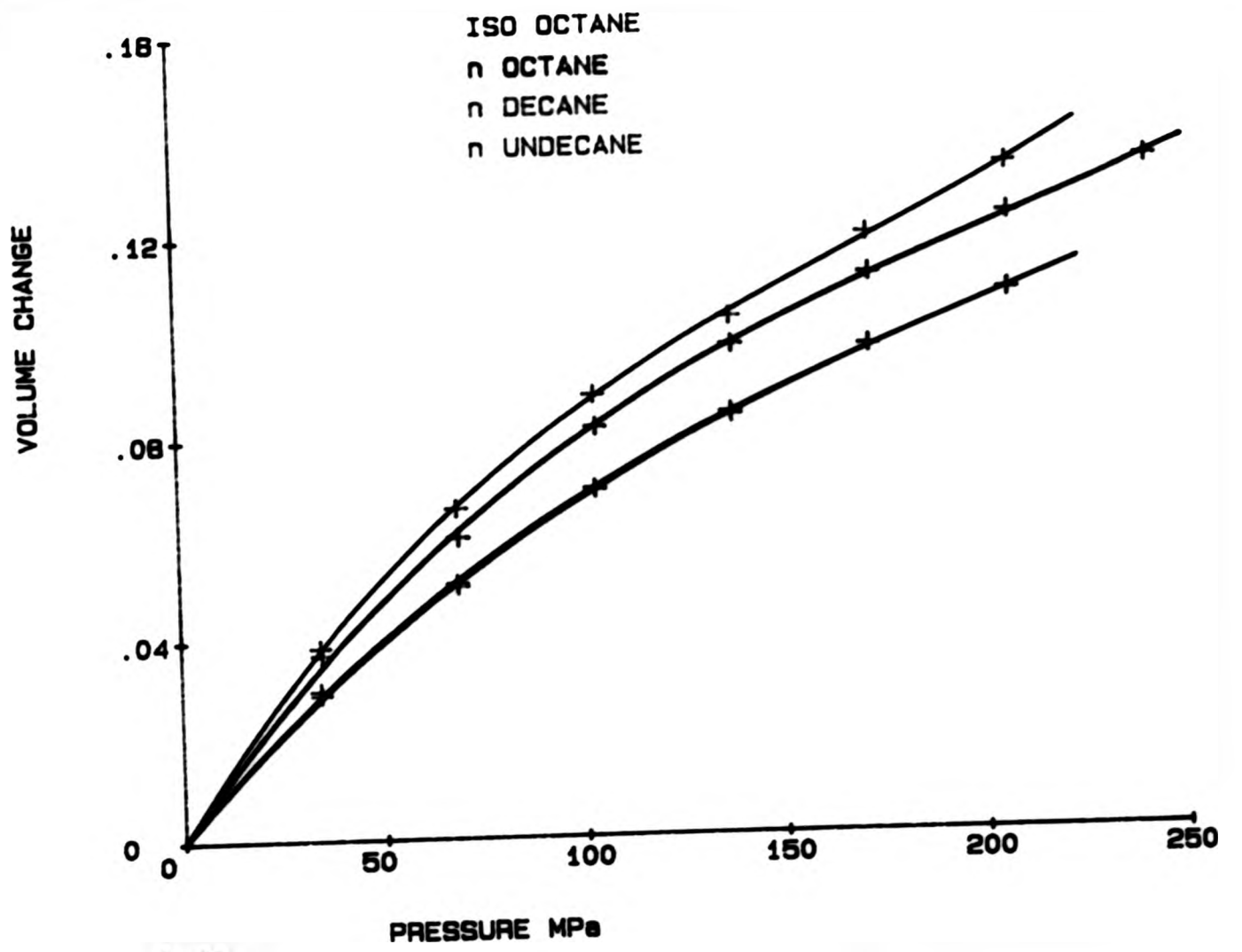
Fig. 4.9

ALKANES C_8 -C_{10} VOLUME CHANGE AS A FUNCTION OF PRESSURE
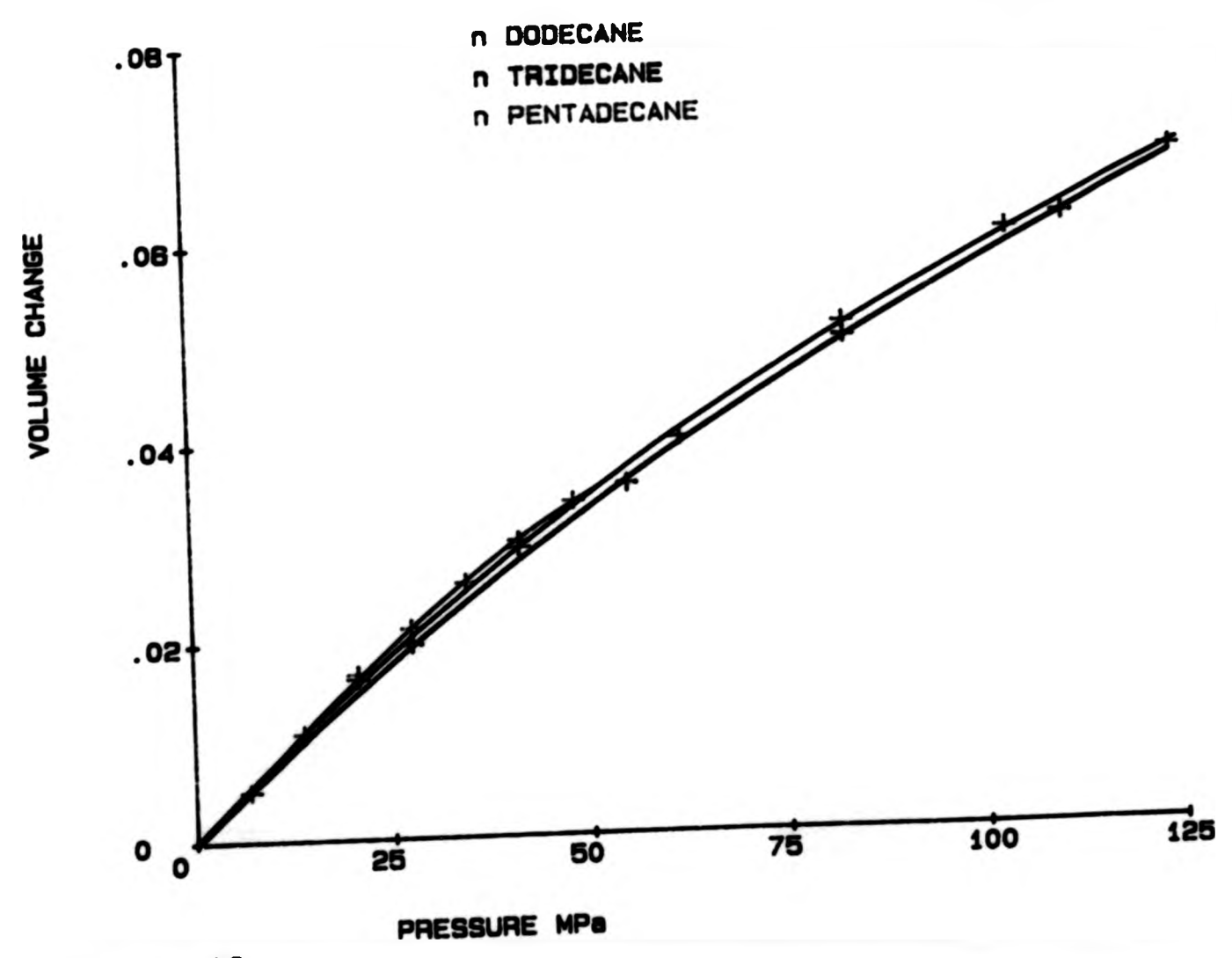
Fig. 4.10

ALKANES C_{12} -C_{15} VOLUME CHANGE AS A FUNCTION OF PRESSURE
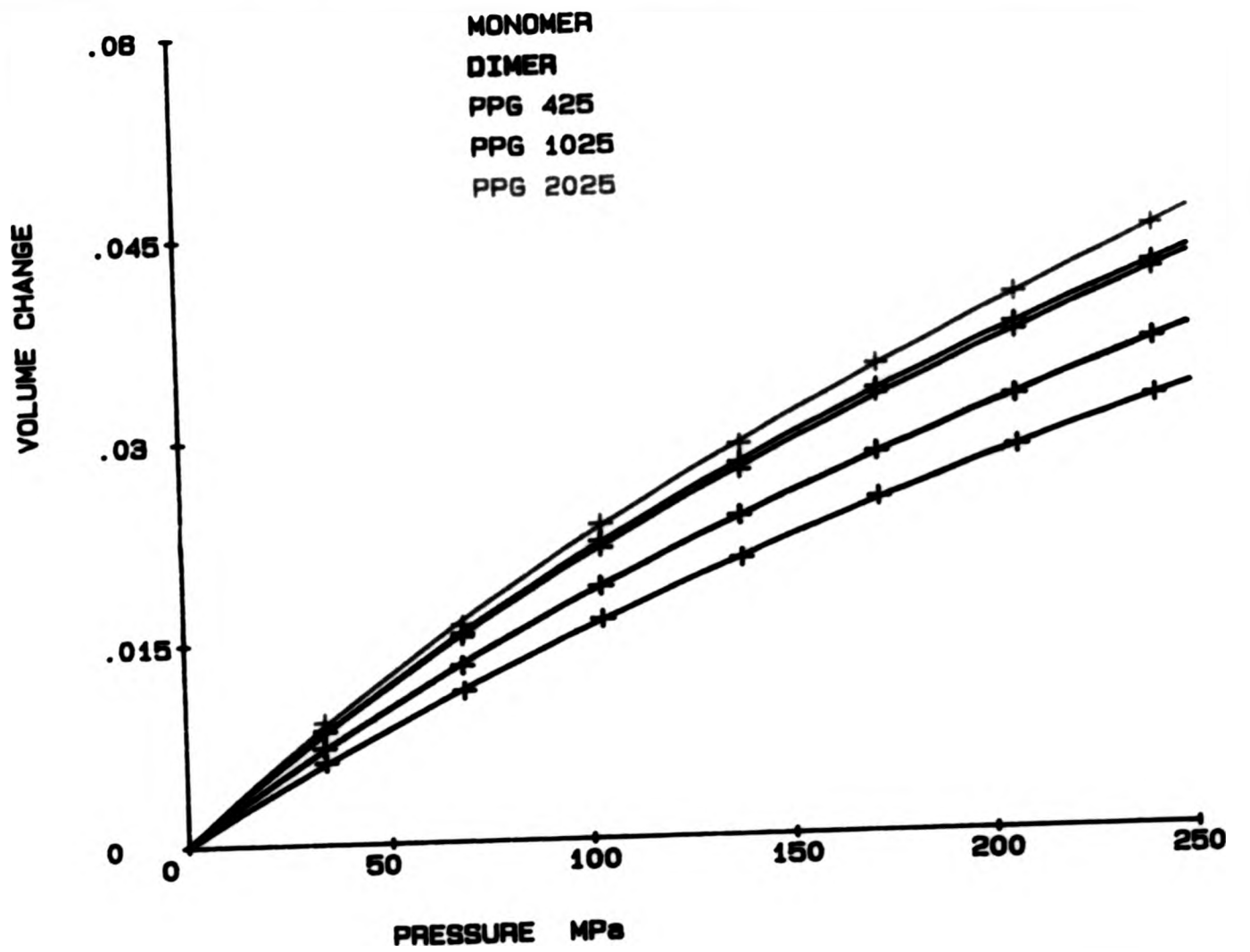
Fig. 4.11

PPG   VOLUME CHANGE AS A FUNCTION OF PRESSURE
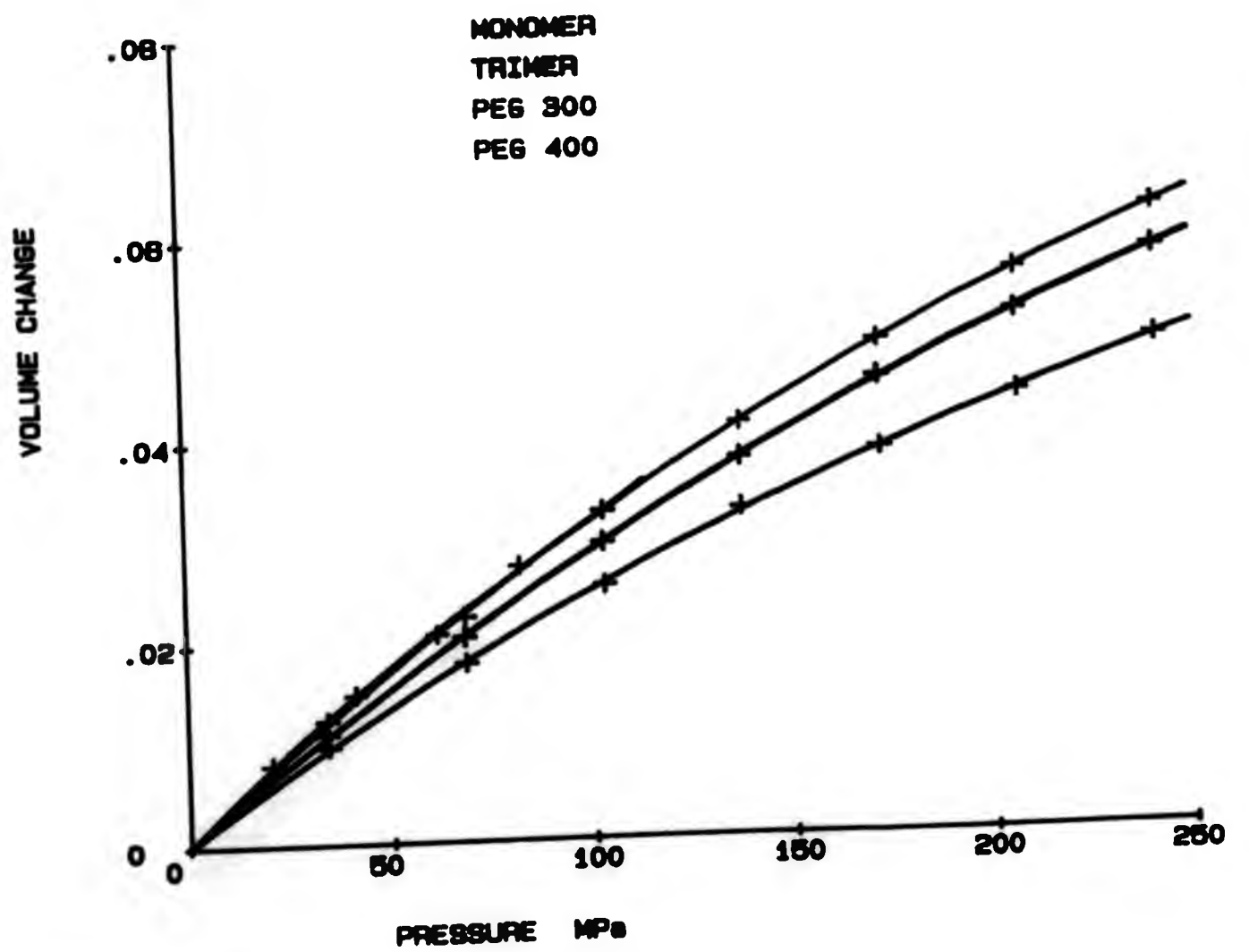
Fig. 4.12

PEG   VOLUME CHANGE AS A FUNCTION OF PRESSURE
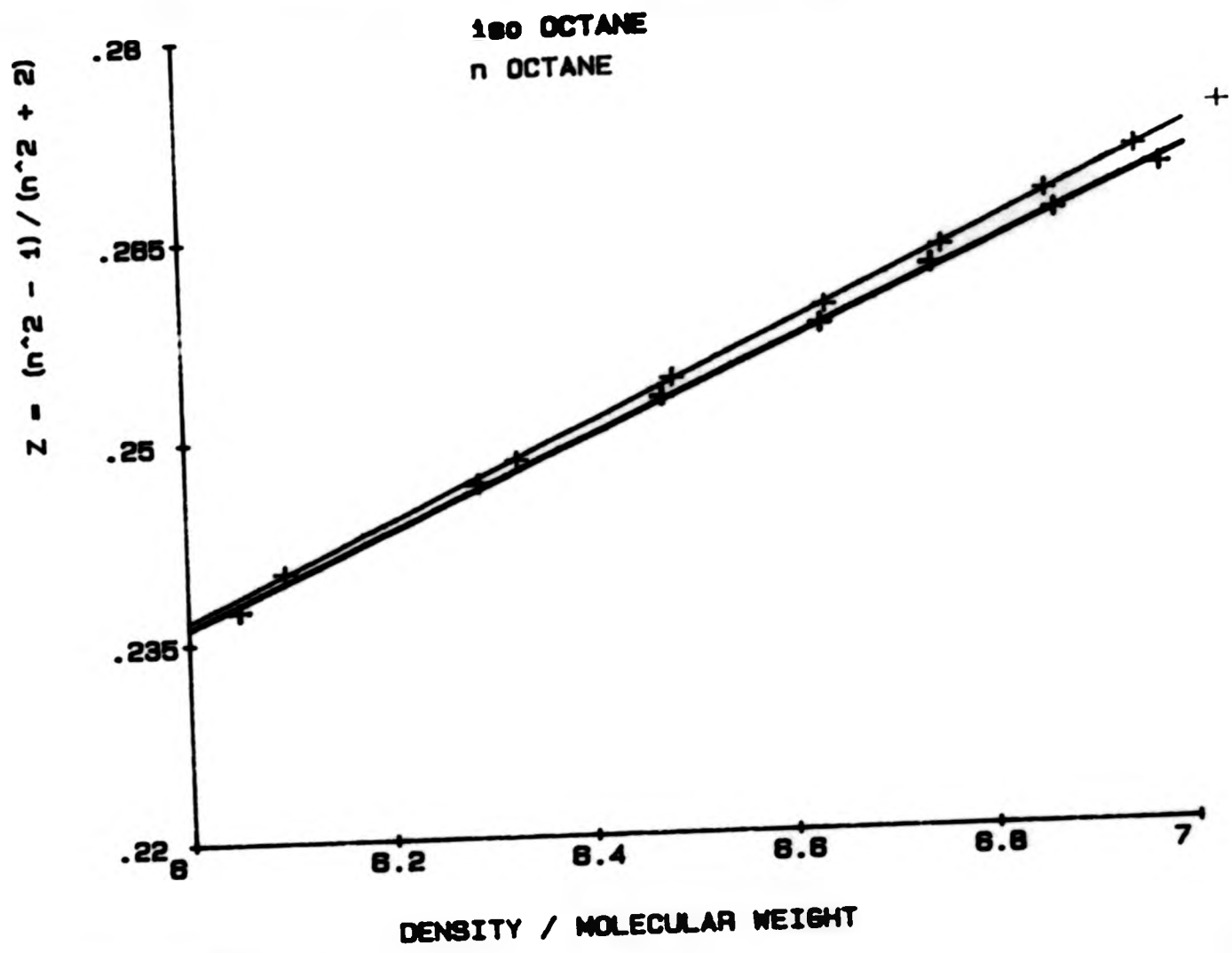
Fig. 4.13

n- & iso- OCTANE MOLAR REFRACTIVITY
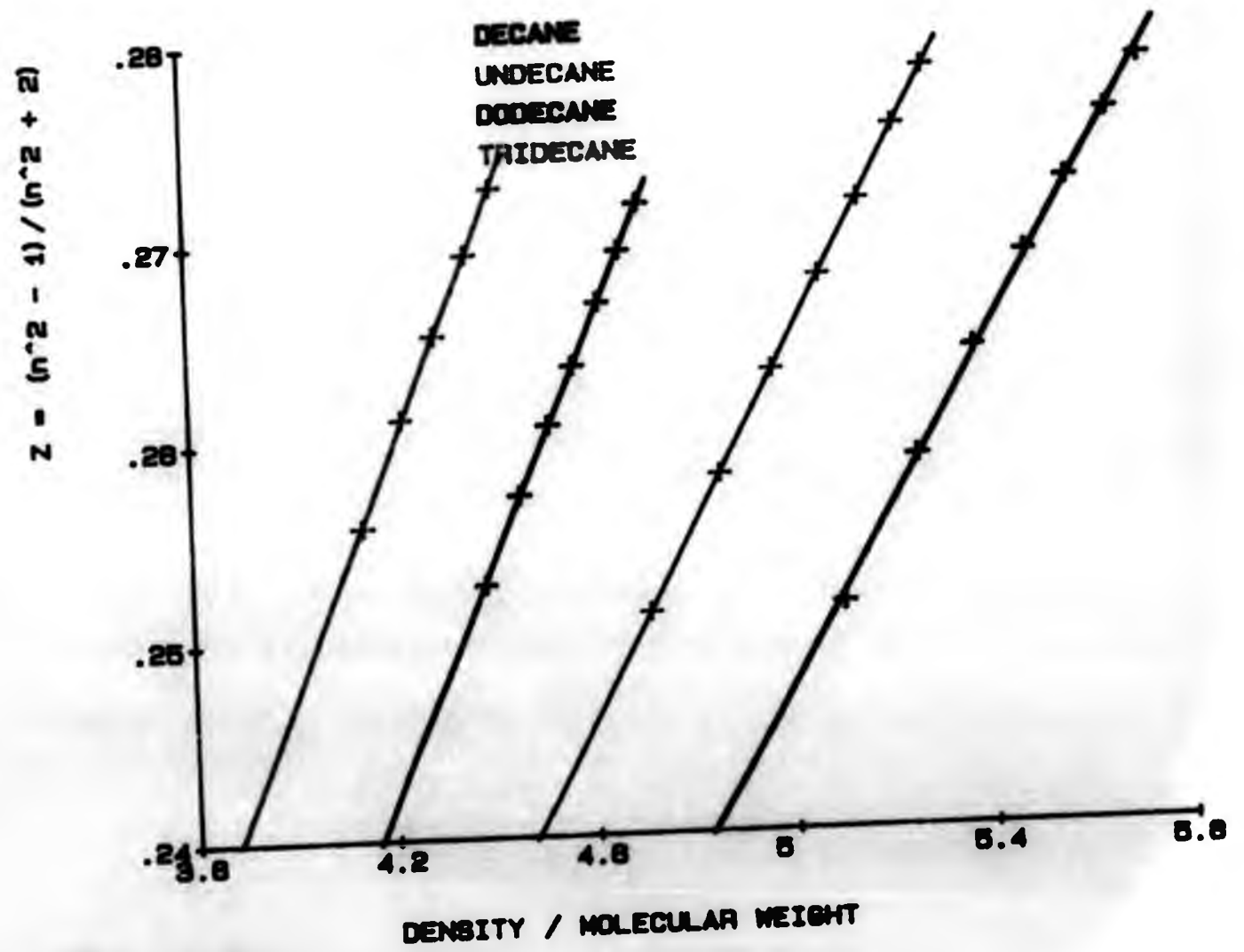
Fig. 4.14

C10 - C13 MOLAR REFRACTIVITY
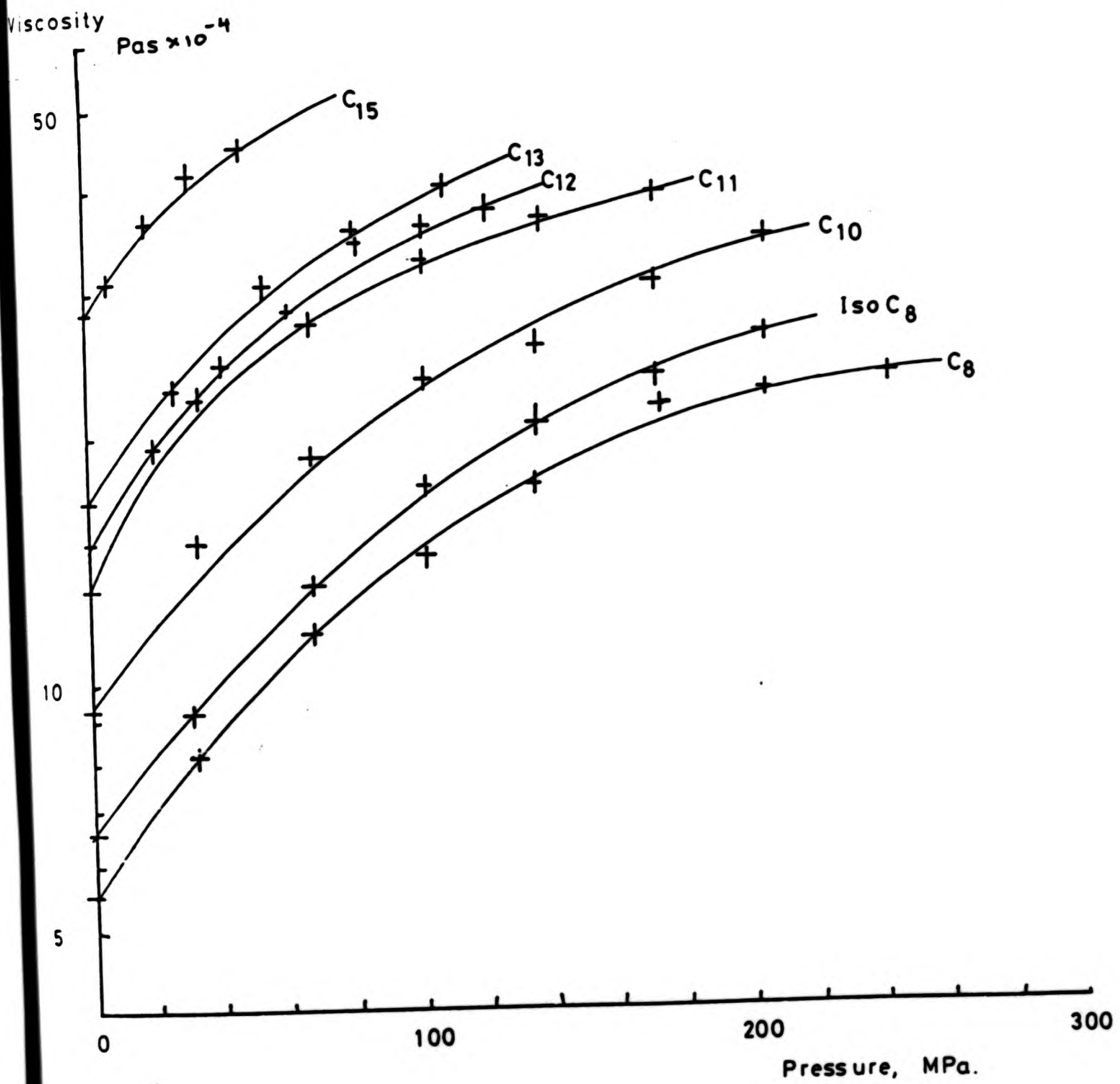
Fig. 4.15   Viscosity of alkanes.
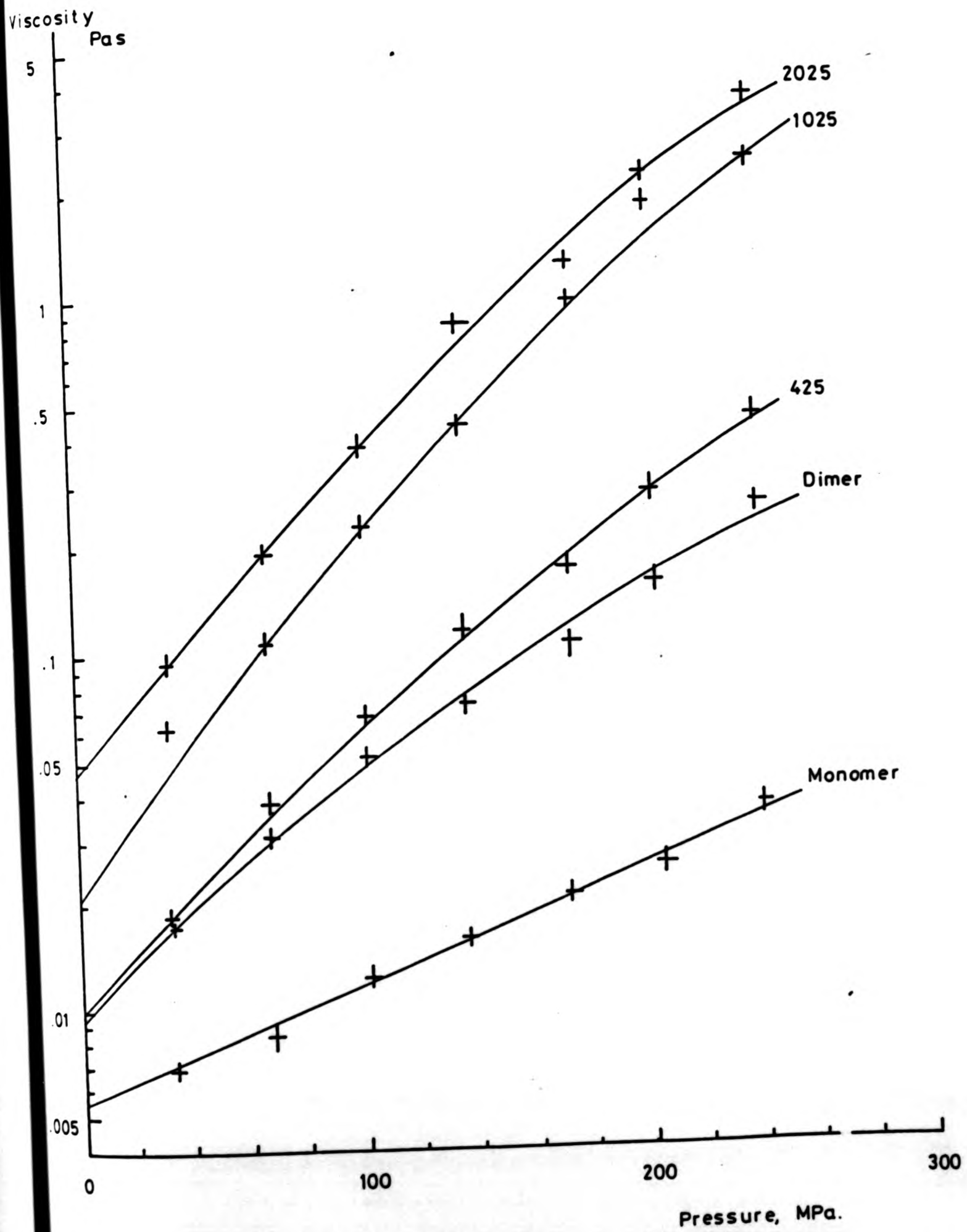
Fig. 4.16   Viscosity of polypropylene glycols.
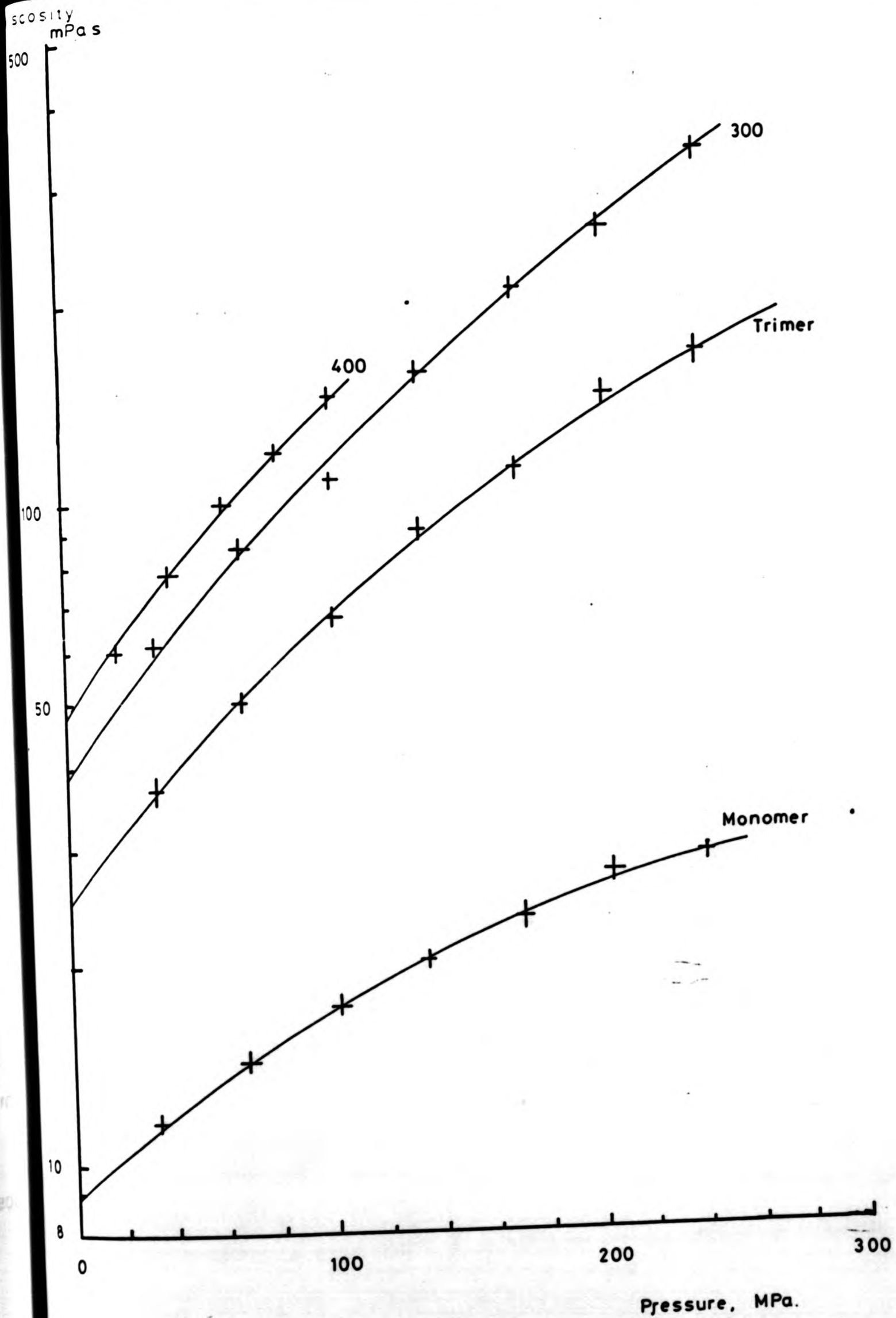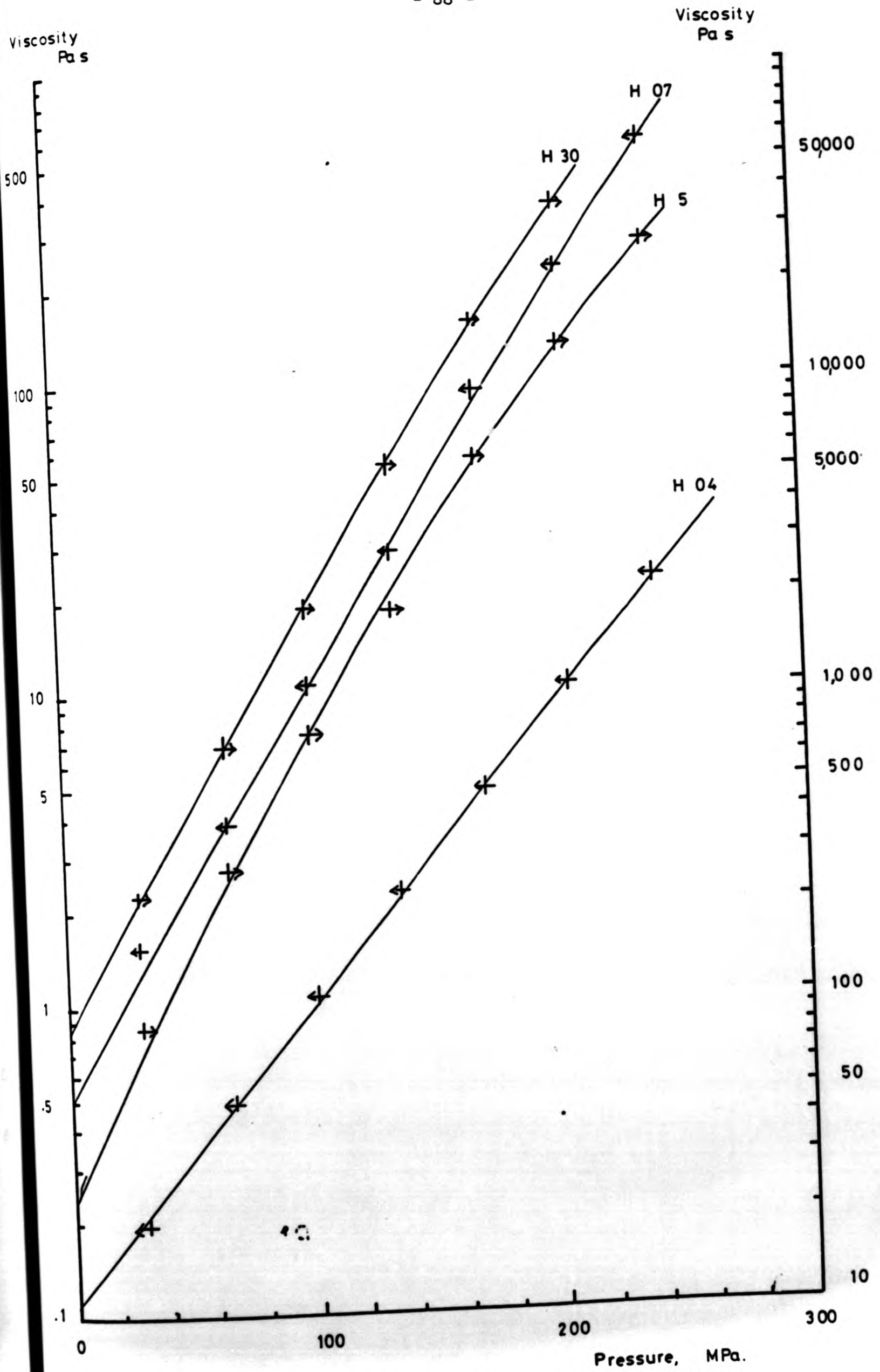
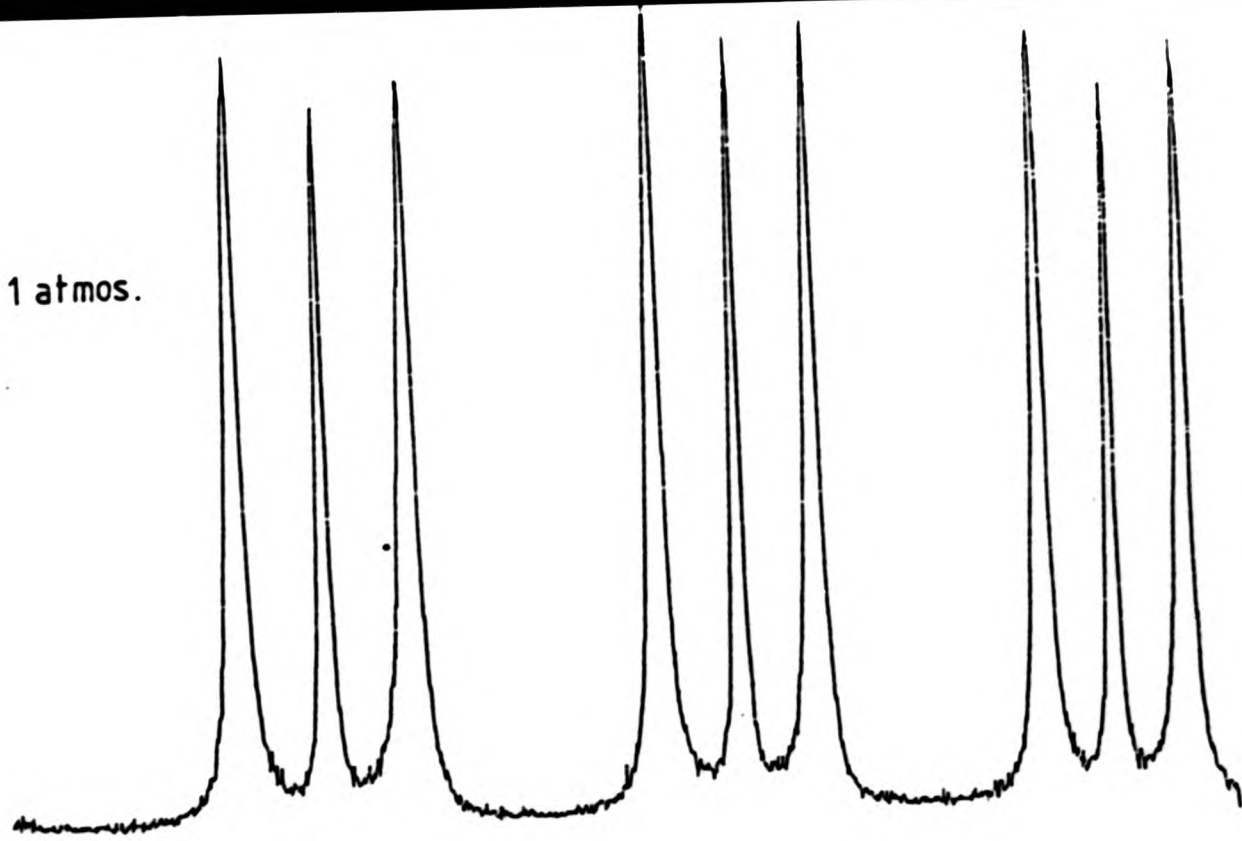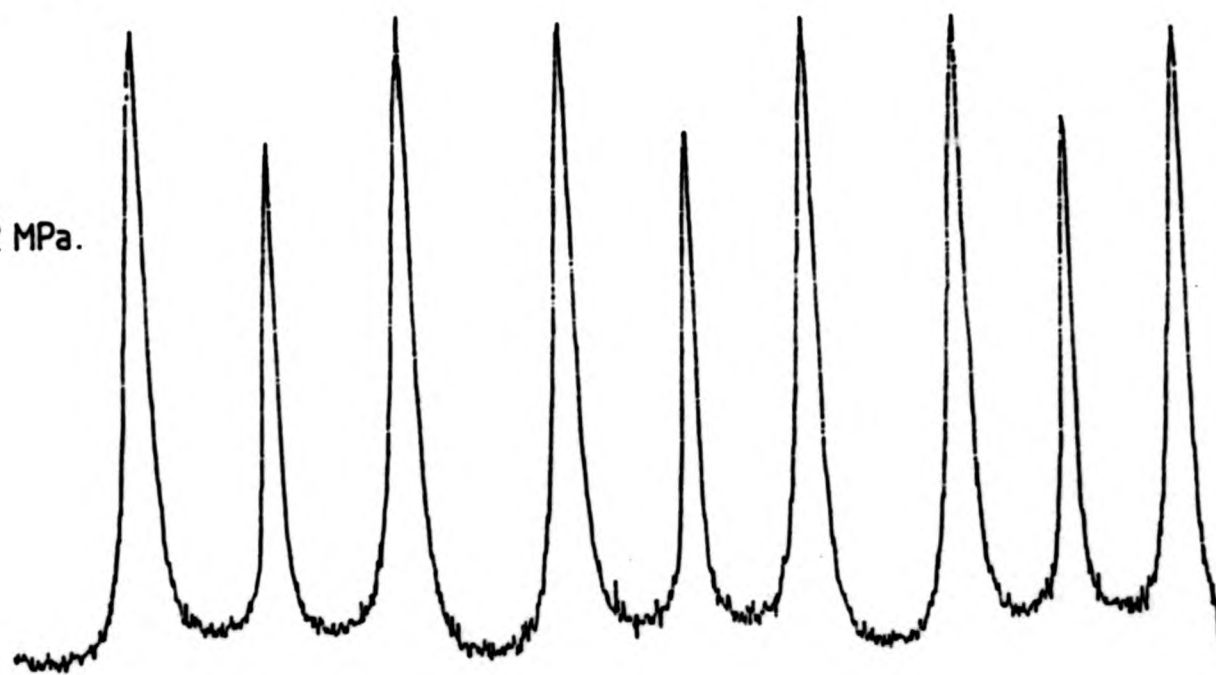Fig. 4.17   Viscosity of polyethylene glycols.
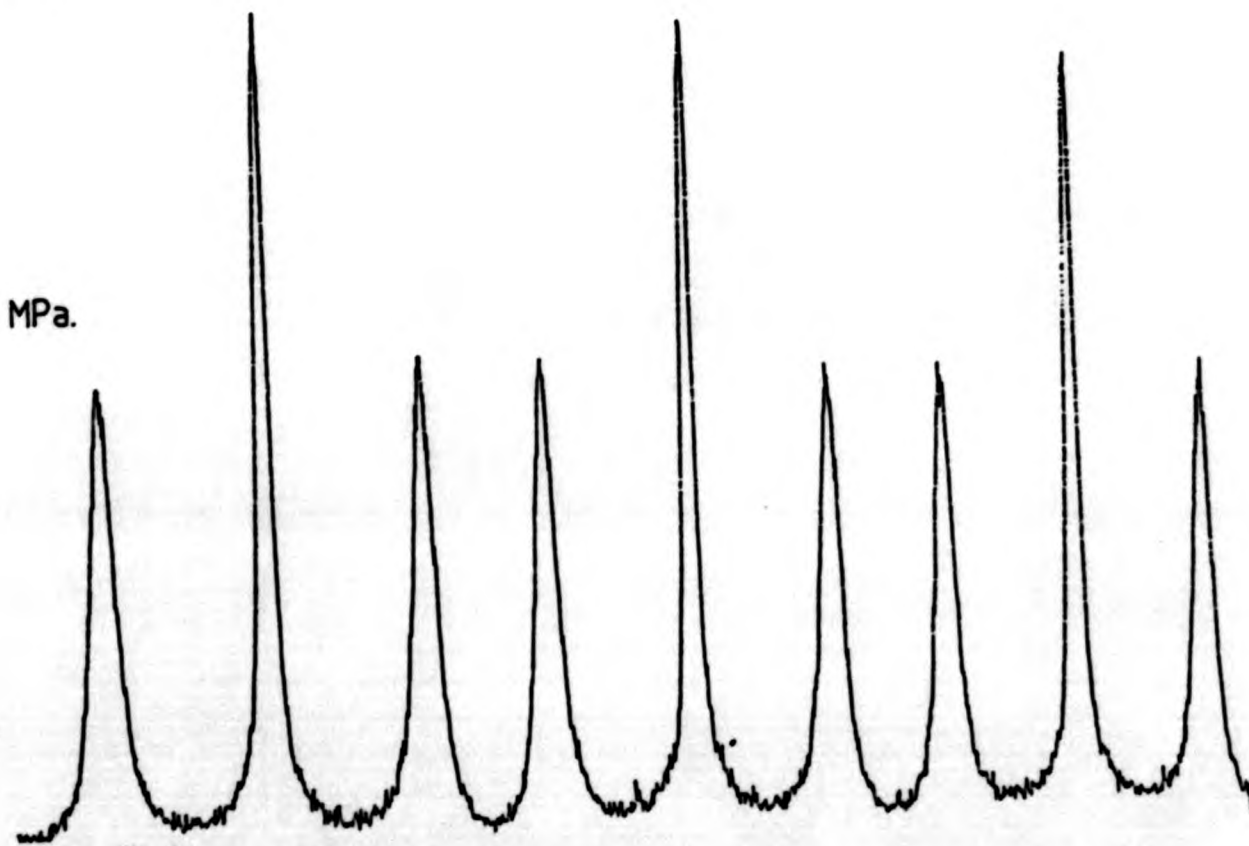
Fig 4.18   Viscosity of   polyisobutenes

Fig. 4.19   Brillouin spectra of n-octane.
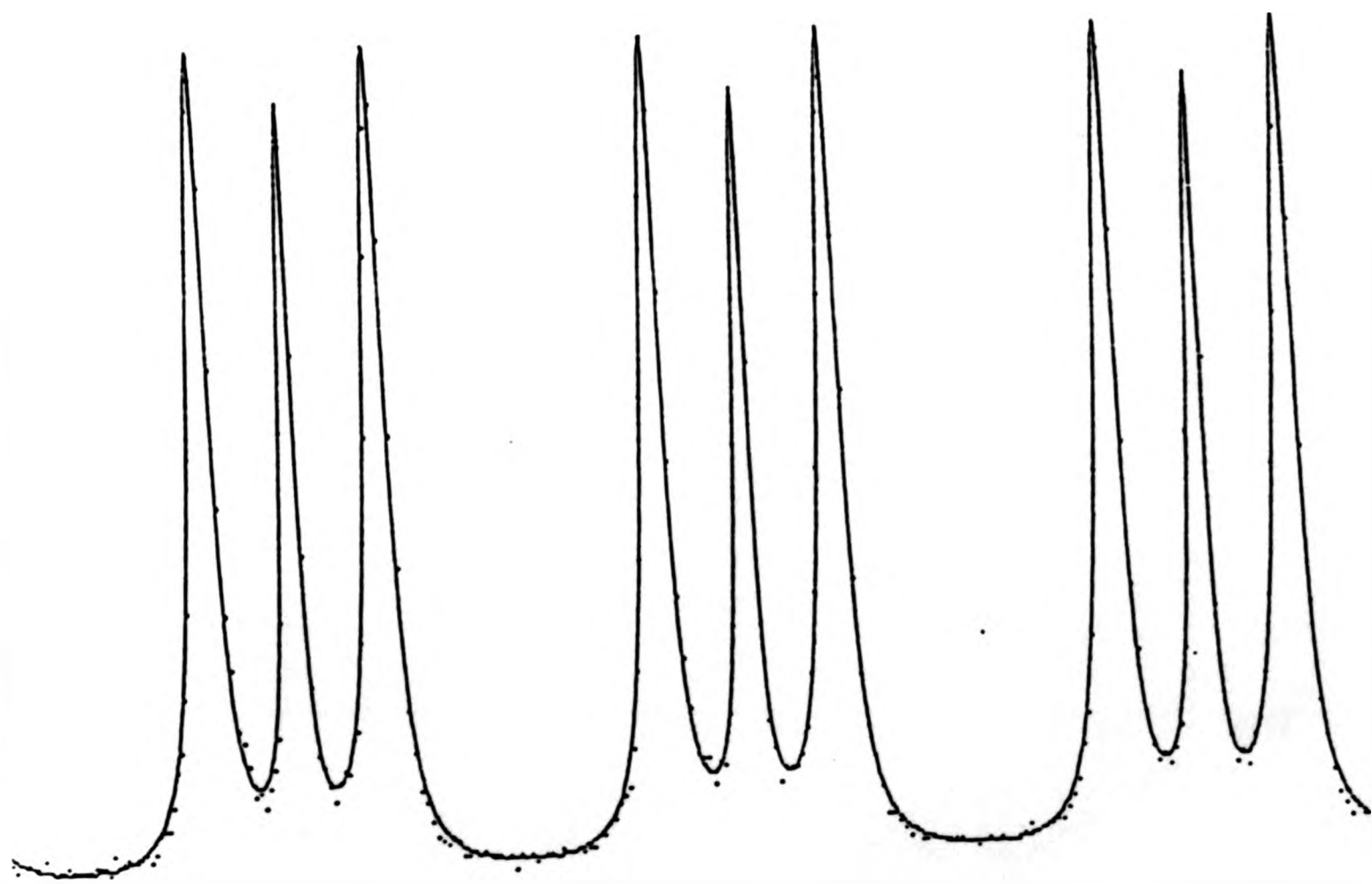FSR =18.45 GHz , T= 22 °c.

Fig. 4.20   Brillouin spectrum of iso-octane
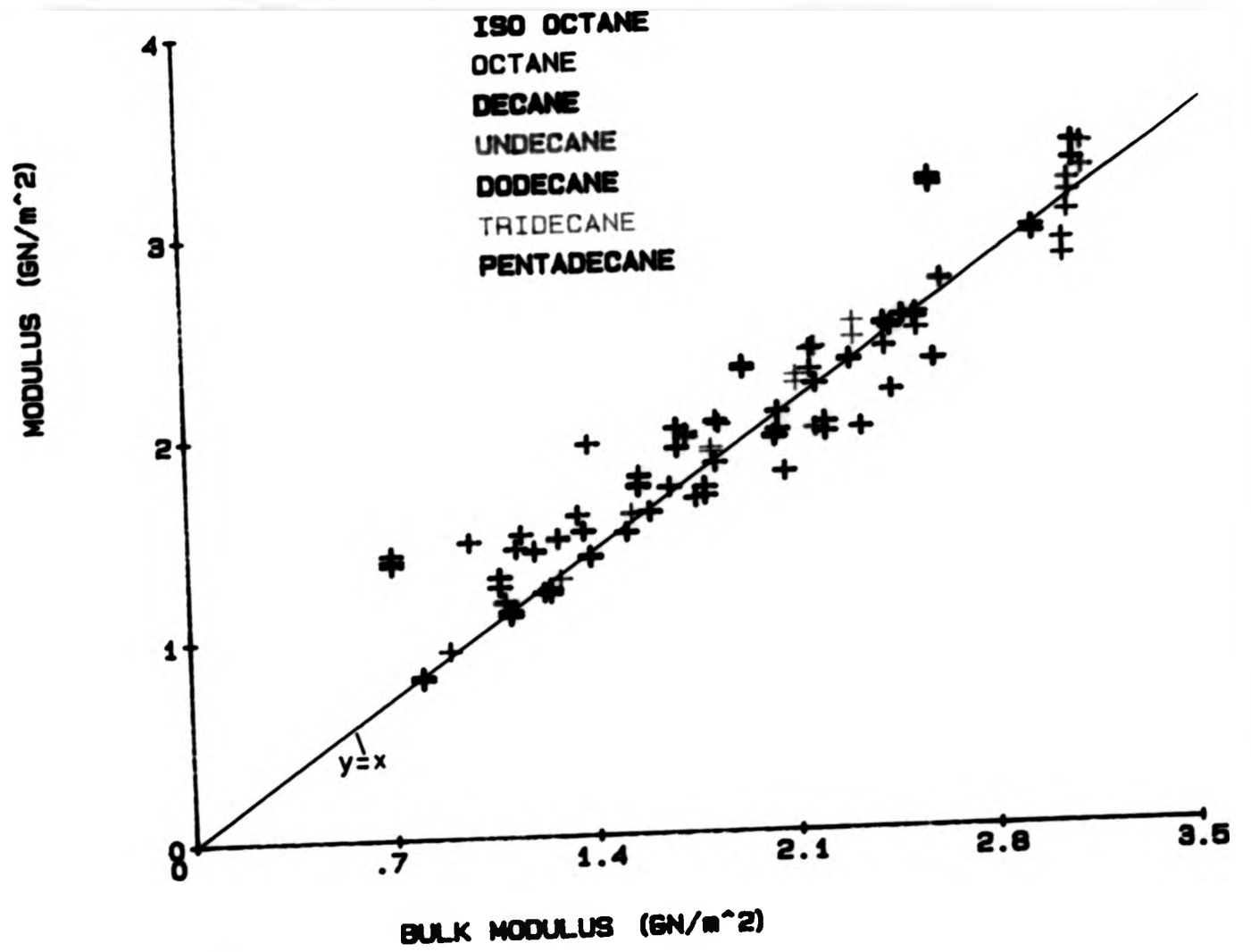showing every 4th datum & the fitted function.
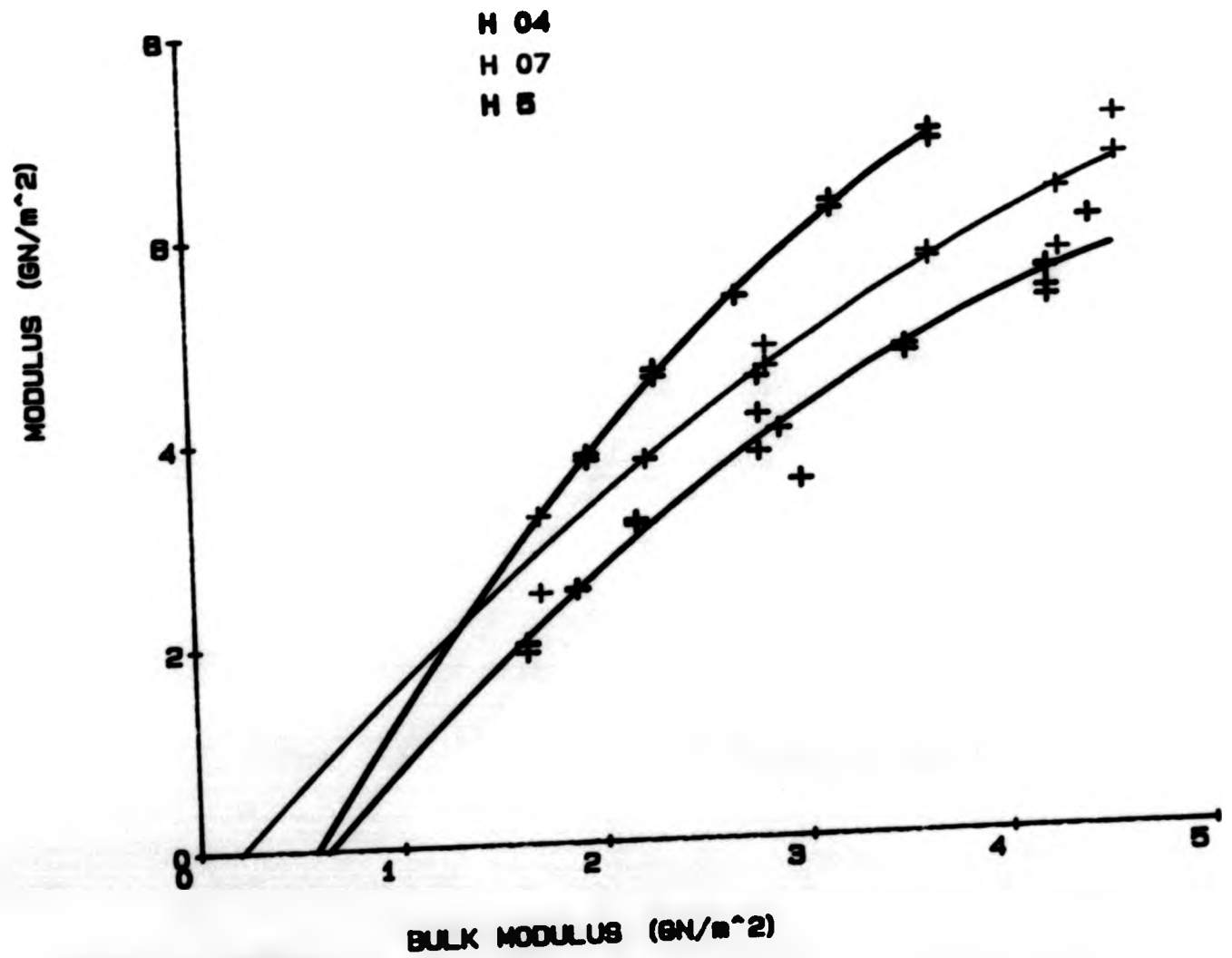
Fig. 4.21(a)

ALKANES : RATIO OF MODULI

Fig. 4.21(b)

POLYISOBUTENES : RATIO OF MODULI

- 91 -
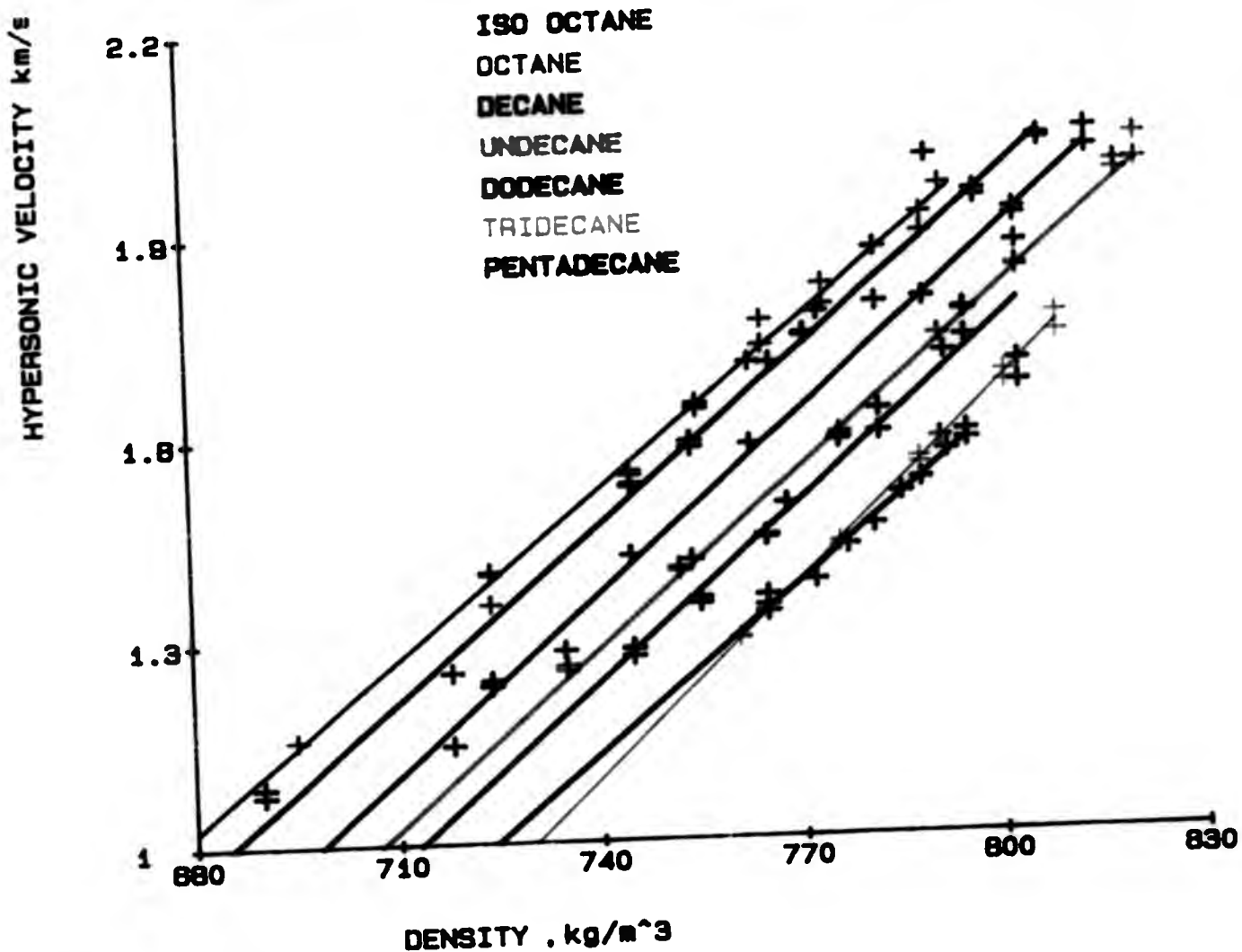
Fig. 4.22a.

ALKANES PHONON VELOCITIES
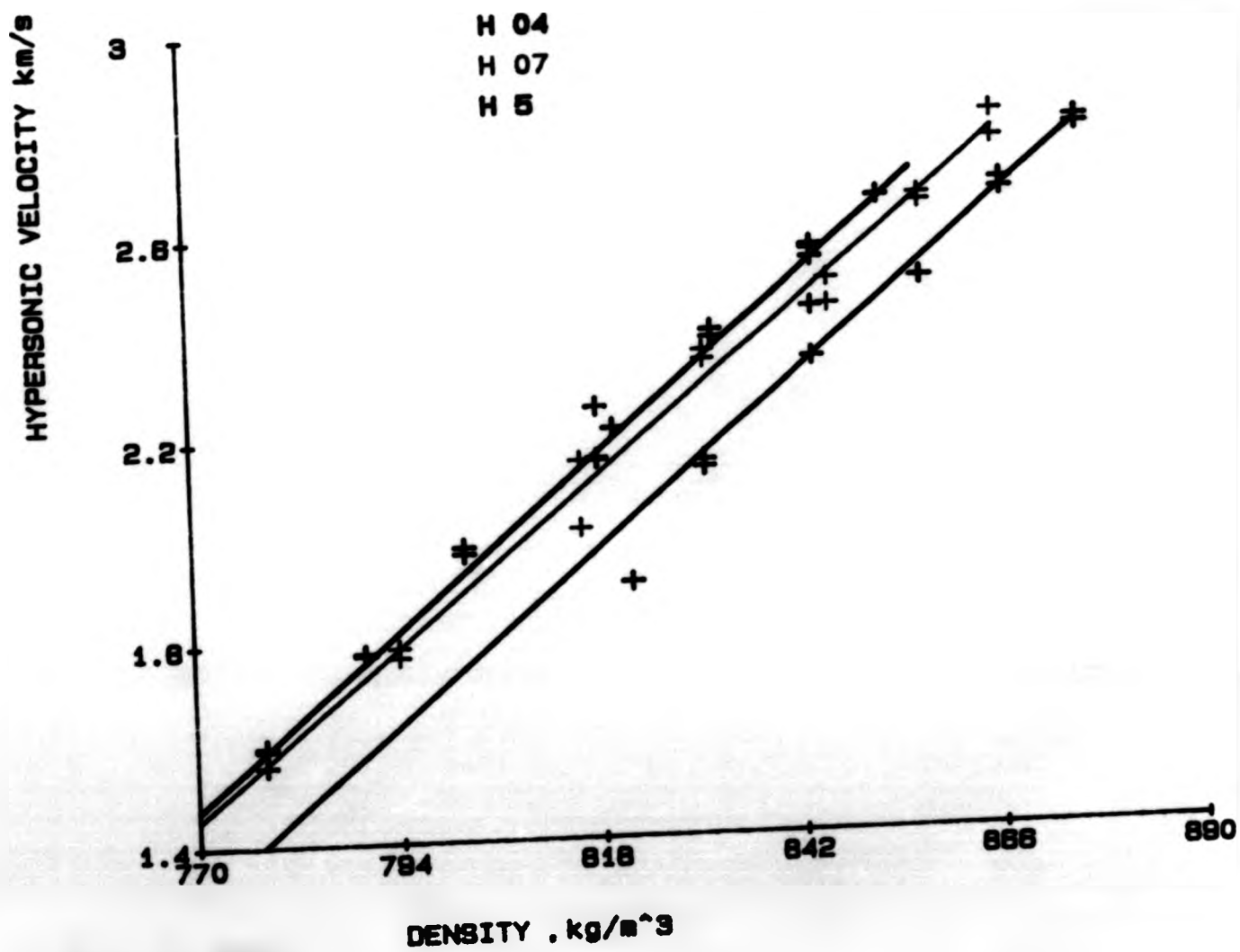
Fig. 4.22b.

POLYISOBUTENES PHONON VELOCITIES

- 92 -

CHAPTER 5

CONCLUSIONS AND DISCUSSION

'We see that wine flows through a strainer as fast as it is poured in; but sluggish oil loiters. This, no doubt, is either because oil consists of larger atoms, or because they are more hooked and intertangled, and, therefore, cannot separate as rapidly, so as to trickle through the holes one by one'

Lucretius (fl 60 BC): 'on the nature of
the universe' Book II

Contents

CHAPTER 5 CONCLUSIONS AND DISCUSSION

1 Comparison of Data with Literature Values

Direct comparison of the high pressure data with literature values is
not possible in most cases, due to the paucity of relevant investigations.
Where data are available, comparison is made difficult, since:

no high pressure dispersion data are available, while any
literature values of refractive index are for other wave-
lengths,

temperatures are generally non-ambient, requiring inter-
polation,

the spacing of pressure datum points may be much greater
than in the present work (eg Bridgmann's data).

In view of this, data comparison depends on atmospheric data, where
available, together with an appraisal of trends where high pressure data
exist. So far as atmospheric pressure data are concerned, the refractive
index, density and viscosity were all measured using instruments calib-
rated with reference to literature values [83,75,84].

The behaviour as a function of pressure, of $\Delta n_{632.8}$ for nC_8 and nC_{10}
at 25 °C is similar to that given for $\Delta n_{546.1}$[30]. Bridgmann's
compressibility data for nC_8, nC_{10}, nC_{12} [85,73], 1SO C_8, ethylene
glycol, diethylene glycol, and propylene glycol [86], as well as his
viscosity data for nC_8 [52] and nC_{10} [87] are all in agreement with the
present data, bearing in mind that his datum points are far more widely
spaced than in the present work. The measurement of viscosity of H5
and H30 [71] by Dandridge and Jackson also agrees within experimental

- 94 -

error. In the case of the Brillouin data, the hypersonic phonon velocities of C_{12} correspond to the literature value [44] at atmospheric pressure, and sound velocities of C_8 and C_{12} at high pressure [45] show a similar trend. The atmospheric pressure data for HO4 and H5 are similar to those obtained by Champion and Dandridge [46] for polyisobutenes of similar molecular weight at 25 °C.

2   Summary

(i)   Experiments have been designed and performed to measure the refractive index, density, viscosity and Rayleigh-Brillouin spectra of liquid samples at ambient temperature, and pressures up to 240 MPa.

(ii)   Data are presented for members of four homologous series of short chain liquid polymers including, and similar to, the n-alkanes.

(iii)   The density has been shown to be adequately described by a cubic polynomial in P.

(iv)   The Lorentz-Lorenz equation has been shown to describe the refractive index as a function of the density.

(v)   The constant molar refractivity implies that the free volume is linearly related to the density, and it has been shown that the viscosity is directly dependent on the density, for a given sample.

(vi)   Hypersonic phonon velocities have been measured for the alkane and some polyisobutene samples and have been shown to be linearly related to the density. This is consistent with pressure data for benzene [13], and with ultrasonic data for

various organic liquids [88], but not with thermal data of Champion and Jackson [44].

(vii) No viscoelastic relaxation was observed for the alkanes, but a fast relaxation was found for the polyisobutene samples.

3 Discussion

Considering the results of this work as a whole, it appears that the important variable is in all cases the density. A model describing the mechanism giving rise to the density, would be invaluable in predicting the pressure dependence of these bulk parameters. The variation in density of members of a homologous series of short chain liquid polymers is due to the change in molecular composition with molecular weight, that is, the comparative chain end: chain segment densities. Tables 3.1 - 3.4 show that, while ρ increases with M for alkanes, PIB and PEG, it decreases for PPG. As found by Champion and Dandridge [46] for PIB, a near-linear relation exists between density and reciprocal molecular weight for all four series (PPG having positive slope). Also, whereas the change in density with pressure decreases with increasing molecular weight in the case of alkanes and PIB, it increases for PPG and PEG (figs 4.8 - 4.12). The phonon velocity, increasing with molecular weight for alkanes and PIB has been found to decrease in the case of PEG and PPG [89,90].

In order to quantify these observations, some method of relating molecular volume to molecular constitution is required. In the following, it is assumed that the molecular volume is composed of additive contributions, ie

$$v = \alpha + \beta + \gamma + \delta \ldots$$

- 96 -

where v is an average volume associated with a molecule, and α, β, γ... are parameters related to molecular contributions, as detailed below.

In the first model, it is assumed that the effective volume occupied by a molecule comprises occupied volume and associated free space, each compounded from two contributions, that due to the sum of the 'chain segments', and that due to the 'chain ends':

$$v = na + lb$$

where n is the number of (repeating) chain elements, a and b are constants for a 'chain' and 'end' unit, respectively and l is the number of 'end units' per molecule. The mass of the molecule is clearly given by

$$m = nc + d$$

where c is the mass of a chain unit and d the summed mass of the end groups. Thus

$$\rho = (nc + d)/(na + lb) \tag{5.1}$$

Since ρ, c, d are known for a range of n and pressure, and since l will be constant for a given series, the ratio a:b, or the relative volumes associated with a chain segment and an 'end group', may be computed. Since the specific molecular volume has been shown to be independent of pressure for the series studied, any changes in a:b must be attributable to changes in the free volume associated with the chain and the chain 'end'.

- 97 -

In order to perform this calculation, it is necessary to define what is meant by an 'end group', ie to assign values to c and d (and hence to n and l). Since the end group is expected to have an associated free volume independent of that associated with the chain, the end groups have been assumed to be the last groups which sweep out a volume upon rotation about the bond attaching them to the chain. Following this argument, the alkane end groups will be CH_3 rather than single - H atoms (see Table 5.1). The end group of the PIB chain has been taken as the $C \genfrac{}{}{0pt}{}{= CH_2}{= CH_3}$ group, though this choice is debatable. However, the choice is arbitrary, since changing the initial magnitudes of a or b simply moves the curve up or down the axis (see Figs 5.1 - 4).

Also shown (Figs 5.5 - 8) is the variation of $\Delta a/a$ and $\Delta b/b$ for a constant increment (10 MPa) in pressure.

An estimate of the specific molecular volume may be obtained by summing the Van der Waal's radii of the constituent species [3]. In a similar manner, the ratio a_o/b_o may be computed for each series, where a_o and b_o are the 'occupied' or Van der Waal's volumes of a chain segment and end group, respectively.

These ratios are shown in Table 5.1, using the Van der Waal's radii: H: 1.0×10^{-10} m, C: 1.7×10^{-10} m, O: 1.4×10^{-10} m.

Some general remarks may be made from this model. Firstly, note that the curves in Figs 5.1 - 4 are smoothly varying: since each datum point is compounded from all the molecular weights studied in each series, this implies that the assumption that the elemental volumes are additive is justified. In the cases of alkanes and PIB a/b is initially less than a_o/b_o, and approaches it as the pressure increases: for PEG and PPG, a/b, (initially greater than a_o/b_o),

- 98 -

also approaches. In the limit of high pressure, the Van der Waal's volume may be seen as an asymptote. Bondi [3], extrapolating Bridgmann's n-heptane data, predicts this to happen around 6600 MPa: a gross linear extrapolation of the present data yields a value in the region 3000 MPa. Considering the inaccuracy of such an extrapolation, this agreement is very good. The characteristics of the curves may be compared with the freezing behaviour of the samples. Whereas n-alkanes freeze to form lamellar crystallites, PEG and PPG both freeze to form spherulites [93]. PIB samples with measurable viscosity at room temperature have been reported, having very high molecular weight (> 6000 [84]), and so it may be hypothesised that PIB will not freeze at any pressure near to those investigated.

The ratios of a/b for alkanes and PIB both increase with pressure, implying that the chain end volume compresses more rapidly than the segmental volume. Fig 5.5 shows that the compression becomes more important as the end volume change decreases: it is possible that above about 150 MPa some ordering of the molecular chain orientation exists. Both curves in Fig 5.6 have the same sense, showing that the PIB molecule compresses reasonably evenly, the fact that neither chain nor end groups dominate the compression implying a lack of ordering and the probability that the material will continue to behave in a glassy state at higher pressures.

The ratios a/b for PEG and PPG both decrease with pressure, though PEG appears to start levelling out while PPG does not. Fig 5.7 shows precisely the opposite features to Fig 5.5, and it may be inferred that in the case of PEG the primary variable is the segmental volume change.

- 99 -

Finally, the similar sense of the greater part of the curves in Fig 5.8 together with the lack of levelling out in Fig 5.4, predict a similar non-freezing behaviour to that seen for PIB.

In an attempt further to quantify these statements, a model involving chain flexibility was employed. In this model, the fit depends on the number of each type of bond, so that the molecular volume is given by:

alkanes $\qquad v = (n - 1)a + (2n + 2)b$

PIB $\qquad v = (4n + 2)a + (8n + 8)b + e$

PEG $\qquad v = na + 4nb + 2nc + 2d$

PPG $\qquad v = 2na + 6nb + 2nc + 2d$

where the variables a, b, c, d, e depend on the C - C, C - H, C - O, O - H and C = C bond volumes, respectively. To test this model, a and b were computed (as functions of pressure) for the alkanes, and these values used to predict e from the PIB data, and c and d from the PEG data. These values were then used to predict density data for PPG. The values of c and e were negative, and of the order -2na and -1000a respectively: the predicted values of ρ_{PPG} were too small by a factor of around 5. The failure of this model shows that the relative position of the bond as well as its type plays an important part, for instance, the volume occupied by the side group Me in polyisobutene is much smaller than that occupied by the same group at the chain end in alkanes.

In this context, it is interesting to note that the constitutive formula for PIB may be written as $C_m H_{2m}$, compared with $C_n H_{2n+2}$ for the alkanes. Although these formulae are similar (especially for

high m and n), the highly branched PIB molecule is much stiffer and less flexible than the (longer, for m = n) alkane chain. Thus it is necessary to take account of the branching, and this may simply be done by introducing variables f and g to account for $C - C_3$ and $C - C_4$ bonds, respectively. Thus the formulae for PIB and PPG become:

$$v_{PIB} = (4n + 2)a + (8n + 8)b + e + ng$$

$$v_{PPG} = 2na + 6nb + 2nc + 2d + (n - 1)f.$$

However, this does little to improve the calculated values. Clearly, the introduction of yet more variables may lead to some sort of a fit, but the proliferation of variables leads to a lack of generality such that the final model would contain no more information than the simple 'chain segment' and 'chain end' model. It is, however, worth noting that in the former model, intermolecular interactions are tacitly included in the averaging nature of 'a' and 'b', whereas this is not the case in the intramolecular bond volume approach.

The Brillouin data show pressure behaviour which is almost independent of molecular weight, as predicted for chain molecules by Lin and Wang [89,90]. This also appears to hold for the thermal spectra of the n-alkanes [44] and PIB [46], supporting the view [90] that Brillouin spectra of polymeric liquids depend on localised motions involving only a few segments. The extremely fast relaxation observed in the PIB data, is presumably attributable to an end group, of which the $C = CH_2$, not present in alkanes, seems most likely. This observation may help to explain the mobility of the polyisobutene chain: while the bulk of the molecules may be more or less constrained, the relaxing end group must be relatively free, providing the cavity necessary for the molecule to move in viscous flow. As the chain length

increases, the probability of coordinated segment movement, necessary for flow to occur, will necessarily decrease. The activation energy for viscous flow will be related to the end group bond energy: the curvature of the plots in Fig 4.21b appears to tend toward X = Y at some higher pressure, implying a decrease in τ with pressure. Thus increasing the pressure will have the effect of increasing the viscous flow activation energy. The dependence of log η on n^a, where a is a constant of value around $\frac{1}{2}$ [91,92], suggests that the probability of coordinated segmental motion is dependent on the mean chain end separation. The increasing rotational isomerism with pressure reported by Schoen et al [8] for the n-alkanes implies a decrease in the mean chain end separation, corresponding to the observation that the increase of η with pressure is less for the n-alkanes than for the other samples investigated.

4   Suggestions for Further Work

In order to obtain meaningful Brillouin data for the PIB samples it would be necessary to provide either a photon-counting system with a logarithmic output, or with a Pockels cell to modify the laser amplitude [5] in order to accommodate the large amount of unshifted scatter. PPG and PEG samples would also require a custom-built variable sample cell of welded, rather than glued, glass. While it would be of great interest to obtain molecular reorientation data for short chain liquid polymers, by depolarised scattering, the instrumentation problem posed by the scrambling of polarisation by the stressed optical windows is not trivial [94]: Raman spectra may prove simpler while yielding much useful data. The addition of thermal control to the massive blocks of steel constituting the bombs, would be relatively easy, and so P - T data could be easily obtained.

TABLE 5.1

Choice of fitted parameters for density:molecular volume relation

Series	Chain segment	c	End segment	d	n	l	a/b	a_o/b_o
n-alkanes	CH_2	14	CH_3	15	n_c-2	2	0.47	0.87
PIB	CH_2CMe_2	56	$CMeCH_2$	41	$n_c/2$	1	0.89	1.4
PEG	CH_2CH_2O	44	HO	17	$n_c/2$	2	2.46	2.2
PPG	CH_2CHMeO	58	HO	17	$n_c/2$	2	4.11	3.1

n_c is the number of backbone Carbon atoms.

Remaining CH_3 of PIB is assumed to 'add on' to the chain.

Values of a/b and a_o/b_o are at atmospheric pressure.

- 103 -

Fig. 5.1   Alkanes: ratio of volumes as a function of pressure.
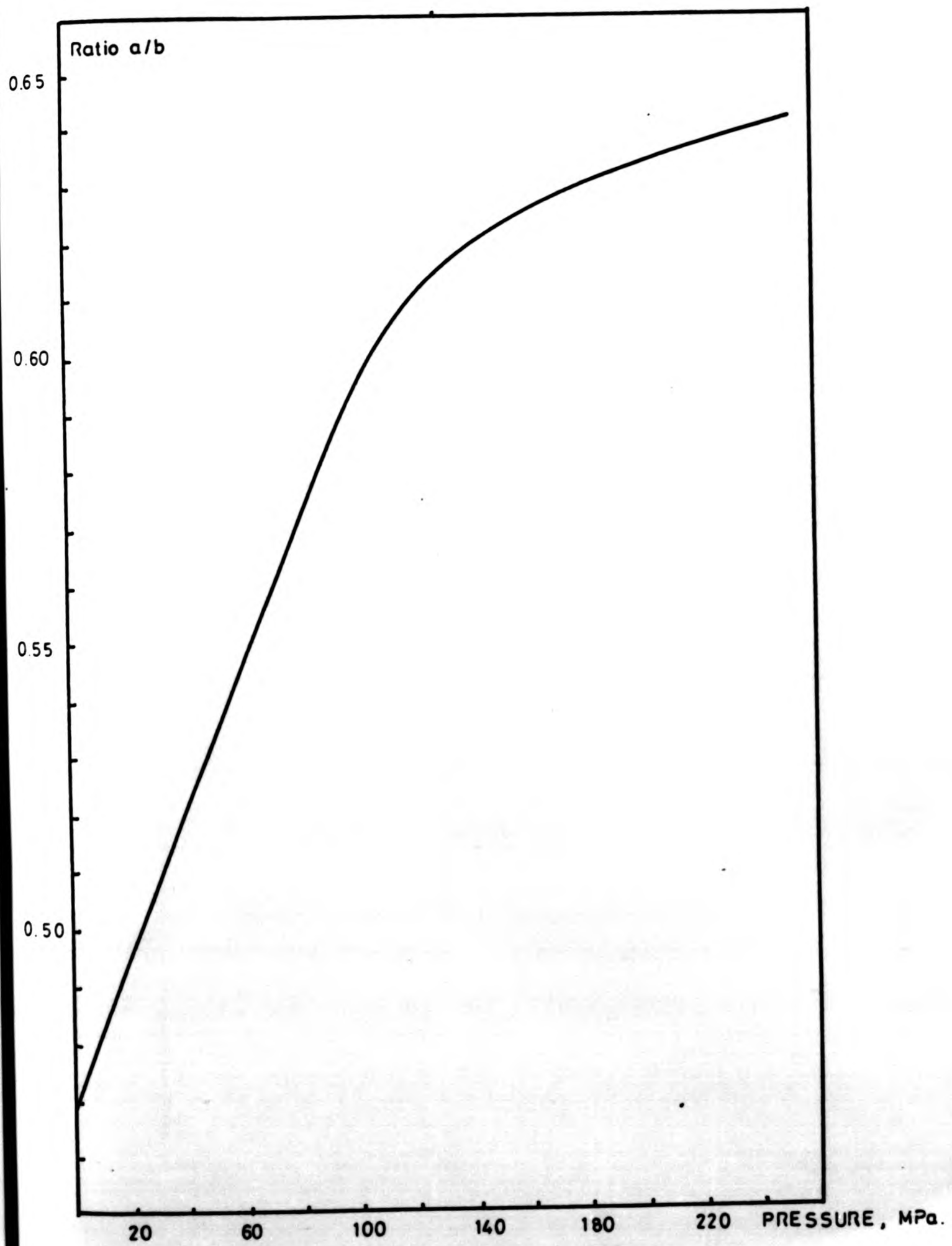
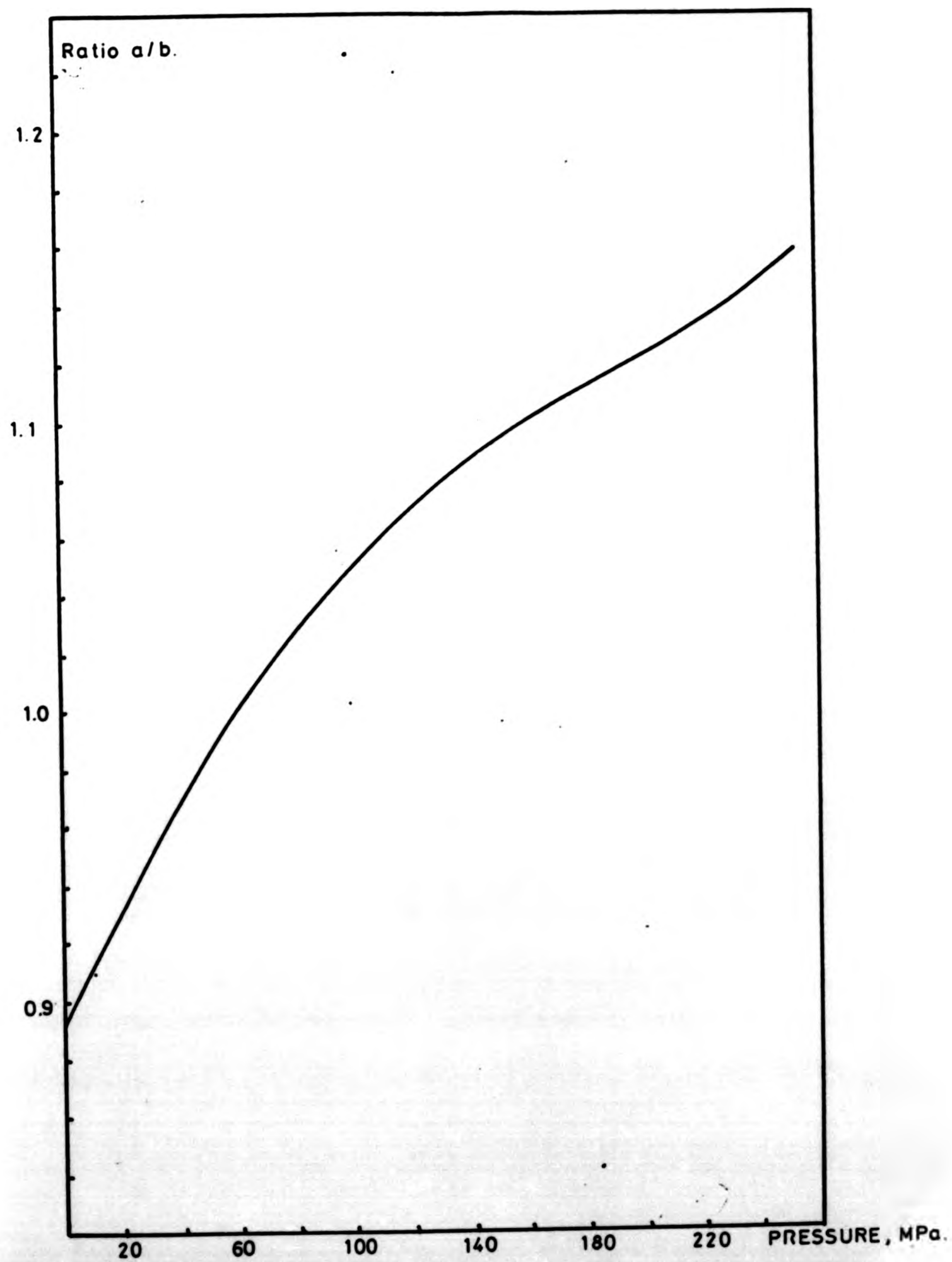Fig. 5.2   Polyisobutenes: ratio of volumes as a function of pressure.

Fig. 5.3 Polyethylene glycols: ratio of
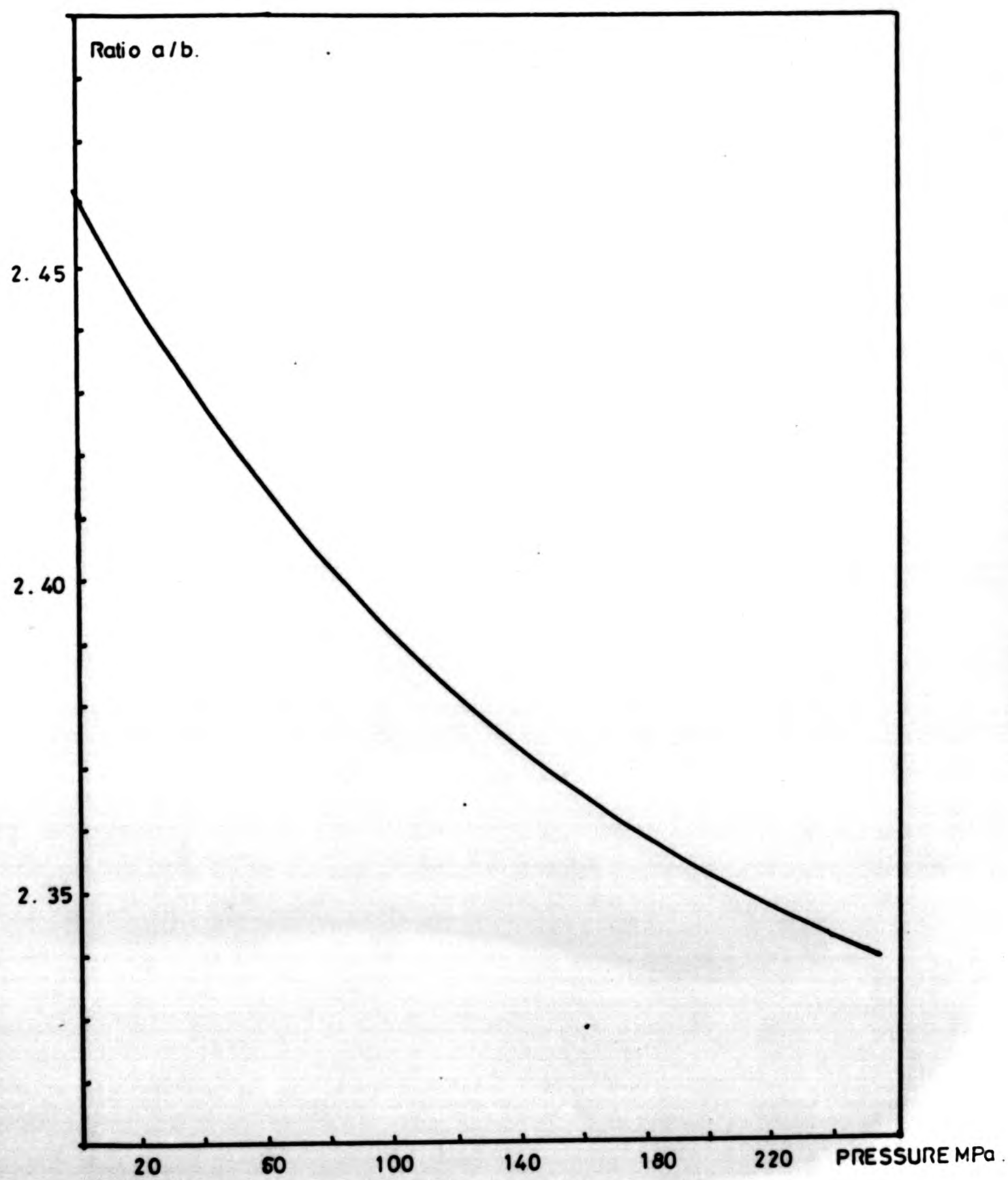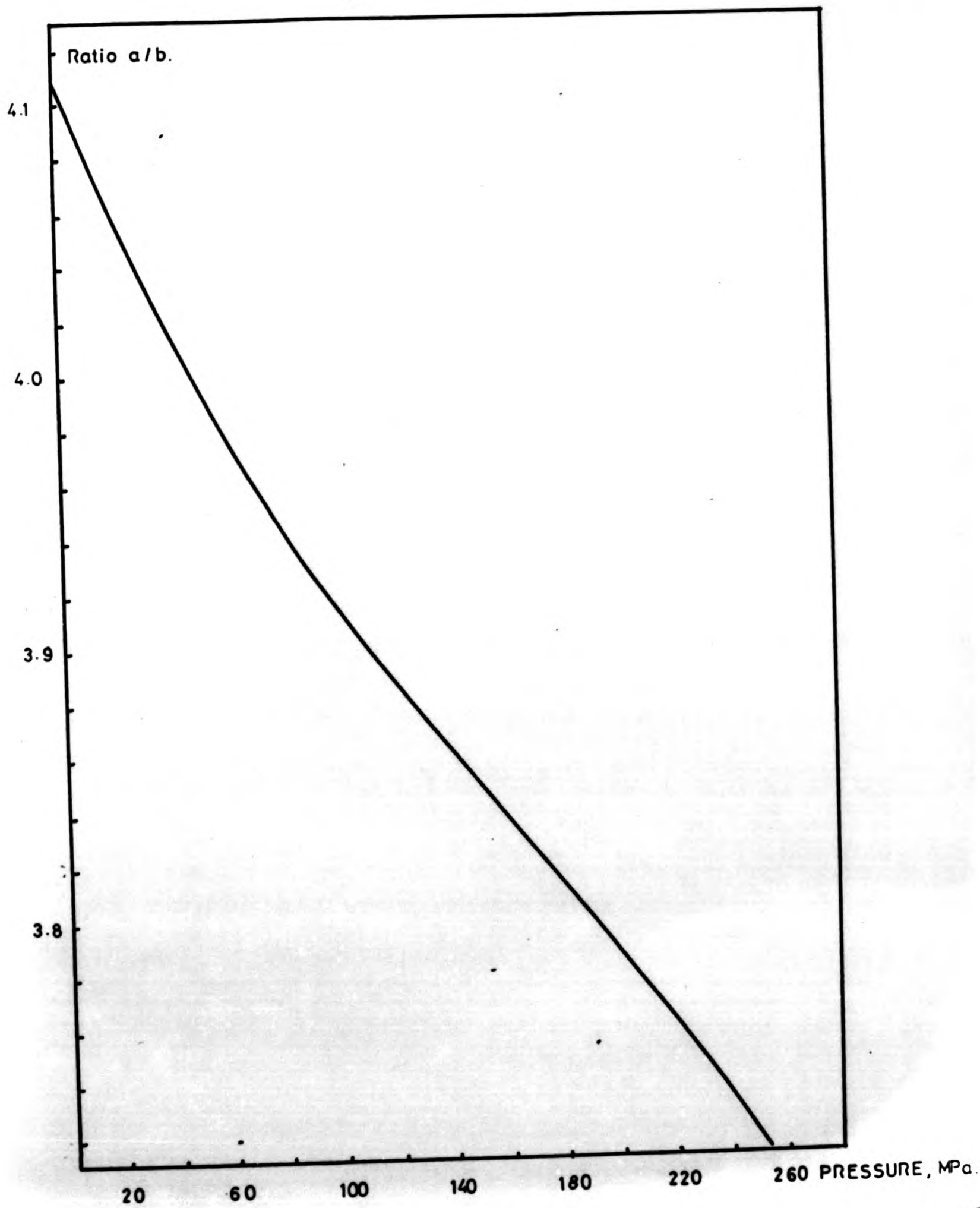   volumes as a function of pressure

Fig.5.4   Polypropylene glycols: ratio of volumes as a function of pressure.
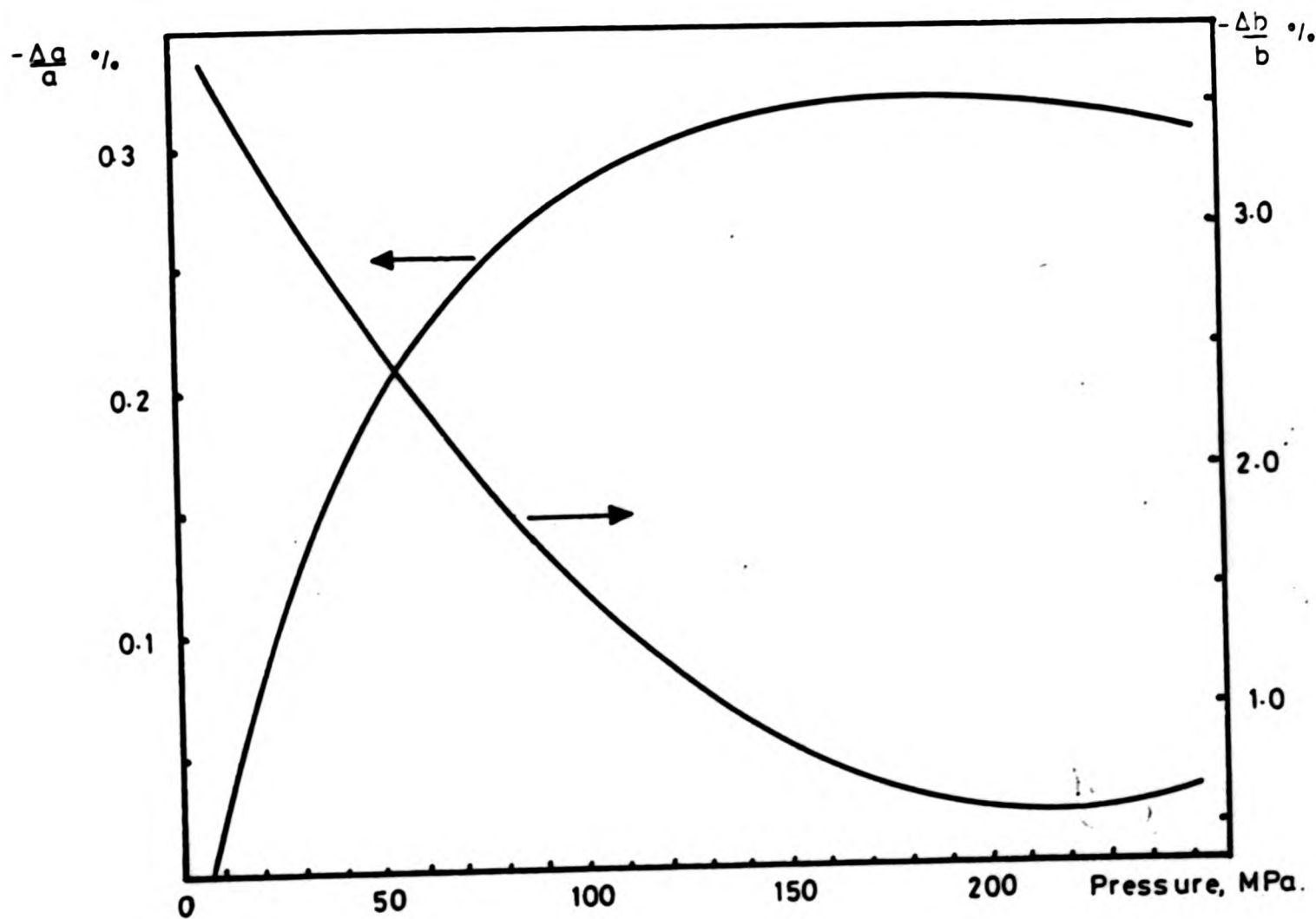
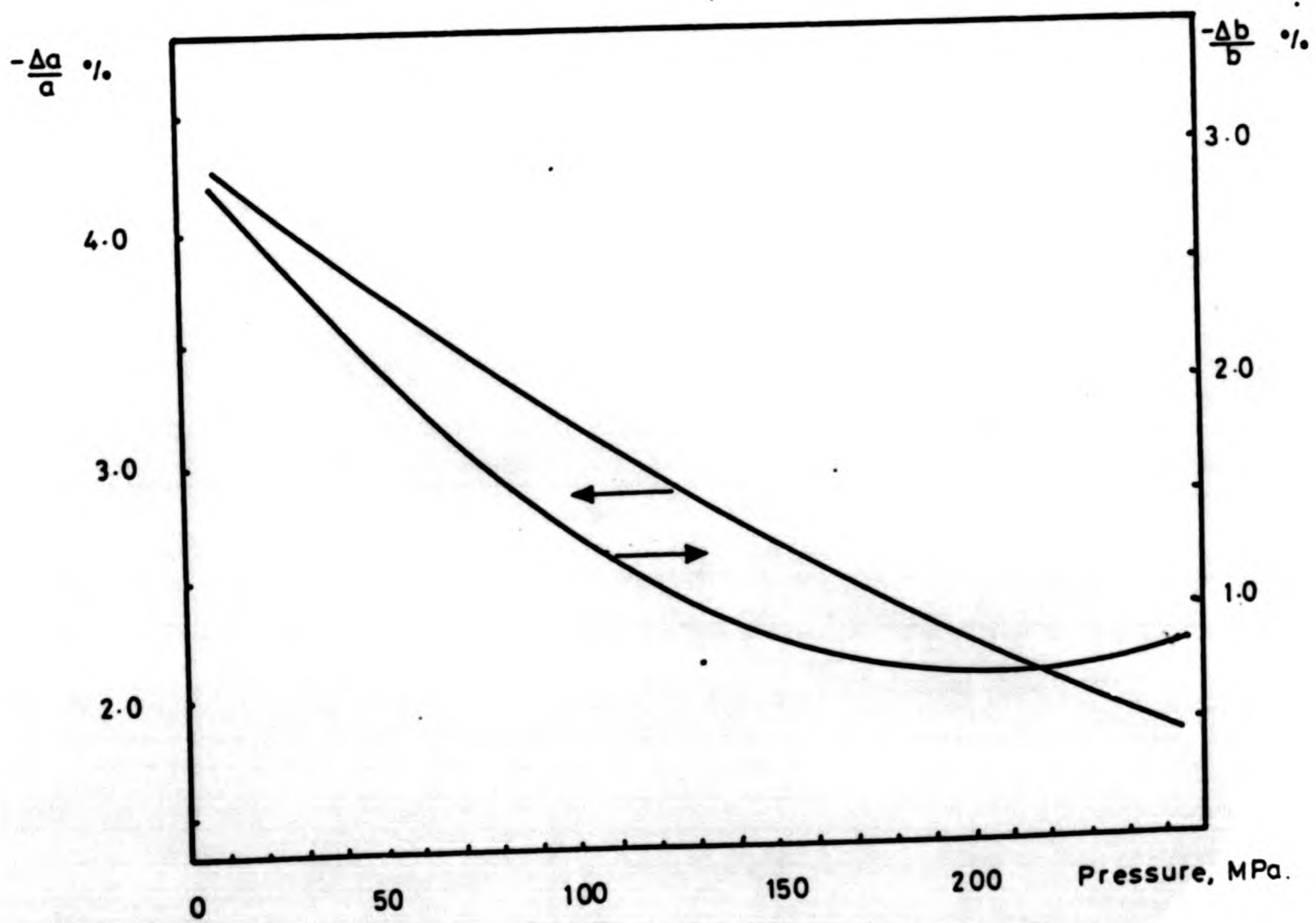Fig. 5.5 Alkanes : rates of change of a & b.

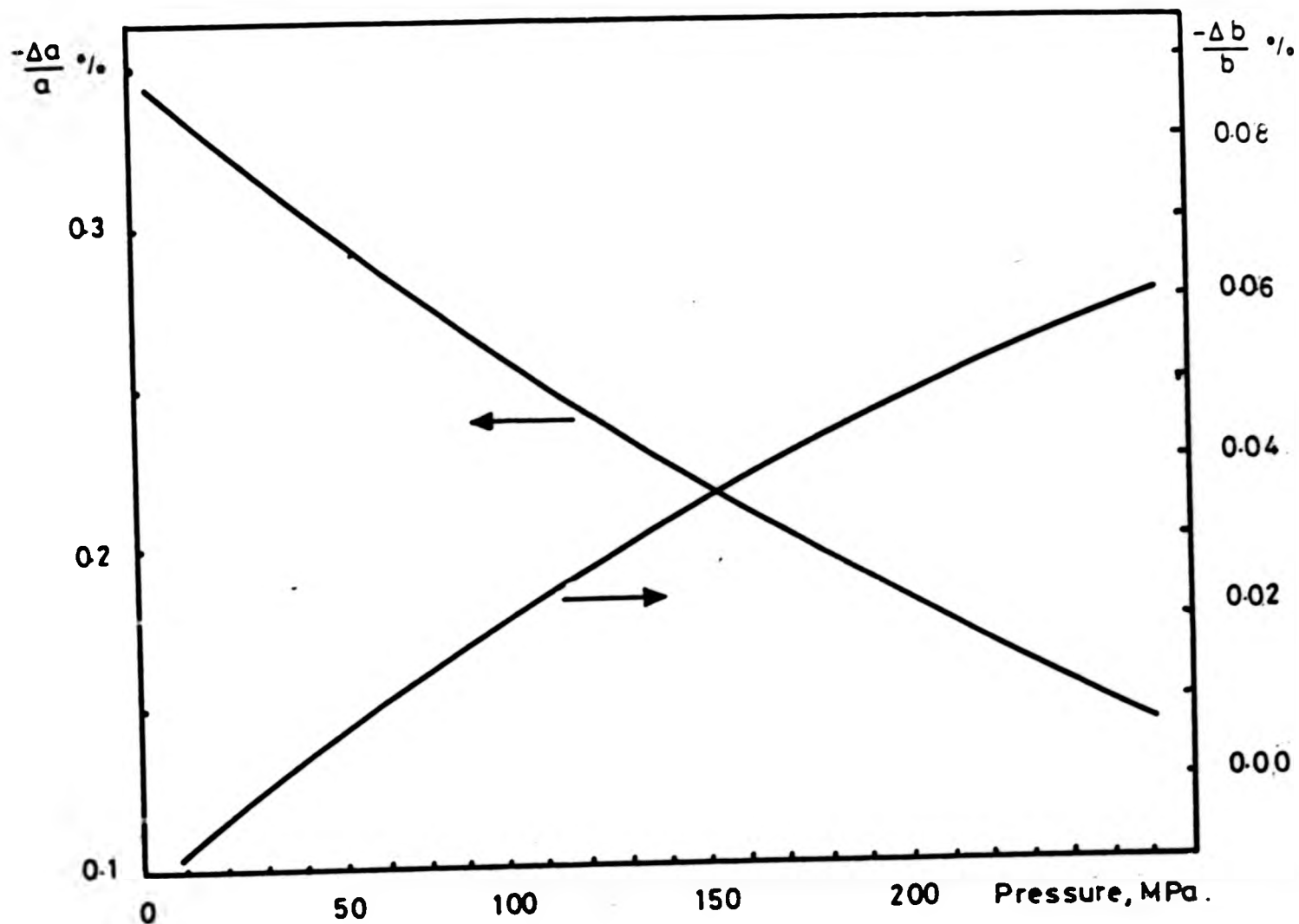Fig. 5.6 Polyisobutenes: rates of change of a & b.

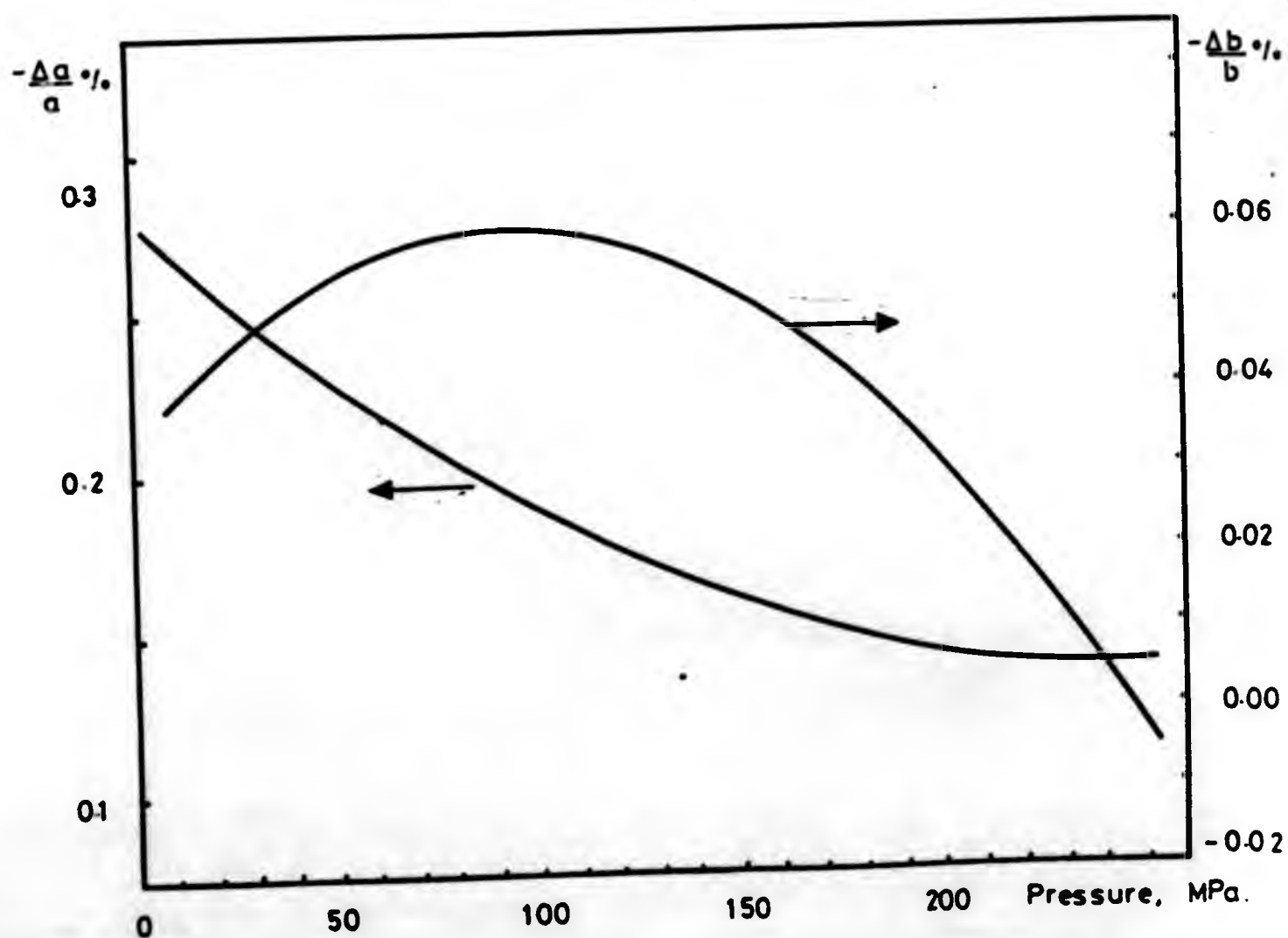Fig. 5.7   Polyethylene glycols: rates of change of a & b.

Fig. 5.8   Polypropylene glycols: rates of change of a & b.

References

1   Schoen, P E, Priest, R G, Sheridan, J P and Schnur, J M.
     Nature 270 412 (1977).

2   Flory, P J.
     "Statistical mechanics of chain molecules"
     John Wiley NY (1969).

3   Bondi, A.
     J Phys Chem 58 (11) 929 (1954).

4   Monobe, K, Fujiwara, Y and Tanaka, I.
     Proc 4th Int Conf on High Pressure
     Kyoto (1974) pp 63,865.

5   Krüger, J K, Peetz, L and Wildner, W.
     Polymer 21 620 (1980).

6   Krüger, J K, Peetz, L, Pietralla, M and Unruh, H G.
     Colloid and Poly Sci 259 215 (1981).

7   Patterson, G D, Carroll, P J and Pearson, D S.
     J Chem Soc Faraday Trans II 79 677 (1983).

8   Schoen, P E, Priest, R G, Sheridan, J P and Schnur, J M
     J Chem Phys 71 (1) 317 (1979).

9   Ikawa, S and Whalley, E.
     J Chem Phys 81 (4) 1620 (1984).

10 Dill, J F, Drake, P W and Litovitz, T A.
     ASLE Trans 18 (3) 202 (1975).

11 Assenbaum, A and Hochenheimer, H D.
     J Chem Phys 74 (1) 1 (1981).

12 Stith, J H, Peterson, L M, Rank, D H and Wiggins, T A.
     J Acoust Soc Am 55 (4) 785 (1974).

13 Medina, F D and O'Shea, D C.
     J Chem Phys 66 (5) 1940 (1977).

14 Tait, R I.
     Acustica 7 (4) 193 (1957).

15 Richardson, E G and Tait, R I.
     Phil Mag (Ser 8) 2 (16) 441 (1957).

16 Eden, H F and Richardson, E G.
     Acustica 10 (5,6) 309 (1960).

17 Wang, C H, Lin, Y H and Jones, D R.
     Mol Phys 37 (1) 287 (1979).

18 Doolittle, A K and Doolittle, D B
     J App Phys 28 (8) 901 (1957).

19   Doolittle, A K.
        J App Phys $\underline{22}$ (12) 1471 (1951).

20   Matheson, A J.
        J Chem Phys $\underline{44}$ (2) 695 (1966).

21   Bridgmann, P W.
        Proc Am Acad Arts and Sci $\underline{44}$ 255 (1909).

22   Gladstone and Dale.
        Phil Trans $\underline{153}$ 337 (1863).

23   Kittel, C.
        Introduction to solid state physics 5th ed.
        John Wiley NY (1976).

24   Lorentz.
        Ann Phys $\underline{9}$ 641 (1880).

25   Lorenz.
        Ann Phys $\underline{11}$ 70 (1880).

26   Glasstone, S.
        Textbook of physical chemistry 2nd ed.
        MacMillan and Co London (1948) p 529 et seq.

27   Böttcher, C J F.
        Theory of electric polarisation.
        Elsevier Amsterdam (1952).

28   Eisenlohr, F.
        Z Phys Chem $\underline{75}$ 585 (1911).

29   Tait, P G.
        Phys Chem $\underline{2}$ 176 (1888).

30   Vedam, K and Limsuwan, P (I and II).
        J Chem Phys $\underline{69}$ (11) 4762 (1978).

31   Vedam, K, Schmidt, E D D and Roy, R.
        J Am Ceram Soc $\underline{49}$ (10) 531 (1966).

32   Vedam, K, Schmidt, E D D, Kirtz, J L and Schneider, W C.
        Mat Res Bul $\underline{4}$ 573 (1969).

33   Vedam, K and Limsuwan, P.
        J App Phys $\underline{50}$ (3) 1328 (1979).

34   Eyring, H.
        J Chem Phys $\underline{4}$ 283 (1936).

35   Gee, G.
        Proc Chem Soc Tilden Lecture 111 (1957).

36   Cogswell, F N and McGowan, J C.
        Br Poly J $\underline{4}$ 183 (1972).

37   Faxen, H.
      Ark Mat Astron Fys 17 1 (1923).

38   Flude, M J C and Daborn, J E.
      J Phys E: 15 1313 (1982).

39   Lorentz.
      Abh Theor Phys 1 23 (1907).

40   Tanner, R I.
      J Fluid Mech 17 161 (1963).

41   Sutterby, J L.
      Trans Soc Rheol 17.4 573 (1973).

42   Isdale, J D and Spence, C M.
      DOI NEL Report 592 June (1975).

43   Chen, M C S and Swift, G W.
      A I Ch E J 18 146 (1972).

44   Champion, J V and Jackson, D A.
      Mol Phys 31 (4) 1169 (1976).

45   Boelhouwer, J W M.
      Physica 34 484 (1967).

46   Champion, J V and Dandridge, A.
      Mol Phys 42 (2) 385 (1981).

47   Litovitz, T A and Davis, C M.
      In "Physical acoustics II A" Mason, W P (ed).
      Academic Press, NY (1965).

48   Berne, B J and Pecora, R.
      "Dynamic light scattering ..." Chapter 10.4.
      John Wiley NY (1976).

49   Huang, Y Y and Wang, C H.
      J Chem Phys 62 (1) 120 (1975).

50   Schaafs, W.
      "Moleckularskustik" Springer-Verlag Berlin (1963) page 243.

51   Michels, B.
      J Chimie Phys 63 1123 (1966).

52   Bridgmann.
      "The Physics of High Pressure" Bell London (1949).

53   Gibson, R E and Kincaid, J F.
      J Am Chem Soc 60 (1) 511 (1938).

54   Langer, D W and Montalvo, R A.
      J Chem Phys 49 (6) 2836 (1968).

55   Waxler, R M and Wier, C E.
      J Res Nat Bur Stand <u>67</u> (A) (2) 163 (1963).

56   Vedam, K and Limsuwan, P.
      Rev Sci Inst <u>48</u> (3) 245 (1977).

57   Canton, J.
      Phil Trans Roy Soc   {640 (1762)
                            {261 (1764)

58   Tait, P G.
      Report of the voyage of HMS Challenger II appendix A (1881).

59   Aimé, G.
      Ann Chim Phys <u>8</u> 257 (1843).

60   Perkins, J.
      Trans Roy Soc <u>72</u> 324 (1819 - 20).

61   Bridgmann, P L J.
      Proc Am Acad Arts and Sci <u>77</u> 117 (1948).

62   Barnett, J D and Bosco, C D.
      J App Phys <u>40</u> (8) 3144 (1969).

63   Birnboim, M H and Weiss, H.
      J Poly Sci Poly Phys Ed <u>17</u> 2225 (1979).

64   Collings, A F and McLaughlin, E.
      Trans Faraday Soc <u>67</u> (578) 340 (1971).

65   Cogswell, F N.
      Plastics and Polymers p 39 Feb (1973).

66   Irving, J B and Barlow, A J.
      J Phys E: Sci Instrum <u>4</u> 232 (1971).

67   McLachlan, R J.
      J Phys E: Sci Instrum <u>9</u> 391 (1976).

68   Kuss, E.
      High T High P <u>9</u> 415 (1977).

69   Piermarini, G J, Forman, R A and Block, S.
      Rev Sci Instrum <u>49</u> (8) 1061 (1978).

70   Jackson, D A and Bedborough, D S.
      J Phys D: Appl Phys <u>11</u> L135 (1978).

71   Dandridge, A and Jackson, D A.
      J Phys D: Appl Phys <u>14</u> 829 (1981).

72   Stith, J H, Peterson, L M, Rank, D H and Wiggins, T A.
      J Acoust Soc Am <u>55</u> (4) 785 (1974).

73   Bridgmann, P W.
      Proc Am Arts and Sci <u>77</u> 129 (1948).

74 American Institute of Physics Handbook (1972).

75 Bradley, R S.
    "High Pressure Physics and Chemistry".
    Vol 1 Academic Press London (1963).

76 Liddell, P.
    PhD Thesis City of London Polytechnic (1979).

77 Bridgmann, P W.
    Rev Mod Phys 18 (1) 1 (1946).

78 Rajagopalan.
    J Phys Soc Jap 26 (6) 1495 (1969).

79 Kaye, G W C and Laby, T H.
    "Tables of Physical and Chemical Constants".
    14th ed Longmans London (1973).

80 Tatam, R and Crilly, J C.
    Internal Report, City of London Polytechnic (1983).

81 Rao.
    Indian J Phys 14 109 (1940).

82 Leidecker, H W and La Macchia, J T.
    J Acoust Soc Am 43 (1) 143 (1968).

83 Timmermans, J.
    "Physico-Chemical Constants of Pure Organic Compounds".
    Elsevier NY (1965).

84 BP Chemicals "Hyvis" technical booklet no HB102/4.

85 Bridgmann, P W.
    Proc Am Acad Arts and Sci 66 (5) 185 (1931).

86 Bridgmann, P W.
    Proc Am Acad Arts and Sci 67 (1) 1 (1932).

87 Bridgmann, P W.
    Proc Nat Acad Arts and Sci USA 11 603 (1925).

88 Mifsud, J F and Nolle, A W.
    J Acoust Soc Am 283 469 (1956).

89 Lin, Y H and Wang, C H.
    J Chem Phys 69 (4) 1546 (1978).

90 Wang, C H, Lin, Y H and Jones, D R.
    Mol Phys 37 (1) 287 (1979).

91 Flory, P J.
    J Am Chem Soc 62 (5) 1057 (1940).

92 Fox, T G and Flory, P J.
    J Am Chem Soc 70 (7) 2384 (1948).

93   Frenkel, J I.
      "Kinetic Theory of Liquids" OUP (1946).

94   Cantor, D M, Schroeder, J and Jonas, J.
      App Spectros $\underline{29}$ (5) 393 (1975).

II

D53687'85

END